Measurement of the weak mixing angle $\sin^2(\theta_W)$ by Coherent Elastic ν-Nucleus Scattering with the RICOCHET experiment

PHD SEMINAR – NEUTRINOS GROUP

SERRA Renaud

27/03/2025

I. Context and state of the art

II. Detection method and calibration

III. Study of $\boldsymbol{\gamma}$-background

IV. Measurement of specific activity

IV. Conclusion and prospects

Physical process : CEνNS

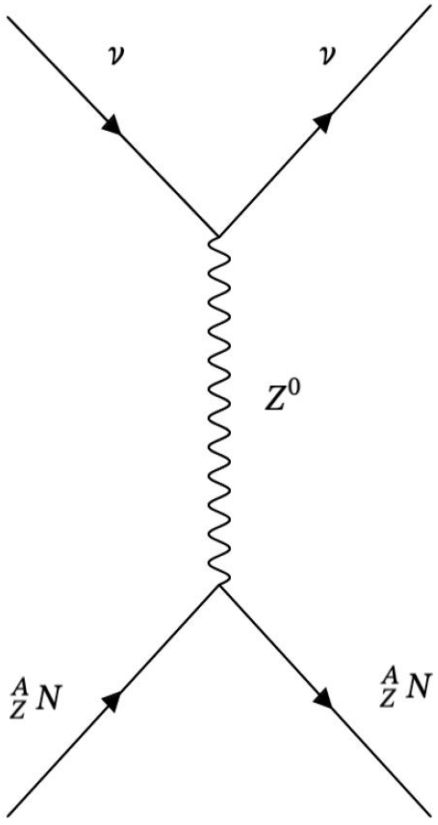

Diagram of $CE\nu NS$

Coherent : in-phase interaction between the neutrino and the nucleus as a whole

Elastic : process in which the total kinetic energy of the particles remains constant

Neutrino : elementary particle of the Standard Model, interacting very weakly with other particles

Nucleus : central part of an atom composed of protons and neutrons

Scattering : process by which one particle is deflected by another

- Theorized in 1974 by Daniel Z. Freedman
- First measurement in 2017 by COHERENT

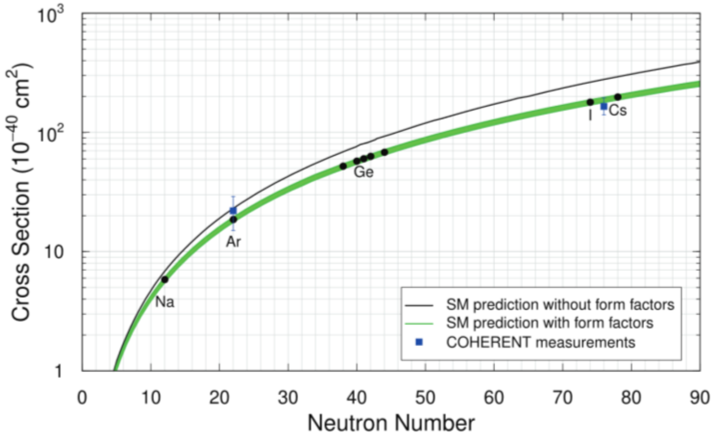

Cross-section measurement on different materials

[EPL, 143 (2023) 34001, M. Cadeddu & al.]

Physical process : CEνNS

[EPL, 143 (2023) 34001, M. Cadeddu & al.]

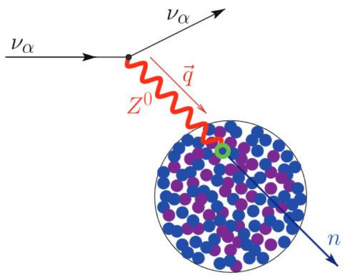

Inelastic and incoherent :

$\lambda_{Z_0} \ll 2R$

Physical process : CEνNS

[EPL, 143 (2023) 34001, M. Cadeddu & al.]

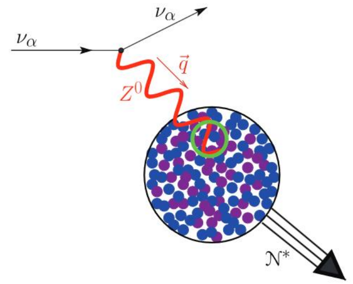

Elastic and incoherent:

$$\lambda_{Z_0} \leq 2R$$

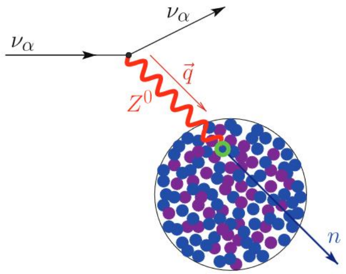

Inelastic and incoherent :

$$\lambda_{Z_0} \ll 2R$$

Physical process : CEνNS

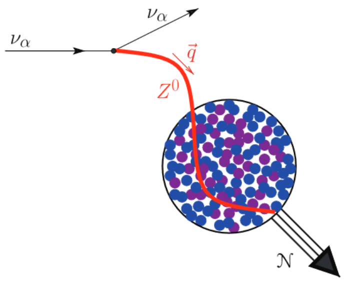

Elastic and coherent :

$$\lambda_{Z_0} \geq 2R$$

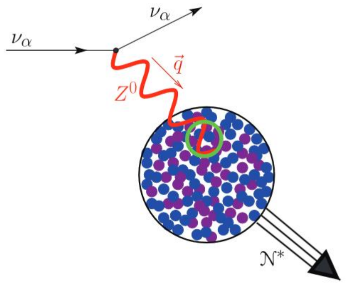

Elastic and incoherent:

$$\lambda_{Z_0} \leq 2R$$

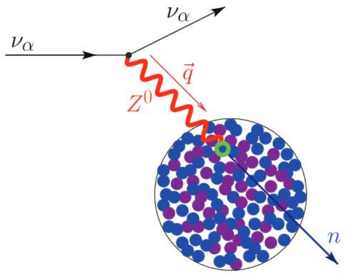

Inelastic and incoherent :

$$\lambda_{Z_0} \ll 2R$$

[EPL, 143 (2023) 34001, M. Cadeddu & al.]

Physical process : CEνNS

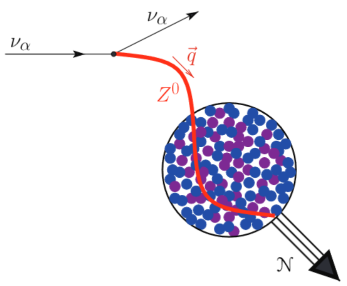

Elastic and coherent :

$\lambda_{Z^0} \geq 2R$

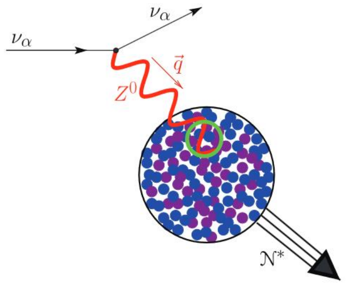

Elastic and incoherent:

$\lambda_{Z^0} \leq 2R$

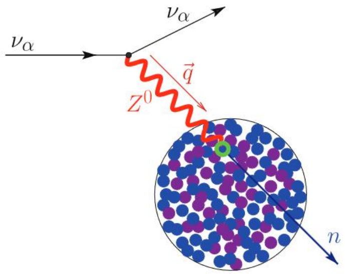

Inelastic and incoherent :

$\lambda_{Z^0} \ll 2R$

[EPL, 143 (2023) 34001, M. Cadeddu & al.]

Cross section predicted by the Standard Model :

$$\frac{d\sigma_{\nu/N}}{dE_R} = \frac{G_F^2}{4\pi} Q_w^2 \, m_N \left(1 - \frac{m_N \, E_R}{2 \, E_\nu^2}\right) F^2(E_R) \sim N^2$$

Physical process : CEνNS

[EPL, 143 (2023) 34001, M. Cadeddu & al.]

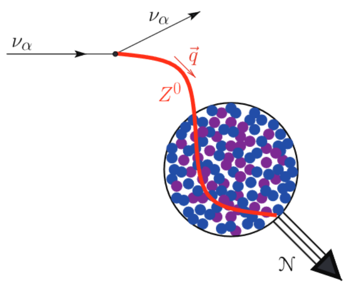

Elastic and coherent :

$\lambda_{Z^0} \geq 2R$

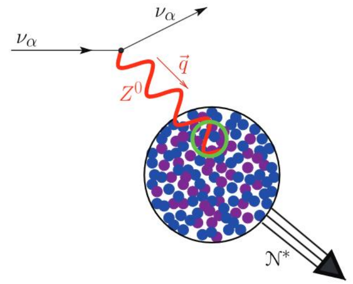

Elastic and incoherent:

$\lambda_{Z^0} \leq 2R$

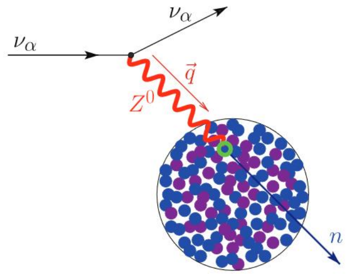

Inelastic and incoherent :

$\lambda_{Z^0} \ll 2R$

Cross section predicted by the Standard Model :

$$\frac{d\sigma_{\nu/N}}{dE_R} = \frac{G_F^2}{4\pi} Q_w^2\, m_N \left(1 - \frac{m_N\, E_R}{2\, E_\nu^2}\right) F^2(E_R) \sim N^2$$

- Technical challenges : very low nuclear recoil
- Ultra-sensitive detectors $\sim 10\ eV$ for Ricochet

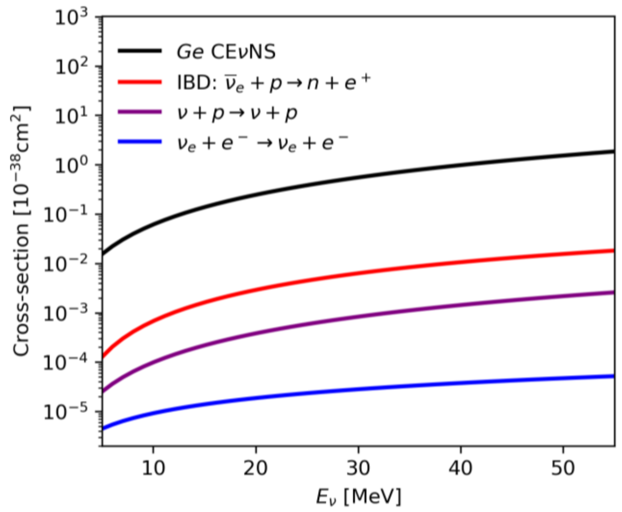

Interactions cross-sections for various processes

Physical process : CEνNS

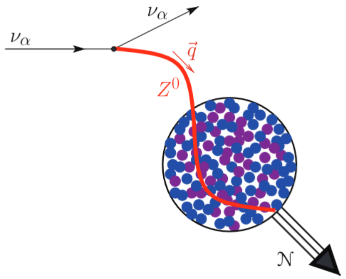

Elastic and coherent :

$$\lambda_{Z_0} \geq 2R$$

[EPL, 143 (2023) 34001, M. Cadeddu & al.]

Cross section predicted by the Standard Model :

$$\frac{d\sigma_{\nu/N}}{dE_R} = \frac{G_F^2}{4\pi} Q_w^2 \, m_N \left(1 - \frac{m_N \, E_R}{2 \, E_\nu^2}\right) F^2(E_R) \sim N^2$$

- Technical challenges : very low nuclear recoil
- Ultra-sensitive detectors $\sim 10 \; eV$ for Ricochet

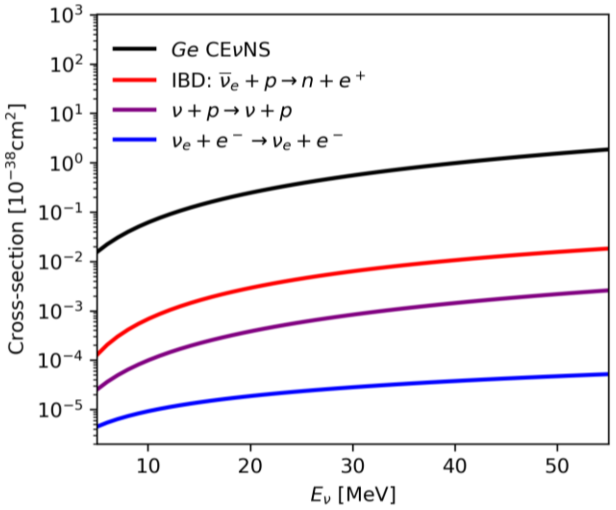

Interactions cross-sections for various processes

1. Sensitivity to new physics :
   - non-standard ν-quark interaction
   - neutrino magnetic moment μ_ν
   - new mediator boson Z'
2. Background for dark matter :
   - same signature and inevitability
   - experimental threshold

[JCAP (2018), J. Billard & al.]

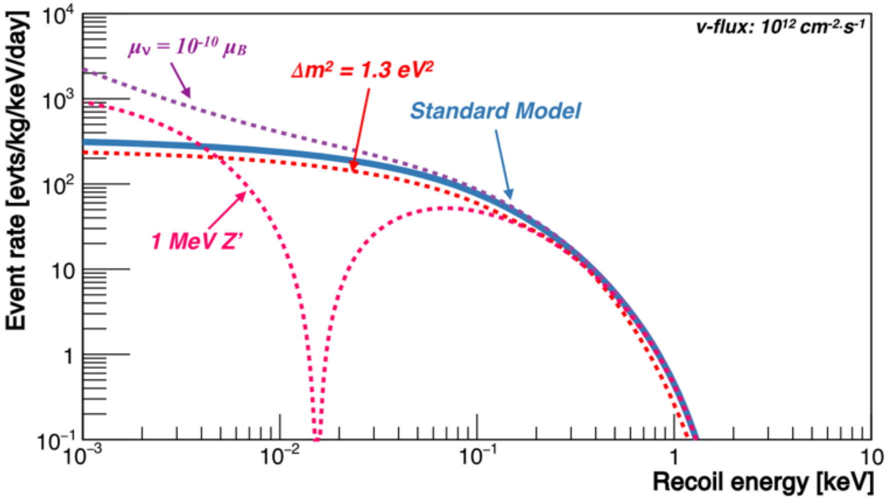

Expected interaction rates for Ricochet

Physical parameter : θ_W

E_R : recoil energy

E_ν : neutrino energy

G_F : Fermi's constant

m_N : nucleus mass

$F(E_R)$: form facteur

Q_w : nucleus weak charge

N : number of neutrons

Z : number of protons

$\boldsymbol{\theta_W}$: weak mixing angle

Cross section predicted by the Standard Model :

$$\frac{d\sigma_{\nu/N}}{dE_R} = \frac{G_F^2}{4\pi} Q_w^2 \, m_N \left(1 - \frac{m_N \, E_R}{2 \, E_\nu^2}\right) F^2(E_R)$$

With : $Q_w = N - \left(1 - 4\sin^2 \boldsymbol{\theta_W}\right) Z$

Unification of the electromagnetic force and the weak interaction :

- Represents the rotation caused by spontaneous symmetry breaking
- Proportion of weak and electromagnetic interactions in particle interactions

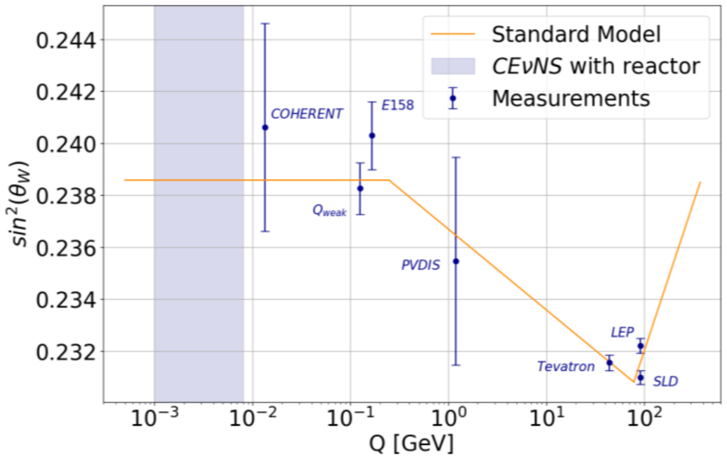

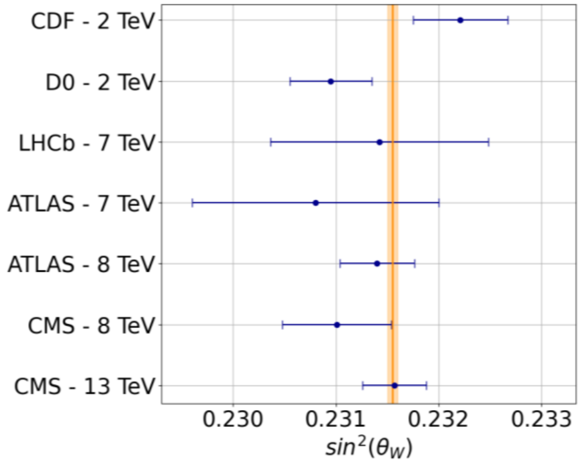

$sin^2\theta_w$ *experimental measurements*

ILL infrastructure : nuclear reactor

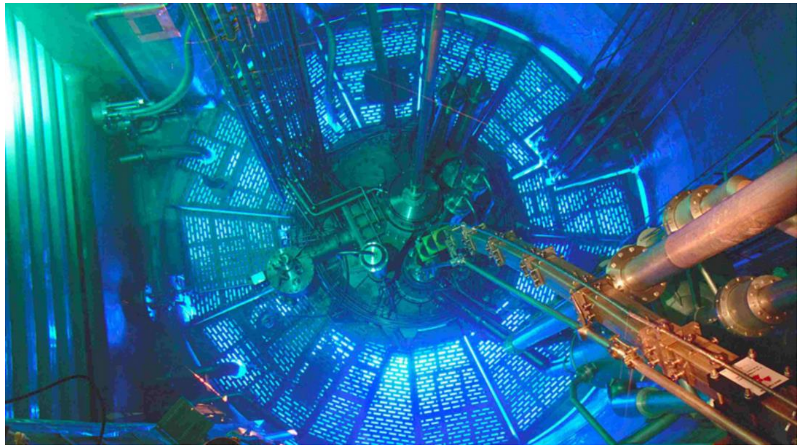

View of the ILL site and reactor pool

[Institut Laue-Langevin (2024)]

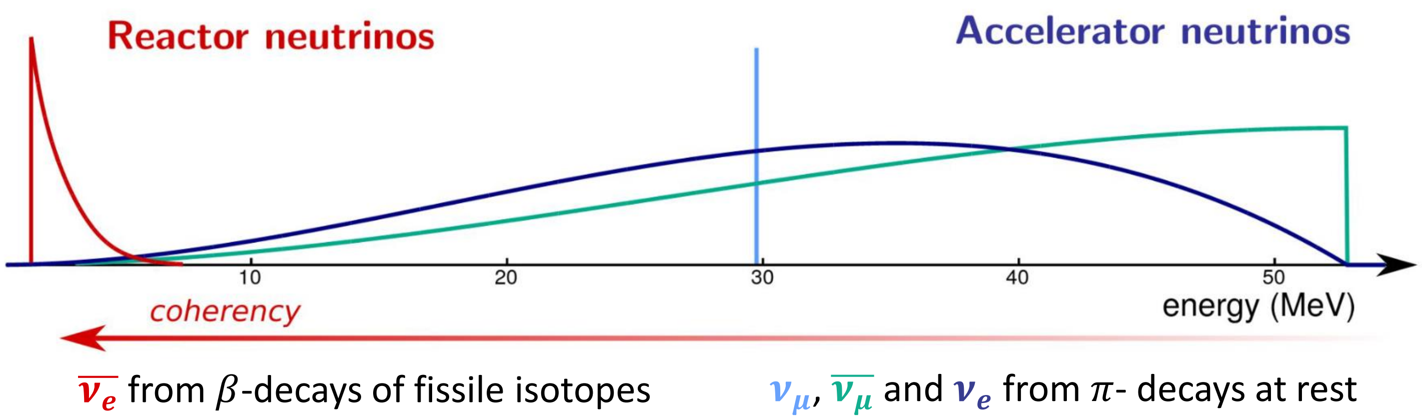

Process coherence as a function of neutrino energy

[HFIR workshop, ORNL (2024)]

- Reactor with **58 MWth** power $\rightarrow\ E_\nu < 10\ MeV$
- Only **8.8 m** to the reactor $\rightarrow\ \sigma_\nu \sim 10^{12}\ cm^{-2}.s^{-1}$

Ricochet detectors

[International Conference on Neutrino Physics and Astrophysics (2024)]

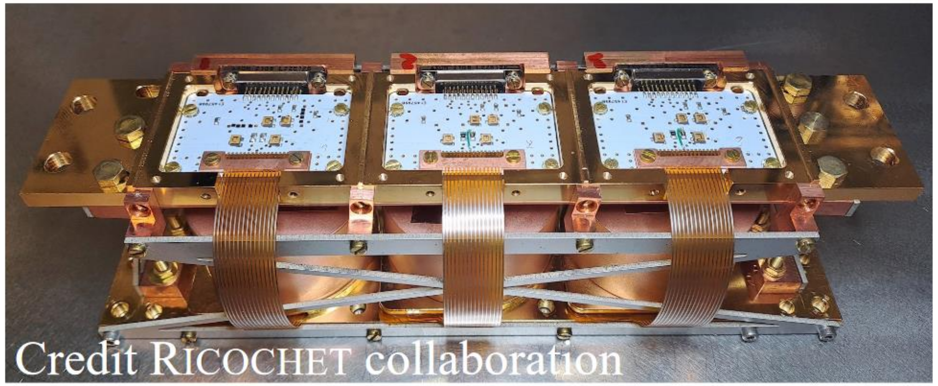

Example of a Mini-Cryocube

- CryoCube : **18** cryogenic calorimeter of **42** grams
- **Mini-CryoCube** : **3** calorimeters (test phase)
- Goal : **20 eV** resolution ionization and heat
- Inherited technology from **FID800** Eldelweiss detectors

Ricochet detectors

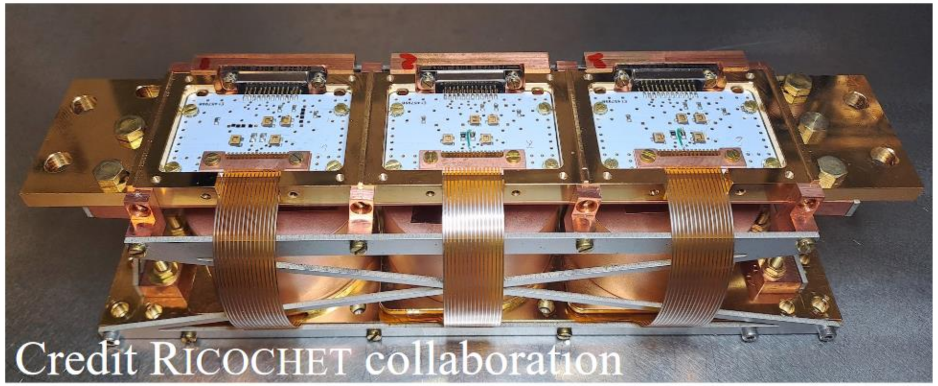

Example of a Mini-Cryocube

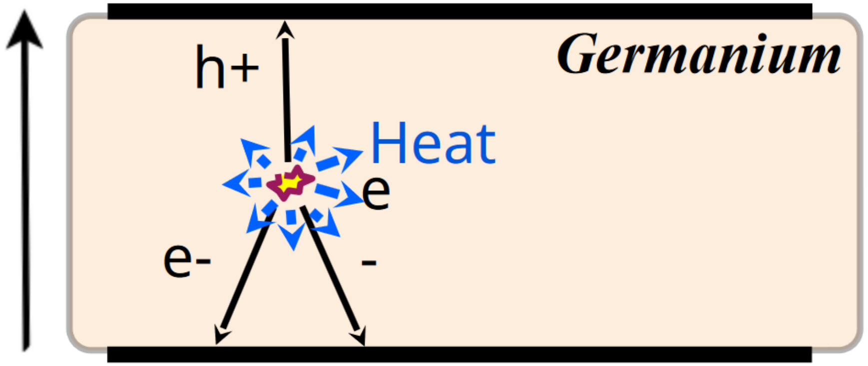

Detector operating diagram

- CryoCube : **18** cryogenic calorimeter of **42** grams
- **Mini-CryoCube** : **3** calorimeters (test phase)
- Goal : **20 eV** resolution ionization and heat
- Inherited technology from **FID800** Eldelweiss detectors
- Signal **discrimination** with ionization/heat ratio
  - ➢ depends on the type of incident particle
  - ➢ and type of recoil

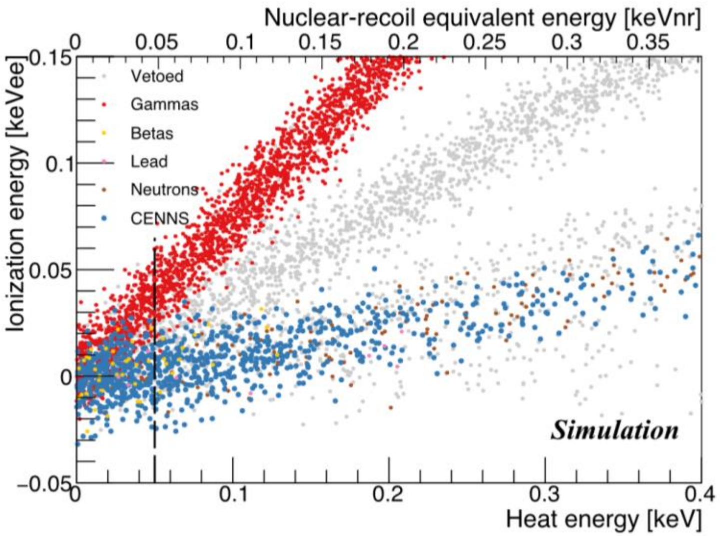

[International Conference on Neutrino Physics and Astrophysics (2024)]

[GDR Neutrino (2020)]

The Ricochet experience at ILL

[EPJC 83:20 (2023) , Ricochet collaboration]

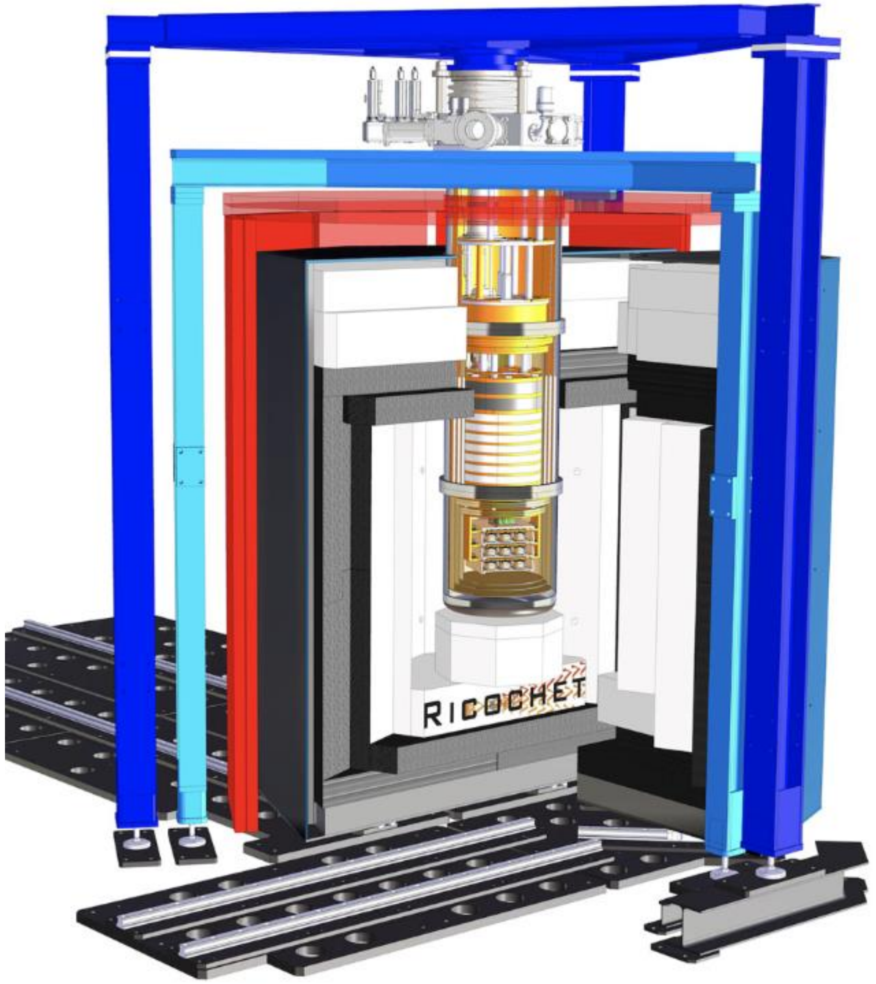

Diagram of Ricochet's shielding and cryostat

Significant raw background level due to :

- the proximity of the reactor core
- the positioning of the detector on earth surface

Background can be divided into **3** categories :

- cosmogenic : from cosmic particles
- reactogenic : isotopes activated by reactor neutrons
- **radiogenic** : natural background of the environment

The Ricochet experience at ILL

[EPJC 83:20 (2023) , Ricochet collaboration]

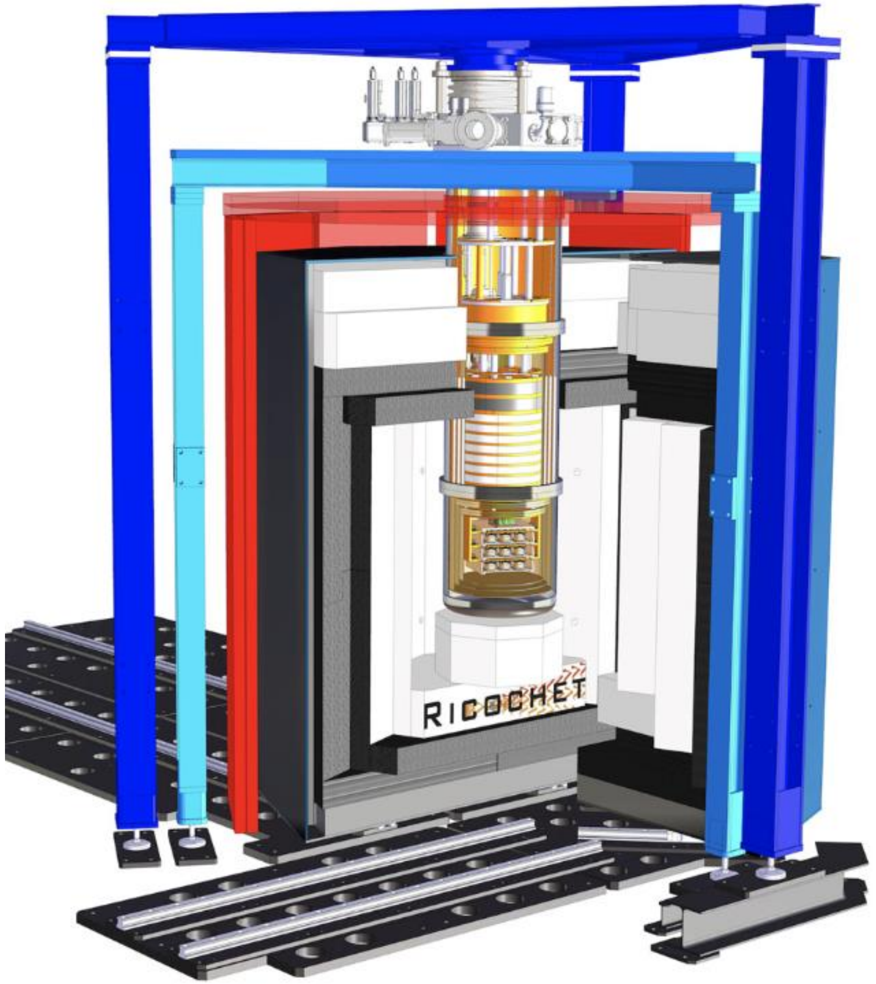

Diagram of Ricochet's shielding and cryostat

- **Blue** : lower and upper triangle (structure)
- **Red** : veto against cosmic muons
- **Gray** : lead photon shielding (20 t)
- **White** : boron-polyethylene neutron shielding (2 t)
- **Yellow** : Ricochet cryostat down to 10 mK

[LPSC Scientific Council (2024), J. Lamblin]

- ILL transfer channel : 15 m.w.e to attenuate cosmic particles

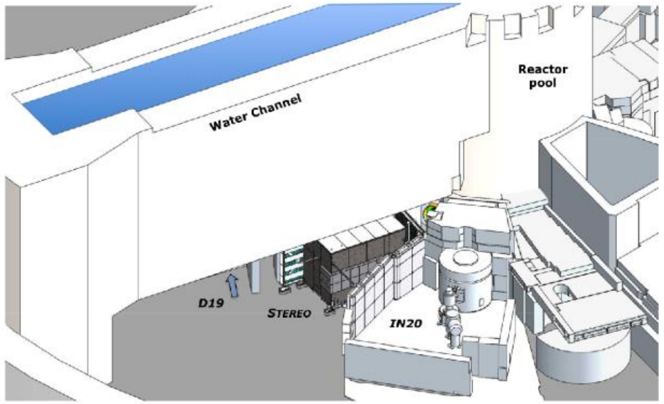

I. Context and state of the art

II. Detection method and calibration

III. Study of γ-background

IV. Measurement of specific activity

IV. Conclusion and prospects

High Purity Germanium detector

- To measure **gamma background** and develop GEANT4 model
- Installed in the shielding until November 2023
- Qualification of the detector with an $^{152}_{63}\boldsymbol{Eu}$ source :
  1. Energy calibration & resolution
  2. GEANT4 simulation
  3. Efficiency
  4. Radiogenic background in shielding
  5. Mass activity for each element
- Objective : extending the model to Ricochet end-detectors

HPGe detector in the shielding of Ricochet

Energy calibration of HPGe detector

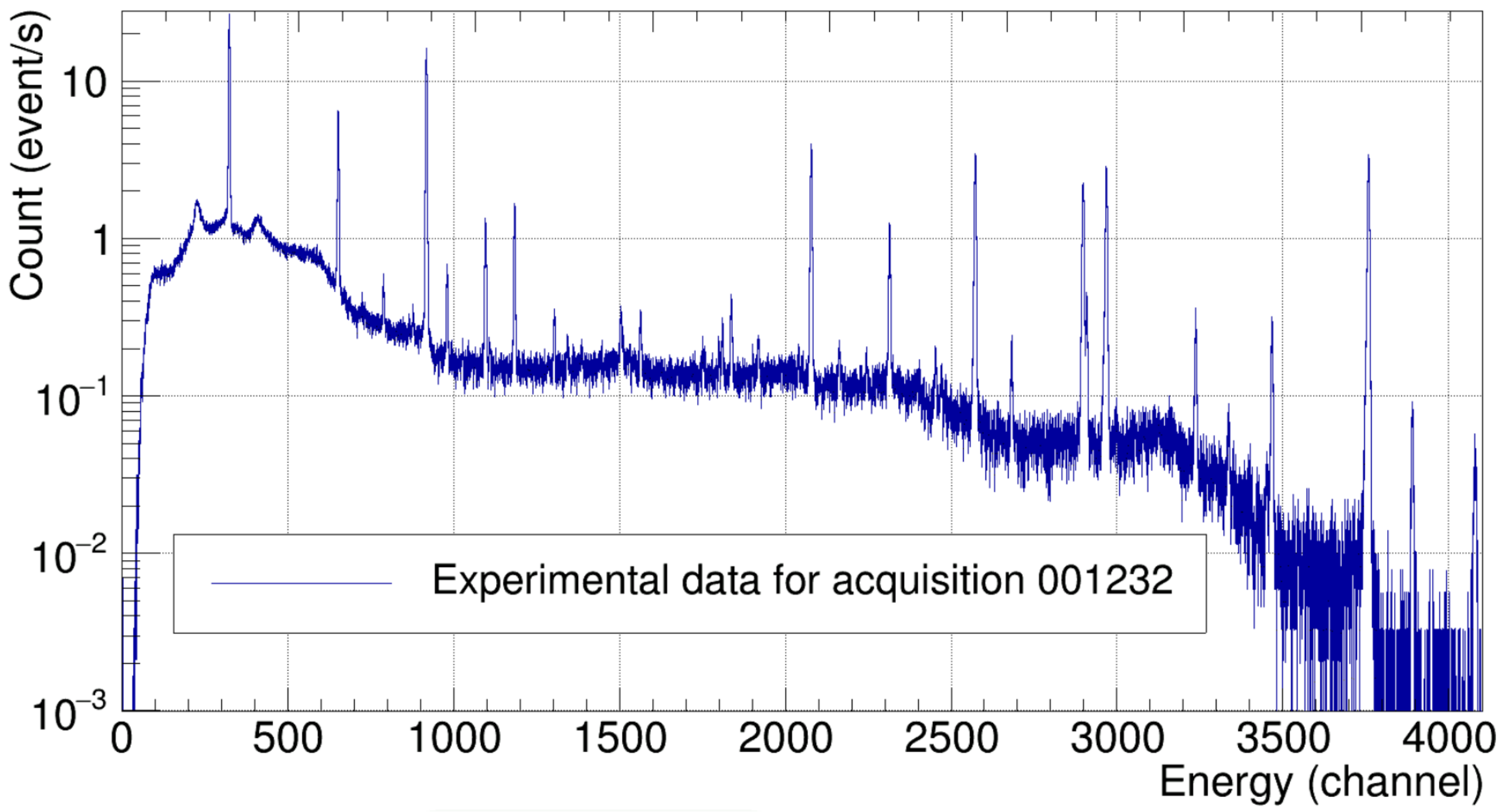

Experimental spectrum of the europium-152 source

- Peak energy of $^{152}\mathrm{Eu}$ known :
  - ➢ calibration possible
  - ➢ nuclear database (NuDat)
- Linear adjustment : $\boldsymbol{E} = \boldsymbol{k} \times \boldsymbol{C}$
  - ➢ E in keV and C in channel

$$k = (0.375 \pm 0.001)\ keV/canal$$

  - ➢ excellent calibration linearity

[Nuclear Data Sheet 114, 1497 (2013)]

Energy calibration of HPGe detector

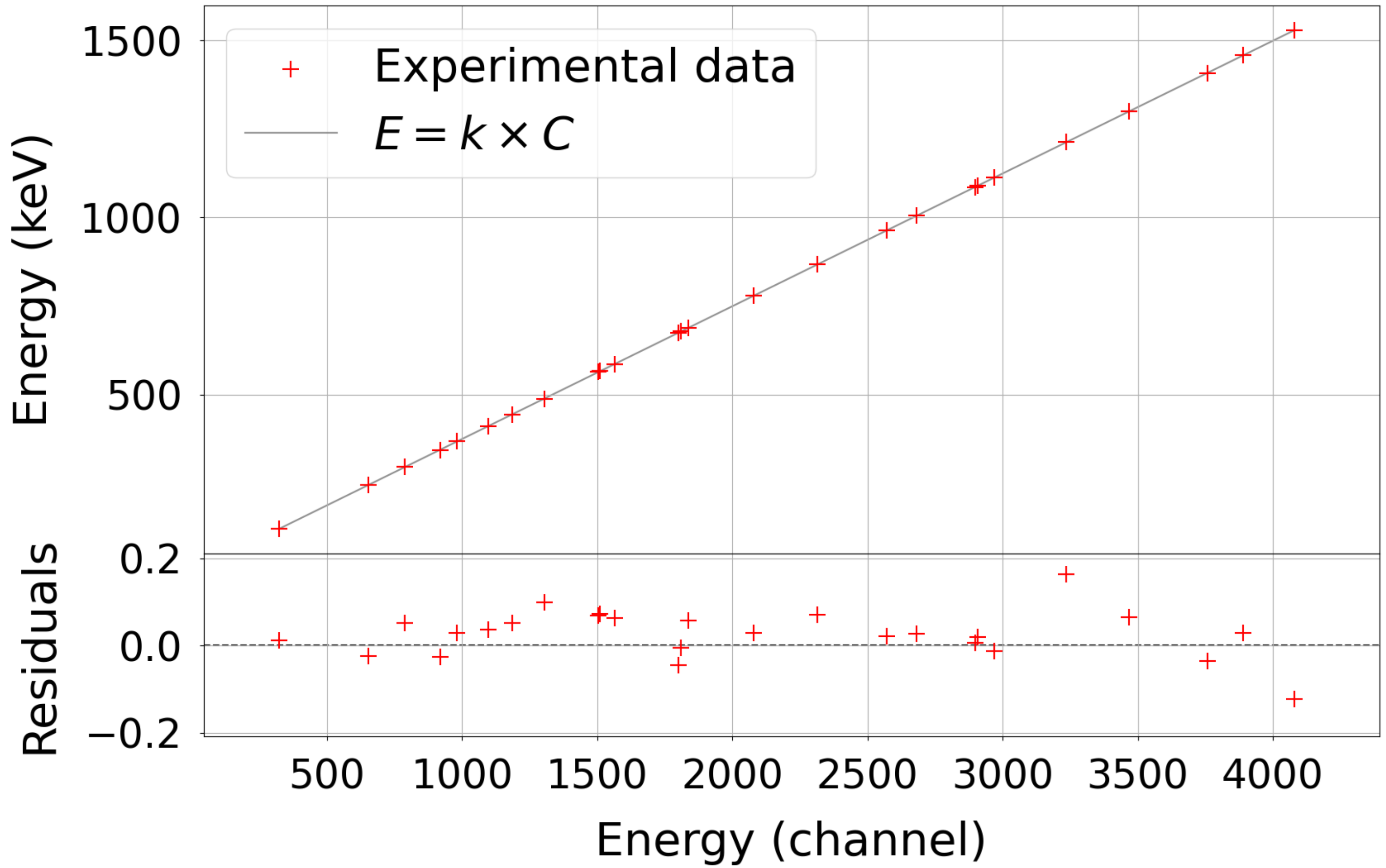

Energy-channel and residuals calibration for the HPGe detector

- Peak energy of ^{152}Eu known :
  - ➢ calibration possible
  - ➢ nuclear database (NuDat)
- Linear adjustment : $\boldsymbol{E} = \boldsymbol{k} \times \boldsymbol{C}$
  - ➢ E in keV and C in channel

$$k = (0.375 \pm 0.001)\ keV/canal$$

  - ➢ excellent calibration linearity

[Nuclear Data Sheet 114, 1497 (2013)]

Energy calibration of HPGe detector

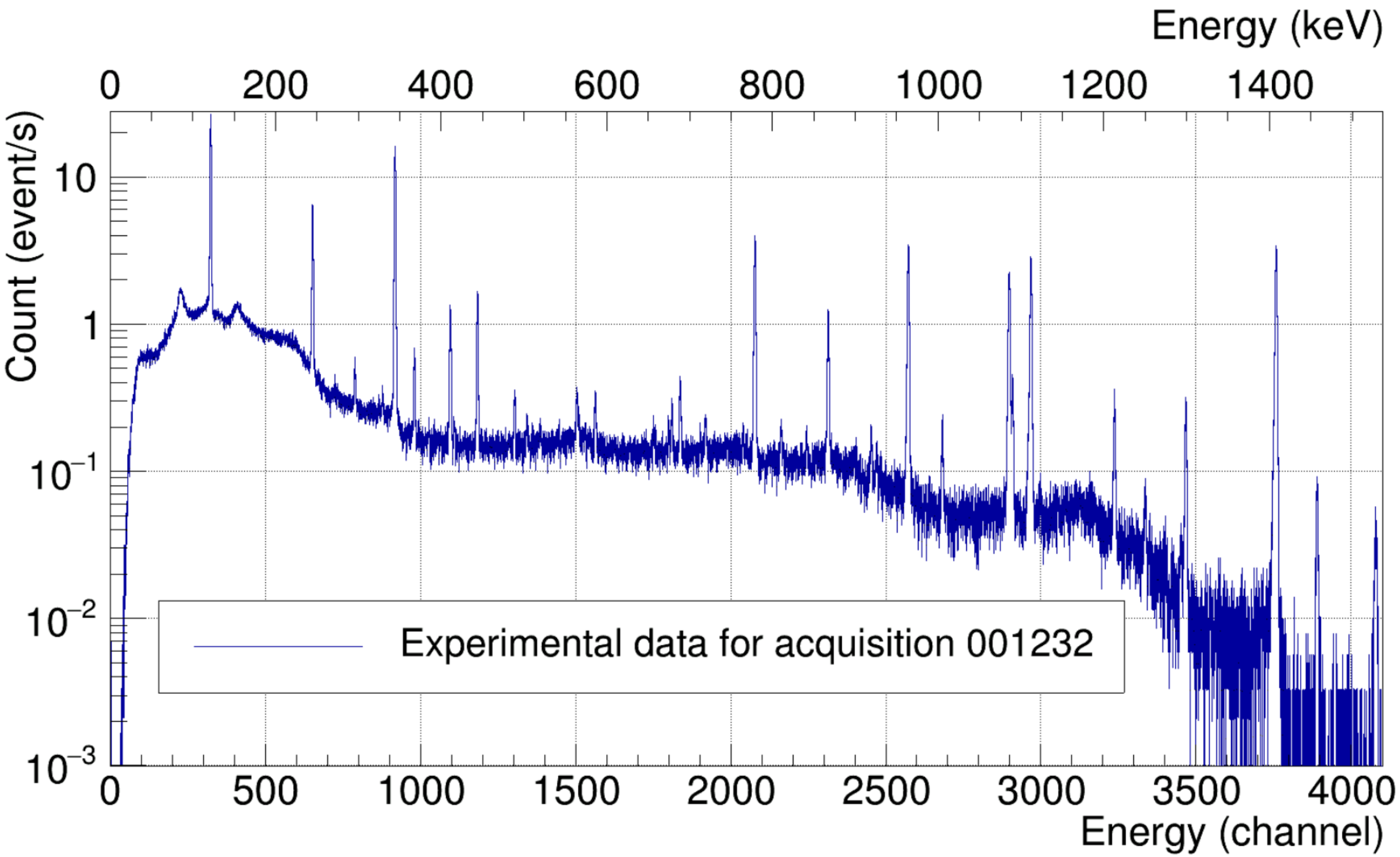

Experimental spectrum of the europium-152 source

- Peak energy of $^{152}\mathrm{Eu}$ known :
  - ➢ calibration possible
  - ➢ nuclear database (NuDat)
- Linear adjustment : $\boldsymbol{E} = \boldsymbol{k} \times \boldsymbol{C}$
  - ➢ E in keV and C in channel

$$k = (0.375 \pm 0.001)\ keV/canal$$

  - ➢ excellent calibration linearity

[Nuclear Data Sheet 114, 1497 (2013)]

Energy resolution of HPGe detector

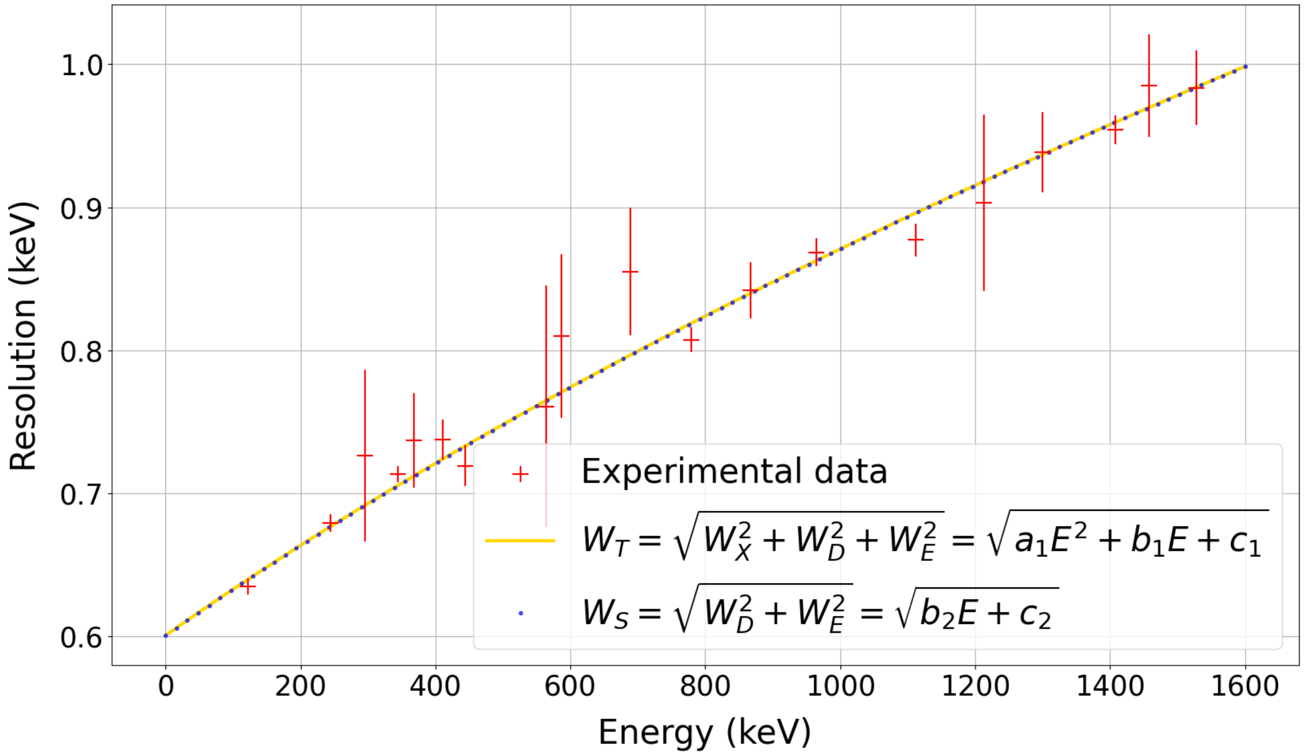

Experimental resolution of the HPGE detector

➢ Will be convoluted with simulated spectrum

Energetic resolution ⇔ sum of 3 contributions :

- $W_X = aE + b$: charges incomplete collection
- $W_E = c = cste$: electronic noise
- $W_D = d\sqrt{E}$: statistical fluctuation linked to the number of charge carriers created

- Better adjustment : $\chi^2/ddl = 1,13$

$$\Rightarrow \begin{cases} b_2 = (3.98 \pm 0.33) \times 10^{-4}\ keV \\ c_2 = (3.60 \pm 0.04) \times 10^{-1}\ keV^2 \end{cases}$$

[G. F. Knoll, Radiation Detection and Measurement : Chapter 12, III.B]

Simulation of detector & source

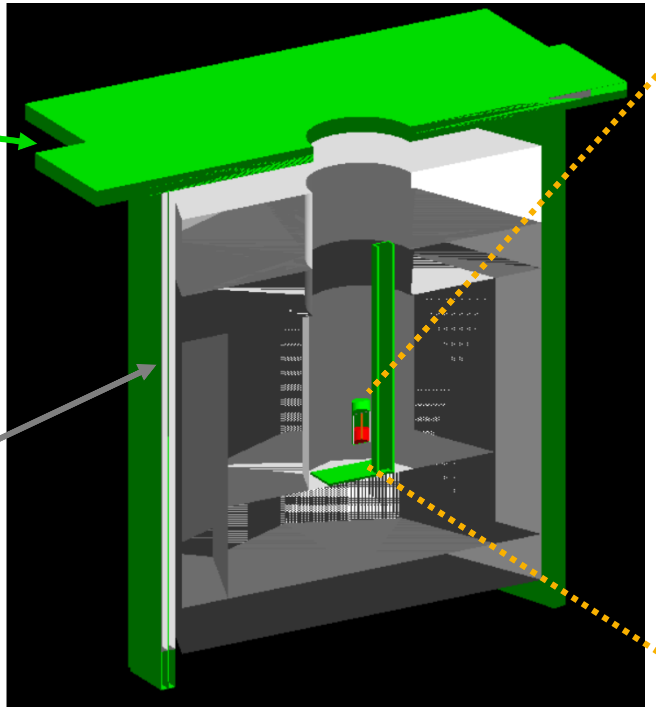

Ricochet shielding

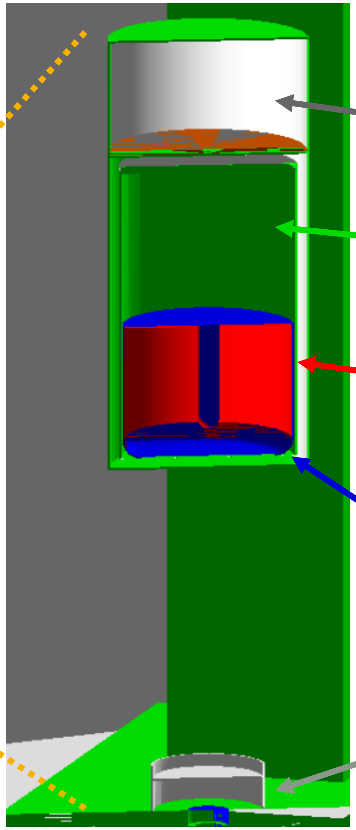

HPGe detector

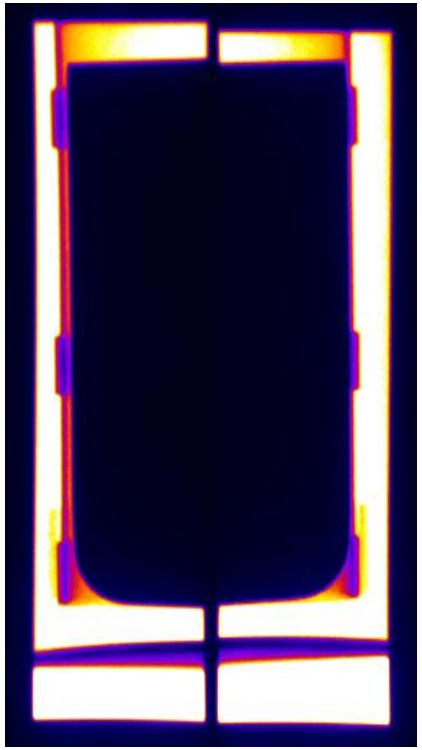

X-ray scan of the detector

GEANT4 simulation : spectrum

$\mathbf{E = 121,8}\ \boldsymbol{keV}$ $\mathbf{E = 688,7}\ \boldsymbol{keV}$ $\mathbf{E = 1299,1}\ \boldsymbol{keV}$

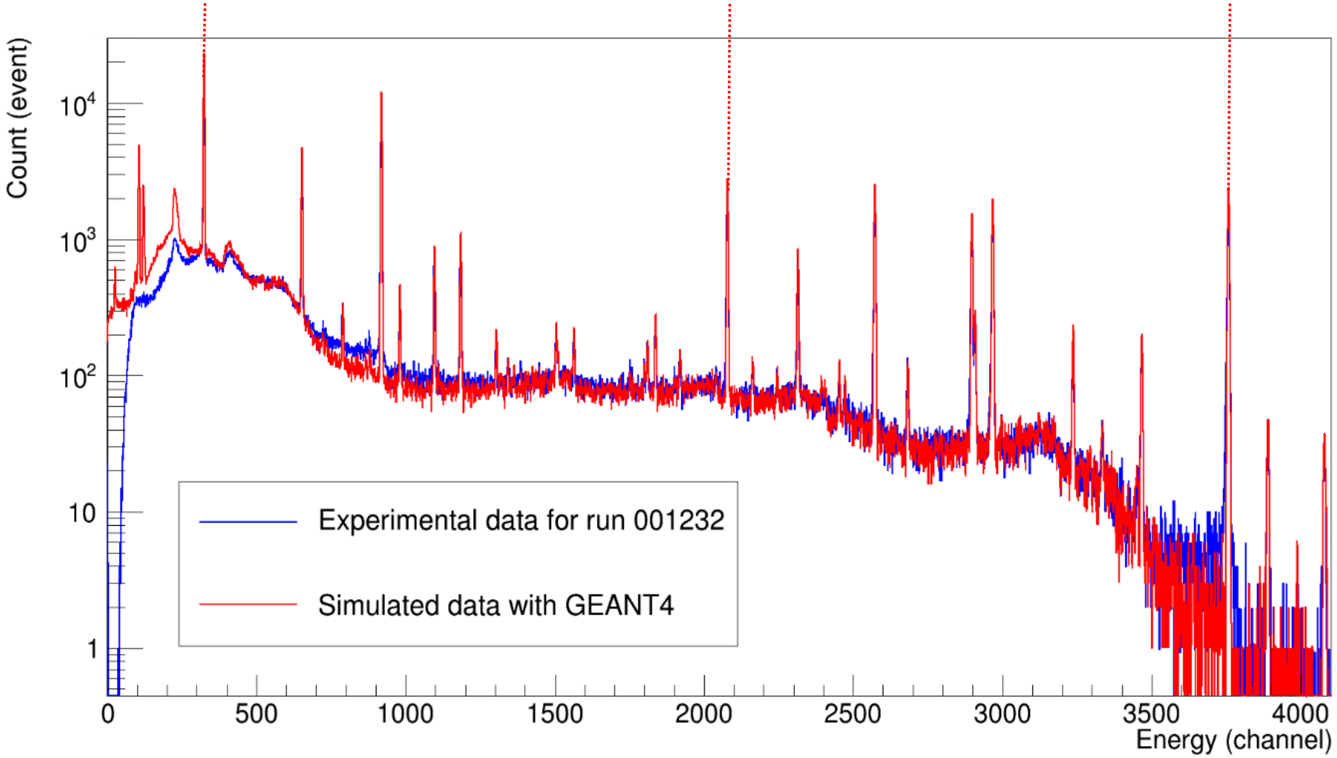

Spectrum comparison between 1232 experimental data and GEANT4 simulation

- Study with different configurations
- Good reproduction of data
- Medium-energy Compton front deficit :

$$E \in [600\,;900]\ channel$$
$$or$$
$$E \in\ [200\,;300]\ \mathrm{keV}$$

- Evidence of threshold at $100\ keV$
- Simulation quality $\pm \sim 10\%$

Threshold effect of the detector

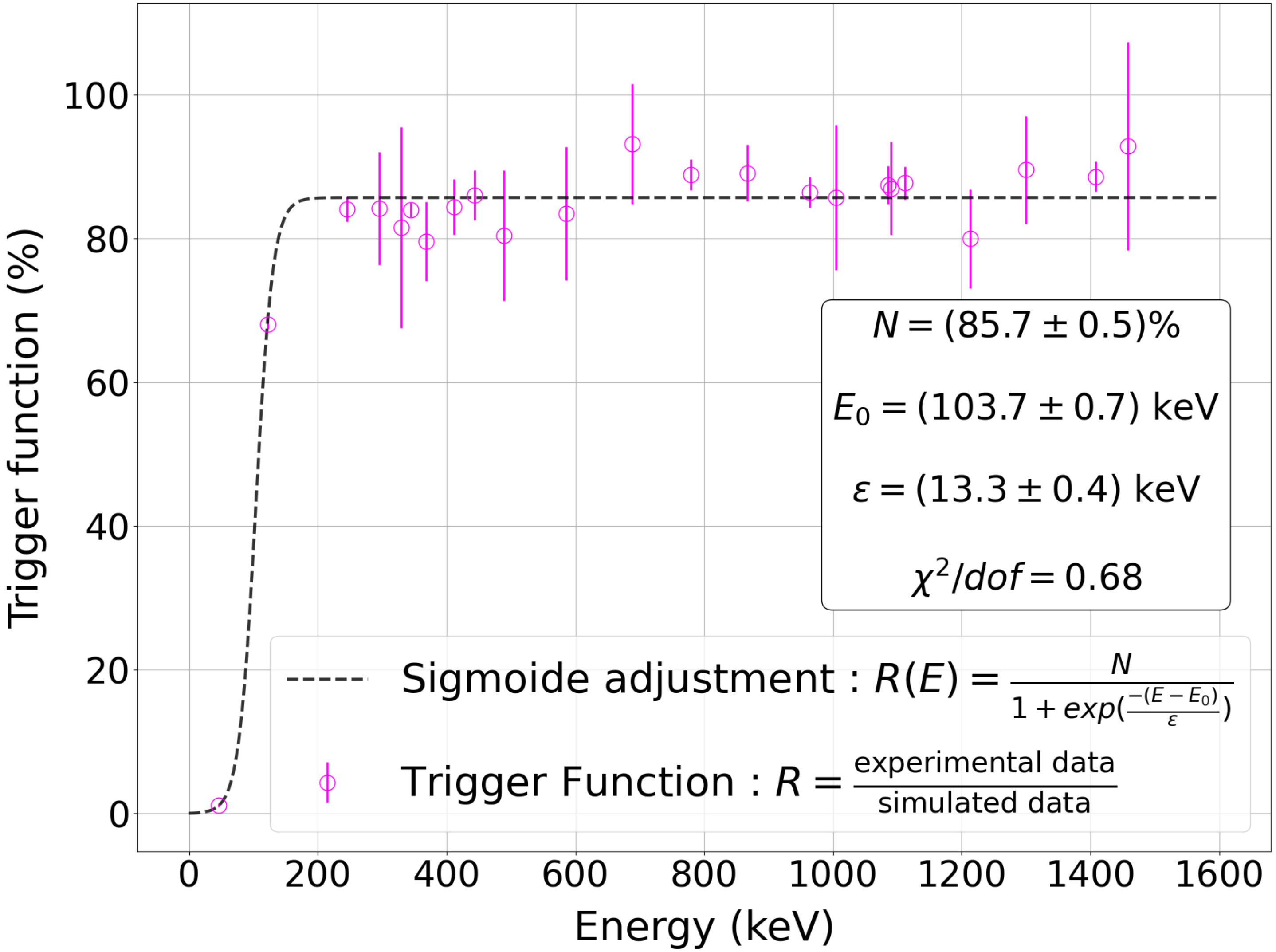

- Ratio of experimental and simulated peak areas :

  → provides information on simulation efficiency

- Adjustment by a sigmoid :

$$R(E) = \frac{N}{1 + e^{-\frac{(E - E_0)}{\epsilon}}}$$

  → to take account of the threshold

I. Context and state of the art

II. Detection method and calibration

III. Study of γ-background

IV. Measurement of specific activity

IV. Conclusion and prospects

Radiogenic γ-background

E (keV)	E (canal)	$^{A}_{Z}X$	E (keV)	E (canal)	$^{A}_{Z}X$	E (keV)	E (canal)	$^{A}_{Z}X$
39.857	108.2	$^{212}_{83}Bi$	510.770	1363	$^{208}_{81}Tl$	1238.110	3302	$^{214}_{83}Bi$
46.539	123.7	$^{210}_{82}Pb$	583.187	1556	$^{208}_{81}Tl$	1332.500	3554	$^{60}_{27}Co$
63.290	169.1	$^{234}_{90}Th$	609.312	1625	$^{214}_{83}Bi$	1377.669	3674	$^{214}_{83}Bi$
92.590	247.2	$^{234}_{90}Th$	727.330	1940	$^{212}_{83}Bi$	1401.515	3737	$^{214}_{83}Bi$
143.760	383.7	$^{235}_{92}U$	768.356	2047	$^{214}_{83}Bi$	1407.988	3755	$^{214}_{83}Bi$
185.715	495.6	$^{235}_{92}U$	860.557	2295	$^{208}_{81}Tl$	1460.832	3896	$^{40}_{19}K$
238.632	636.7	$^{212}_{82}Pb$	911.204	2430	$^{228}_{89}Ac$	1588.220	4239	$^{228}_{89}Ac$
241.995	644.5	$^{214}_{82}Pb$	964.766	2573	$^{228}_{89}Ac$	1729.595	4613	$^{214}_{83}Bi$
295.213	787.4	$^{214}_{82}Pb$	968.971	2585	$^{228}_{89}Ac$	1764.494	4706	$^{214}_{83}Bi$
338.320	902.3	$^{228}_{89}Ac$	1001.030	2670	$^{234m}_{91}Pa$	1847.433	4927	$^{214}_{83}Bi$
351.921	938.7	$^{214}_{82}Pb$	1120.287	2988	$^{214}_{83}Bi$	2204.210	5879	$^{214}_{83}Bi$
463.004	1236	$^{228}_{89}Ac$	1173.228	3129	$^{60}_{27}Co$	2614.511	6973	$^{208}_{81}Tl$

$^{232}_{90}Th$ decay chain

E (keV)	E (canal)	$^{A}_{Z}X$
39.857	108.2	$^{212}_{83}Bi$
46.539	123.7	$^{210}_{82}Pb$
63.290	169.1	$^{234}_{90}Th$
92.590	247.2	$^{234}_{90}Th$
143.760	383.7	$^{235}_{92}U$
185.715	495.6	$^{235}_{92}U$
238.632	636.7	$^{212}_{82}Pb$
241.995	644.5	$^{214}_{82}Pb$
295.213	787.4	$^{214}_{82}Pb$
338.320	902.3	$^{228}_{89}Ac$
351.921	938.7	$^{214}_{82}Pb$
463.004	1236	$^{228}_{89}Ac$

E (keV)	E (canal)	$^{A}_{Z}X$
510.770	1363	$^{208}_{81}Tl$
583.187	1556	$^{208}_{81}Tl$
609.312	1625	$^{214}_{83}Bi$
727.330	1940	$^{212}_{83}Bi$
768.356	2047	$^{214}_{83}Bi$
860.557	2295	$^{208}_{81}Tl$
911.204	2430	$^{228}_{89}Ac$
964.766	2573	$^{228}_{89}Ac$
968.971	2585	$^{228}_{89}Ac$
1001.030	2670	$^{234m}_{91}Pa$
1120.287	2988	$^{214}_{83}Bi$
1173.228	3129	$^{60}_{27}Co$

E (keV)	E (canal)	$^{A}_{Z}X$
1238.110	3302	$^{214}_{83}Bi$
1332.500	3554	$^{60}_{27}Co$
1377.669	3674	$^{214}_{83}Bi$
1401.515	3737	$^{214}_{83}Bi$
1407.988	3755	$^{214}_{83}Bi$
1460.832	3896	$^{40}_{19}K$
1588.220	4239	$^{228}_{89}Ac$
1729.595	4613	$^{214}_{83}Bi$
1764.494	4706	$^{214}_{83}Bi$
1847.433	4927	$^{214}_{83}Bi$
2204.210	5879	$^{214}_{83}Bi$
2614.511	6973	$^{208}_{81}Tl$

$^{238}_{92}U$ decay chain

E (keV)	E (canal)	$^{A}_{Z}X$	E (keV)	E (canal)	$^{A}_{Z}X$	E (keV)	E (canal)	$^{A}_{Z}X$
39.857	108.2	$^{212}_{83}Bi$	510.770	1363	$^{208}_{81}Tl$	1238.110	3302	$^{214}_{83}Bi$
46.539	123.7	$^{210}_{82}Pb$	583.187	1556	$^{208}_{81}Tl$	1332.500	3554	$^{60}_{27}Co$
63.290	169.1	$^{234}_{90}Th$	609.312	1625	$^{214}_{83}Bi$	1377.669	3674	$^{214}_{83}Bi$
92.590	247.2	$^{234}_{90}Th$	727.330	1940	$^{212}_{83}Bi$	1401.515	3737	$^{214}_{83}Bi$
143.760	383.7	$^{235}_{92}U$	768.356	2047	$^{214}_{83}Bi$	1407.988	3755	$^{214}_{83}Bi$
185.715	495.6	$^{235}_{92}U$	860.557	2295	$^{208}_{81}Tl$	1460.832	3896	$^{40}_{19}K$
238.632	636.7	$^{212}_{82}Pb$	911.204	2430	$^{228}_{89}Ac$	1588.220	4239	$^{228}_{89}Ac$
241.995	644.5	$^{214}_{82}Pb$	964.766	2573	$^{228}_{89}Ac$	1729.595	4613	$^{214}_{83}Bi$
295.213	787.4	$^{214}_{82}Pb$	968.971	2585	$^{228}_{89}Ac$	1764.494	4706	$^{214}_{83}Bi$
338.320	902.3	$^{228}_{89}Ac$	1001.030	2670	$^{234m}_{91}Pa$	1847.433	4927	$^{214}_{83}Bi$
351.921	938.7	$^{214}_{82}Pb$	1120.287	2988	$^{214}_{83}Bi$	2204.210	5879	$^{214}_{83}Bi$
463.004	1236	$^{228}_{89}Ac$	1173.228	3129	$^{60}_{27}Co$	2614.511	6973	$^{208}_{81}Tl$

$^{235}_{92}U$ decay chain

E (keV)	E (canal)	$^{A}_{Z}X$	E (keV)	E (canal)	$^{A}_{Z}X$	E (keV)	E (canal)	$^{A}_{Z}X$
39.857	108.2	$^{212}_{83}Bi$	510.770	1363	$^{208}_{81}Tl$	1238.110	3302	$^{214}_{83}Bi$
46.539	123.7	$^{210}_{82}Pb$	583.187	1556	$^{208}_{81}Tl$	1332.500	3554	$^{60}_{27}Co$
63.290	169.1	$^{234}_{90}Th$	609.312	1625	$^{214}_{83}Bi$	1377.669	3674	$^{214}_{83}Bi$
92.590	247.2	$^{234}_{90}Th$	727.330	1940	$^{212}_{83}Bi$	1401.515	3737	$^{214}_{83}Bi$
143.760	383.7	$^{235}_{92}U$	768.356	2047	$^{214}_{83}Bi$	1407.988	3755	$^{214}_{83}Bi$
185.715	495.6	$^{235}_{92}U$	860.557	2295	$^{208}_{81}Tl$	1460.832	3896	$^{40}_{19}K$
238.632	636.7	$^{212}_{82}Pb$	911.204	2430	$^{228}_{89}Ac$	1588.220	4239	$^{228}_{89}Ac$
241.995	644.5	$^{214}_{82}Pb$	964.766	2573	$^{228}_{89}Ac$	1729.595	4613	$^{214}_{83}Bi$
295.213	787.4	$^{214}_{82}Pb$	968.971	2585	$^{228}_{89}Ac$	1764.494	4706	$^{214}_{83}Bi$
338.320	902.3	$^{228}_{89}Ac$	1001.030	2670	$^{234m}_{91}Pa$	1847.433	4927	$^{214}_{83}Bi$
351.921	938.7	$^{214}_{82}Pb$	1120.287	2988	$^{214}_{83}Bi$	2204.210	5879	$^{214}_{83}Bi$
463.004	1236	$^{228}_{89}Ac$	1173.228	3129	$^{60}_{27}Co$	2614.511	6973	$^{208}_{81}Tl$

Remaining isotopes : $^{60}_{27}\mathrm{Co}$ & $^{40}_{19}\mathrm{K}$

E (keV)	E (canal)	$^{A}_{Z}X$
39.857	108.2	$^{212}_{83}\mathrm{Bi}$
46.539	123.7	$^{210}_{82}\mathrm{Pb}$
63.290	169.1	$^{234}_{90}\mathrm{Th}$
92.590	247.2	$^{234}_{90}\mathrm{Th}$
143.760	383.7	$^{235}_{92}\mathrm{U}$
185.715	495.6	$^{235}_{92}\mathrm{U}$
238.632	636.7	$^{212}_{82}\mathrm{Pb}$
241.995	644.5	$^{214}_{82}\mathrm{Pb}$
295.213	787.4	$^{214}_{82}\mathrm{Pb}$
338.320	902.3	$^{228}_{89}\mathrm{Ac}$
351.921	938.7	$^{214}_{82}\mathrm{Pb}$
463.004	1236	$^{228}_{89}\mathrm{Ac}$

E (keV)	E (canal)	$^{A}_{Z}X$
510.770	1363	$^{208}_{81}\mathrm{Tl}$
583.187	1556	$^{208}_{81}\mathrm{Tl}$
609.312	1625	$^{214}_{83}\mathrm{Bi}$
727.330	1940	$^{212}_{83}\mathrm{Bi}$
768.356	2047	$^{214}_{83}\mathrm{Bi}$
860.557	2295	$^{208}_{81}\mathrm{Tl}$
911.204	2430	$^{228}_{89}\mathrm{Ac}$
964.766	2573	$^{228}_{89}\mathrm{Ac}$
968.971	2585	$^{228}_{89}\mathrm{Ac}$
1001.030	2670	$^{234m}_{91}\mathrm{Pa}$
1120.287	2988	$^{214}_{83}\mathrm{Bi}$
1173.228	3129	$^{60}_{27}\mathrm{Co}$

E (keV)	E (canal)	$^{A}_{Z}X$
1238.110	3302	$^{214}_{83}\mathrm{Bi}$
1332.500	3554	$^{60}_{27}\mathrm{Co}$
1377.669	3674	$^{214}_{83}\mathrm{Bi}$
1401.515	3737	$^{214}_{83}\mathrm{Bi}$
1407.988	3755	$^{214}_{83}\mathrm{Bi}$
1460.832	3896	$^{40}_{19}\mathrm{K}$
1588.220	4239	$^{228}_{89}\mathrm{Ac}$
1729.595	4613	$^{214}_{83}\mathrm{Bi}$
1764.494	4706	$^{214}_{83}\mathrm{Bi}$
1847.433	4927	$^{214}_{83}\mathrm{Bi}$
2204.210	5879	$^{214}_{83}\mathrm{Bi}$
2614.511	6973	$^{208}_{81}\mathrm{Tl}$

Linear combination of simulations

Linear combination of GEANT4 simulations :

$$S^{sim} = \sum_{i=1}^{N} a_i^{PE} s_i^{PE} + \sum_{j=1}^{M} a_j^{Pb} s_j^{Pb} = \sum a_k s_k$$

- S^{sim} : linear reconstruction
- $s_k^{PE/Pb}$: simulated spectra in PE or Pb
- a_k : linear coefficients

Objective : find the a_k coefficients to combine simulated spectra in order to reproduce the experimental radiogenic background spectrum

Radiogenic background spectrum with examples

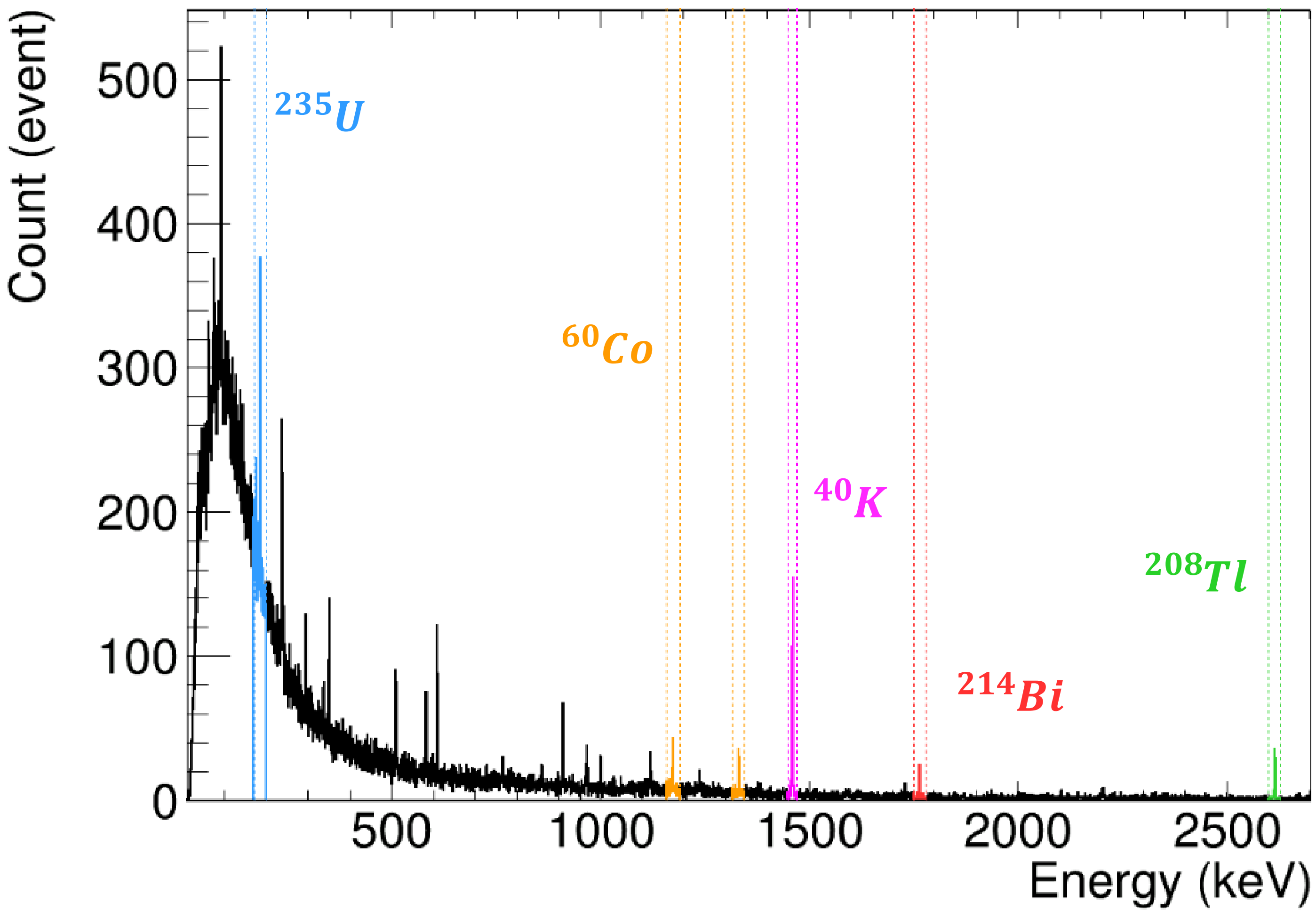

Linear combination of simulations

<u>*Example of peak selection using the weight function*</u>

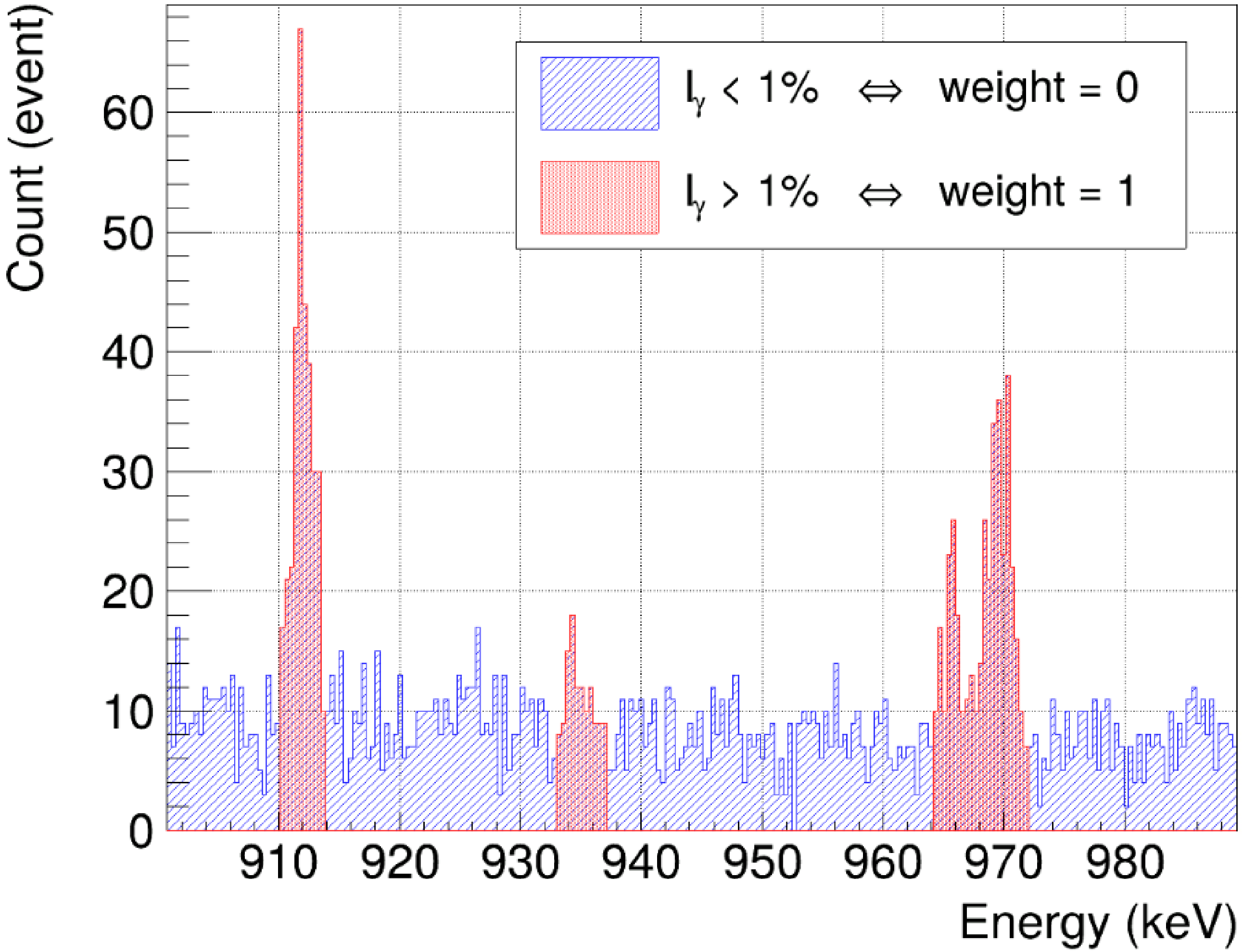

Add a function assigning a weight $\boldsymbol{W}$ based on the bin :

$$W(E \pm \sigma_E) = \begin{cases} 1 \; if \; I_\gamma > 1\% \\ 0 \; otherwise \end{cases}$$

- Using decay databases (NuDat)
- Refine the linear combination of simulated spectra
- Adjustment on photopeaks only

Linear combination of simulations

Adjustment method : χ^2 minimization

$$\chi^2 = \sum_{i=1}^{N_{bin}} \left[\frac{S_i^{exp} - S_i^{sim}(s_k^{PE}, s_k^{Pb}, a_k)}{\sigma_i} \right]^2$$

- S^{exp} : experimental spectrum
- S^{sim} : linear reconstruction
- $s_k^{PE/Pb}$: simulated spectra
- a_k : linear coefficients
- $\sigma_i = \sqrt{N_i}$: poissonian error

- Number of generations required in **polyethylene** shielding :

$^{232}\text{Th} \rightarrow (1.96 \pm 0.07) \times 10^7$

$^{238}\text{U} \rightarrow (1.67 \pm 0.07) \times 10^7$

$^{40}\text{K} \rightarrow (6.56 \pm 0.88) \times 10^7$

$^{235}\text{U} \rightarrow (1.56 \pm 0.07) \times 10^7$

Polyethylene

- Number of generations required in **lead** shielding :

$^{232}\text{Th} \rightarrow (4.06 \pm 0.54) \times 10^7$

$^{238}\text{U} \rightarrow (6.08 \pm 0.64) \times 10^7$

$^{40}\text{K} \rightarrow (8.82 \pm 0.54) \times 10^8$

$^{235}\text{U} \rightarrow (4.97 \pm 2.84) \times 10^7$

$^{60}\text{Co} \rightarrow (3.70 \pm 0.02) \times 10^7$

Lead

Linear combination of simulations

Reconstruction of the experimental spectrum with simulated spectra

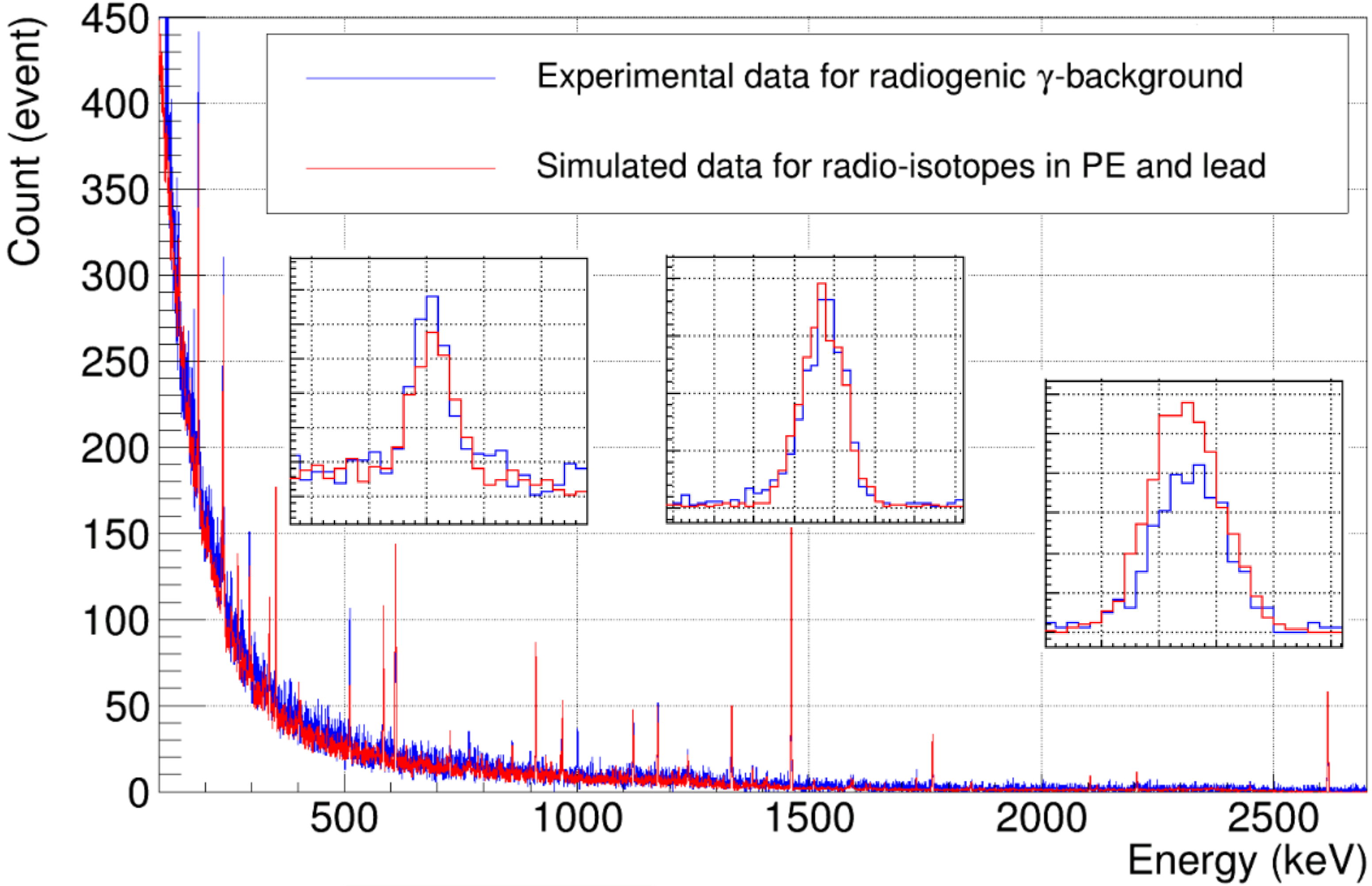

Best adjustment : $\chi^2/dof = 1.9$

	k_1	k_2	k_3	k_4	k_5	k_6	k_7	k_8	k_9
k_9	-0.0163	0.023	0.0822	-0.0428	-0.0981	-0.115	-0.16	-0.0372	1
k_8	-0.0159	-0.0194	0.0564	-0.495	-0.0735	-0.0847	-0.0994	1	-0.0372
k_7	0.0279	0.0363	-0.802	-0.0231	-0.163	-0.148	1	-0.0994	-0.16
k_6	0.0189	-0.734	0.0532	0.02	-0.211	1	-0.148	-0.0847	-0.115
k_5	-0.751	0.0404	0.0929	0.00216	1	-0.211	-0.163	-0.0735	-0.0981
k_4	-0.108	-0.129	-0.00204	1	0.00216	0.02	-0.0231	-0.495	-0.0428
k_3	-0.0372	-0.0275	1	-0.00204	0.0929	0.0532	-0.802	0.0564	0.0822
k_2	-0.00425	1	-0.0275	-0.129	0.0404	-0.734	0.0363	-0.0194	0.023
k_1	1	-0.00425	-0.0372	-0.108	-0.751	0.0189	0.0279	-0.0159	-0.0163

Correlation matrix

I. Context and state of the art

II. Detection method and calibration

III. Study of $\boldsymbol{\gamma}$-background

IV. Measurement of specific activity

IV. Conclusion and prospects

Activity measurement : peak by peak

Activity calculated from :

$$A^{G4}_{peak}\left({}^{A}_{Z}X\right) = \frac{a_k \times N^{G4}_{peak}}{T_{RUN} \times I_\gamma \times \epsilon_{G4}}$$

Where $a_k \times N^{G4}_{peak} \rightarrow N^{exp}_{peak}$ and with :

- $a_k = \frac{EXP}{SIM}$: linear coefficient
- N^{G4}_{peak} : number of events in the peak
- T_{RUN} : acquisition time
- I_γ : intensity of the peak
- ϵ_{G4} : total efficiency at peak energy

Activity measurement : peak by peak

Activity calculated from :

$$A^{G4}_{peak}\left({}^{A}_{Z}X\right) = \frac{a_k \times N^{G4}_{peak}}{T_{RUN} \times I_\gamma \times \epsilon_{G4}}$$

Where $a_k \times N^{G4}_{peak} \rightarrow N^{exp}_{peak}$ and with :

- $a_k = \frac{EXP}{SIM}$: linear coefficient
- N^{G4}_{peak} : number of events in the peak
- T_{RUN} : acquisition time
- I_γ : intensity of the peak
- ϵ_{G4} : total efficiency at peak energy

Efficiency obtained only with GEANT4 : generation of **mono-energetic** peaks

Activity measurement : peak by peak

Activity calculated from :

$$A^{G4}_{peak}\left({}^{A}_{Z}X\right) = \frac{a_k \times N^{G4}_{peak}}{T_{RUN} \times I_\gamma \times \epsilon_{G4}}$$

Where $a_k \times N^{G4}_{peak} \rightarrow N^{exp}_{peak}$ and with :

- $a_k = \frac{EXP}{SIM}$: linear coefficient
- N^{G4}_{peak} : number of events in the peak
- T_{RUN} : acquisition time
- I_γ : intensity of the peak
- ϵ_{G4} : total efficiency at peak energy

Efficiency obtained only with GEANT4 : generation of **mono-energetic** peaks

Total efficiency calculated from :

$$\epsilon_{G4}(E) = \frac{N_{peak}(E)}{N_{gen}}$$

- $N_{peak}(E)$: peak area at energy E
- N_{gen} : number of single-energy photons generated

Energy efficiency: GEANT4

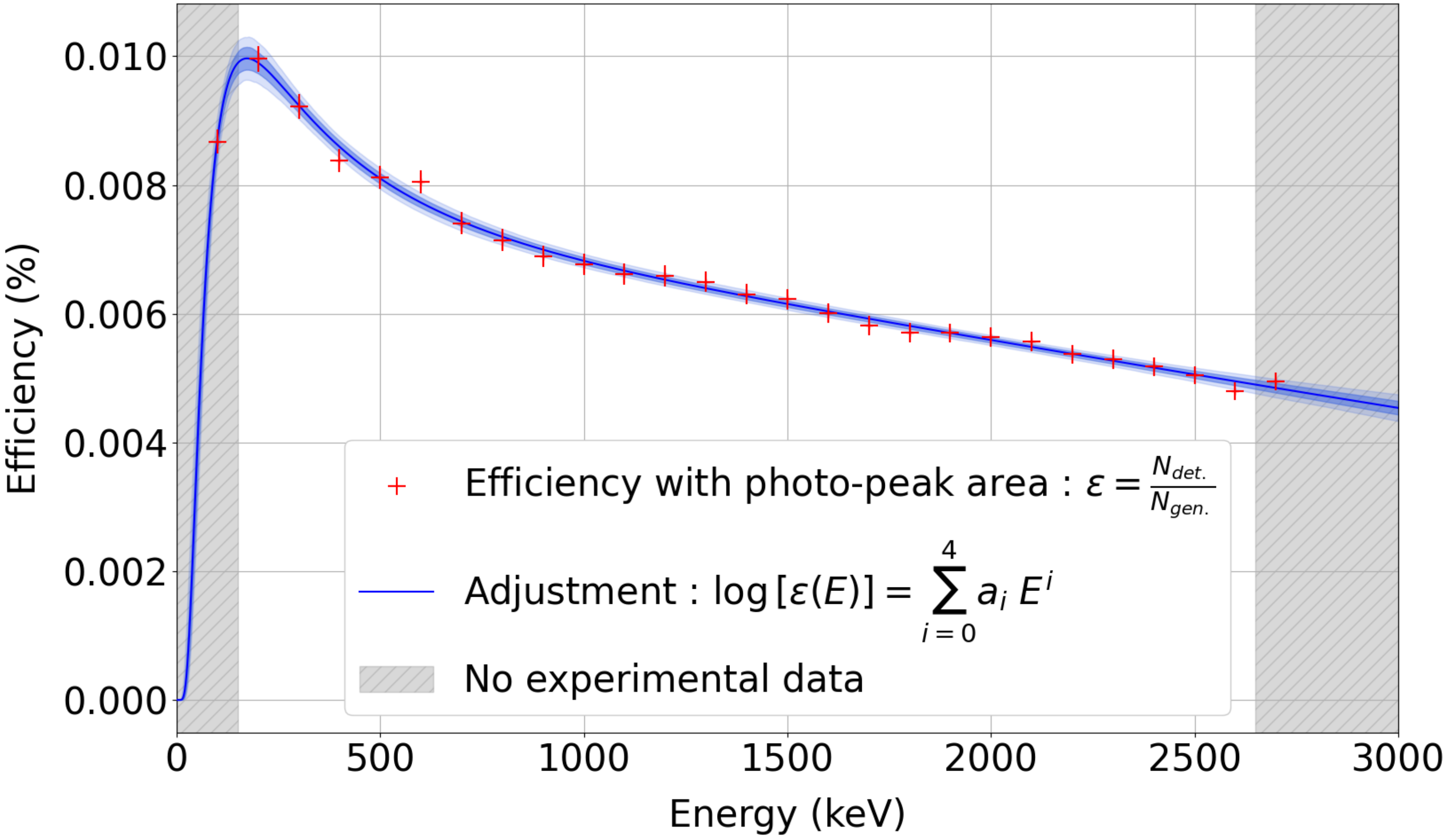

Energy efficiency with GEANT4 simulations for polyethylene shielding

Total efficiency calculated from :

$$\epsilon_{G4}(E) = \frac{N_{peak}(E)}{N_{gen}}$$

- $N_{peak}(E)$: peak area at energy E
- N_{gen} : number of single-energy photons generated

Polynomial fit in log-log space :

$$\log[\epsilon(E)] = \sum_{i=0}^{4} (a_i \, E^i)$$

Energy efficiency: GEANT4

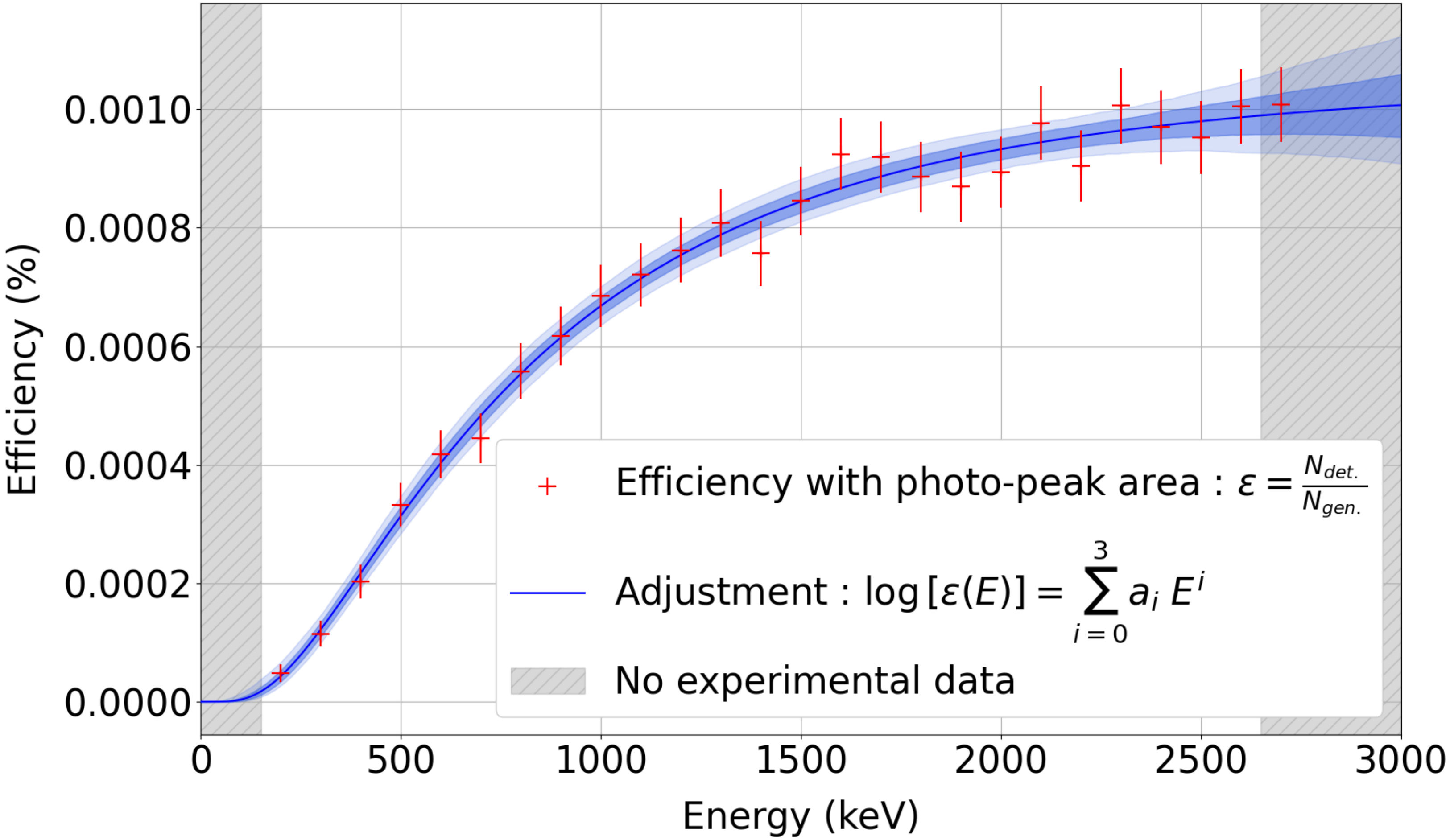

Energy efficiency with GEANT4 simulations for lead shielding

Total efficiency calculated from :

$$\epsilon_{G4}(E) = \frac{N_{peak}(E)}{N_{gen}}$$

- $N_{peak}(E)$: peak area at energy E
- N_{gen} : number of single-energy photons generated

Polynomial fit in log-log space :

$$\log[\epsilon(E)] = \sum_{i=0}^{3} (a_i E^i)$$

Activity measurement : equilibrium

Chains in secular equilibrium with GEANT4 :

$$\Rightarrow \mathrm{A}^{\mathrm{G4}}_{eq.}\left({}^{A}_{Z}Y\right) = \frac{a_k \times \mathrm{N_{gen}}}{\mathrm{T_{RUN}}}$$ with :

- $a_k = \frac{EXP}{SIM}$: linear coefficient
- $\mathrm{N_{gen}}$: total number of particles generated
- $\mathrm{T_{RUN}}$: acquisition time

➢ Independent of isotope ⇔ **same activity for the entire chain !**

Polyethylene

- $A_{PE}^{eq}({}^{232}Th) = (1.62 \pm 0.06) \times 10^2\ mBq/kg$
- $A_{PE}^{eq}({}^{238}U) = (1.38 \pm 0.06) \times 10^2\ mBq/kg$
- $A_{PE}^{eq}({}^{40}K) = (5.44 \pm 0.73) \times 10^2\ mBq/kg$
- $A_{PE}^{eq}({}^{235}U) = (1.29 \pm 0.05) \times 10^2\ mBq/kg$

Lead

- $A_{Pb}^{eq}({}^{232}Th) = (7.18 \pm 0.97) \times 10^2\ mBq/kg$
- $A_{Pb}^{eq}({}^{238}U) = (1.02 \pm 0.12) \times 10^3\ mBq/kg$
- $A_{Pb}^{eq}({}^{40}K) = (1.56 \pm 0.10) \times 10^4\ mBq/kg$
- $A_{Pb}^{eq}({}^{235}U) = (8.80 \pm 5.02) \times 10^2\ mBq/kg$
- $A_{Pb}^{eq}({}^{60}Co) = (6.56 \pm 0.28) \times 10^1\ mBq/kg$

Activity measurement : peak by peak

Activity peak by peak with GEANT4 :

- $A^{G4}_{peak}\left({}^{A}_{Z}X\right) = \frac{a_k \times N^{G4}_{peak}}{T_{RUN} \times I_\gamma \times \epsilon_{G4}}$

Activity at equilibrium with GEANT4 :

- $A^{G4}_{eq.}\left({}^{A}_{Z}Y\right) = \frac{a_k \times N_{gen}}{T_{RUN}}$

Activity measured at the LSM :

- Carried out on PE and **Pb** samples from the Ricochet shoring prior to this study

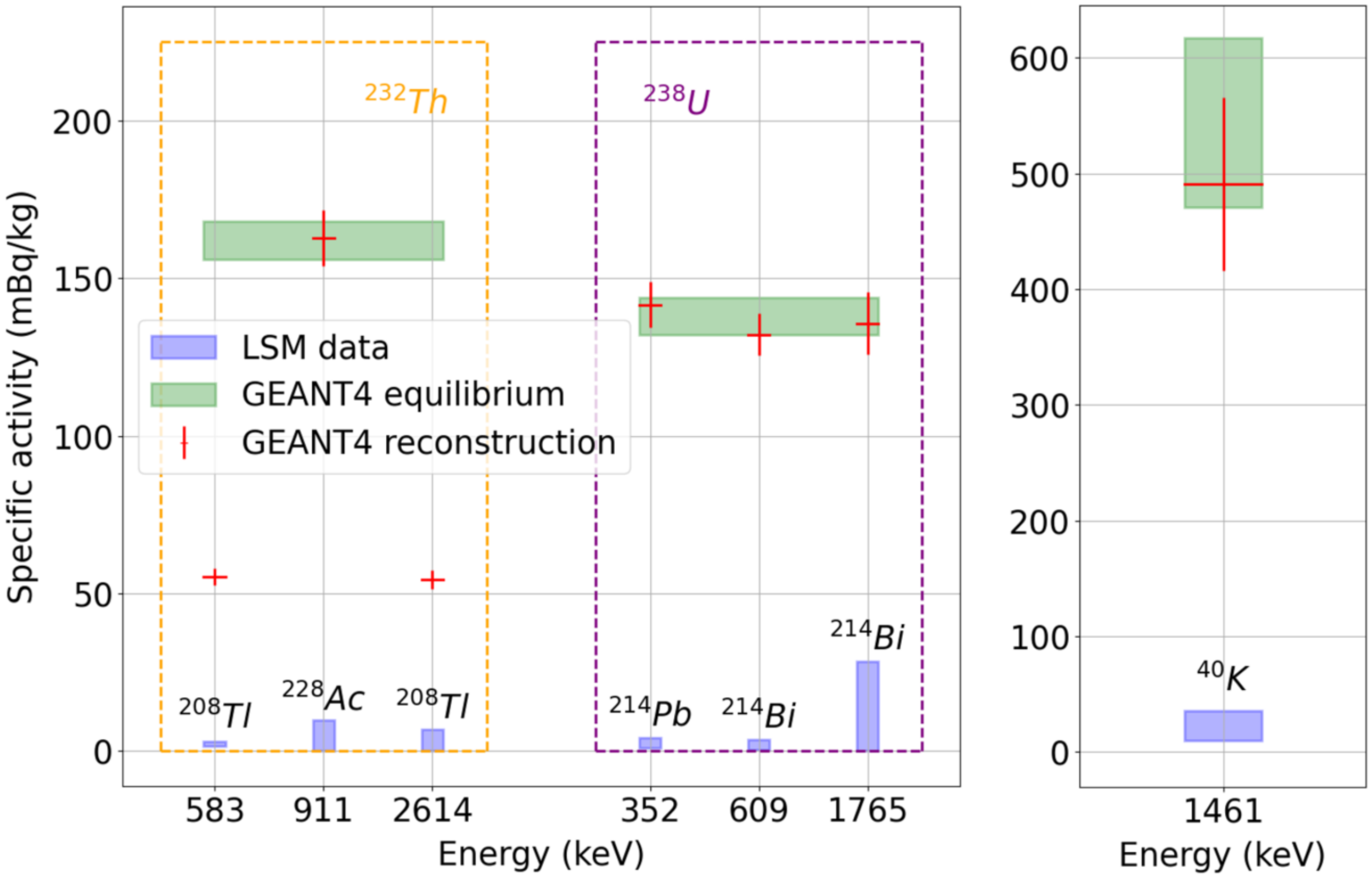

Specific activity for each chains and comparison with LSM data for PE contamination

Activity measurement : peak by peak

Activity peak by peak with GEANT4 :

➢ $$A^{G4}_{peak}\left({}^{A}_{Z}X\right) = \frac{a_k \times N^{G4}_{peak}}{T_{RUN} \times I_{\gamma} \times \epsilon_{G4}}$$

Activity at equilibrium with GEANT4 :

➢ $$A^{G4}_{eq.}\left({}^{A}_{Z}Y\right) = \frac{a_k \times N_{gen}}{T_{RUN}}$$

Activity measured at the LSM :

➢ Carried out on PE and **Pb** samples from the Ricochet shoring prior to this study

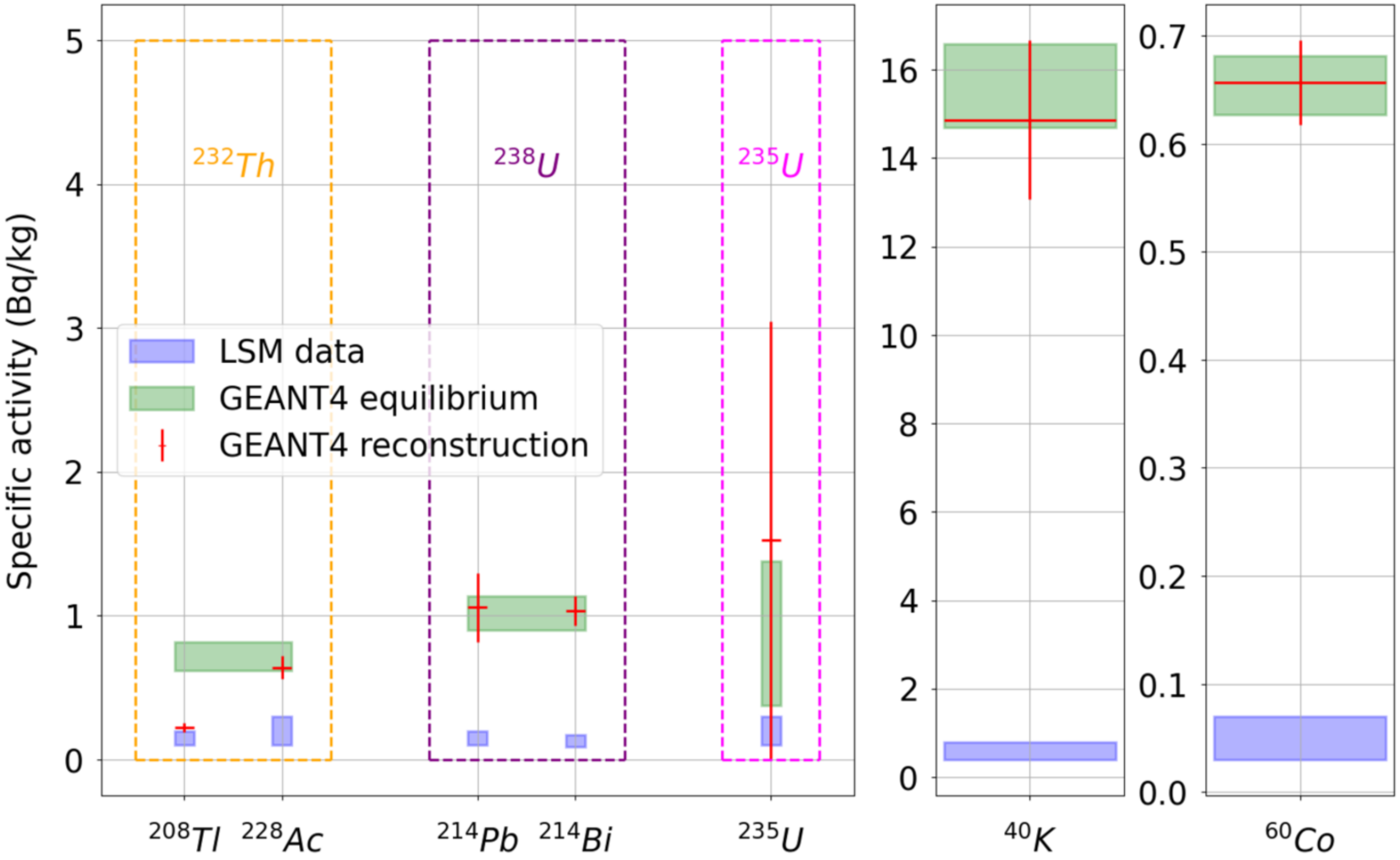

Specific activity for each chains and comparison with LSM data for Pb contamination

Sources of external contamination

Comparison of photoelectric peak areas as a function of energy

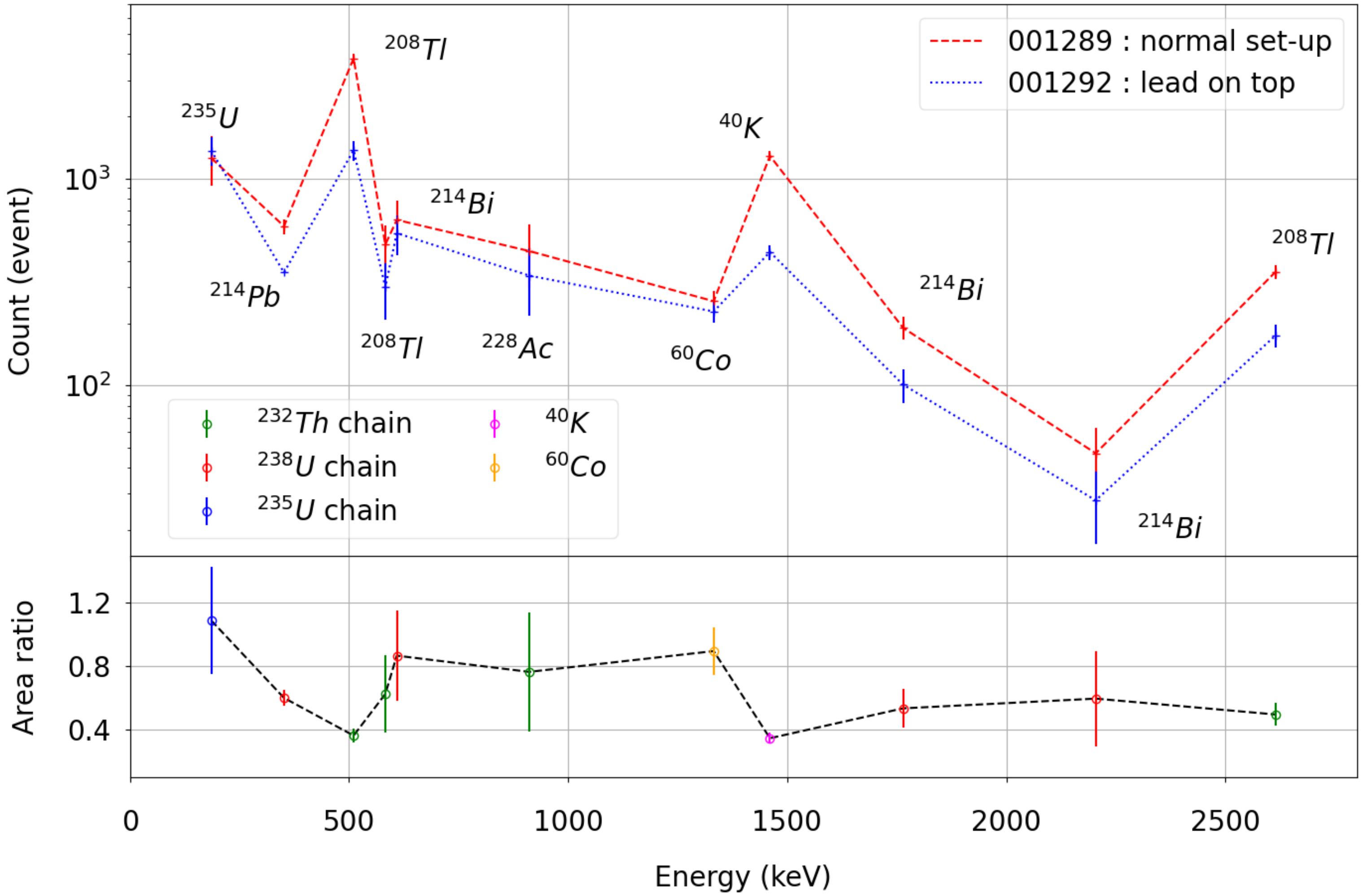

1. Contamination of aluminum parts (supports, cover, etc.)
   - ➢ no significant improvement

Sources of external contamination

Comparison of photoelectric peak areas as a function of energy

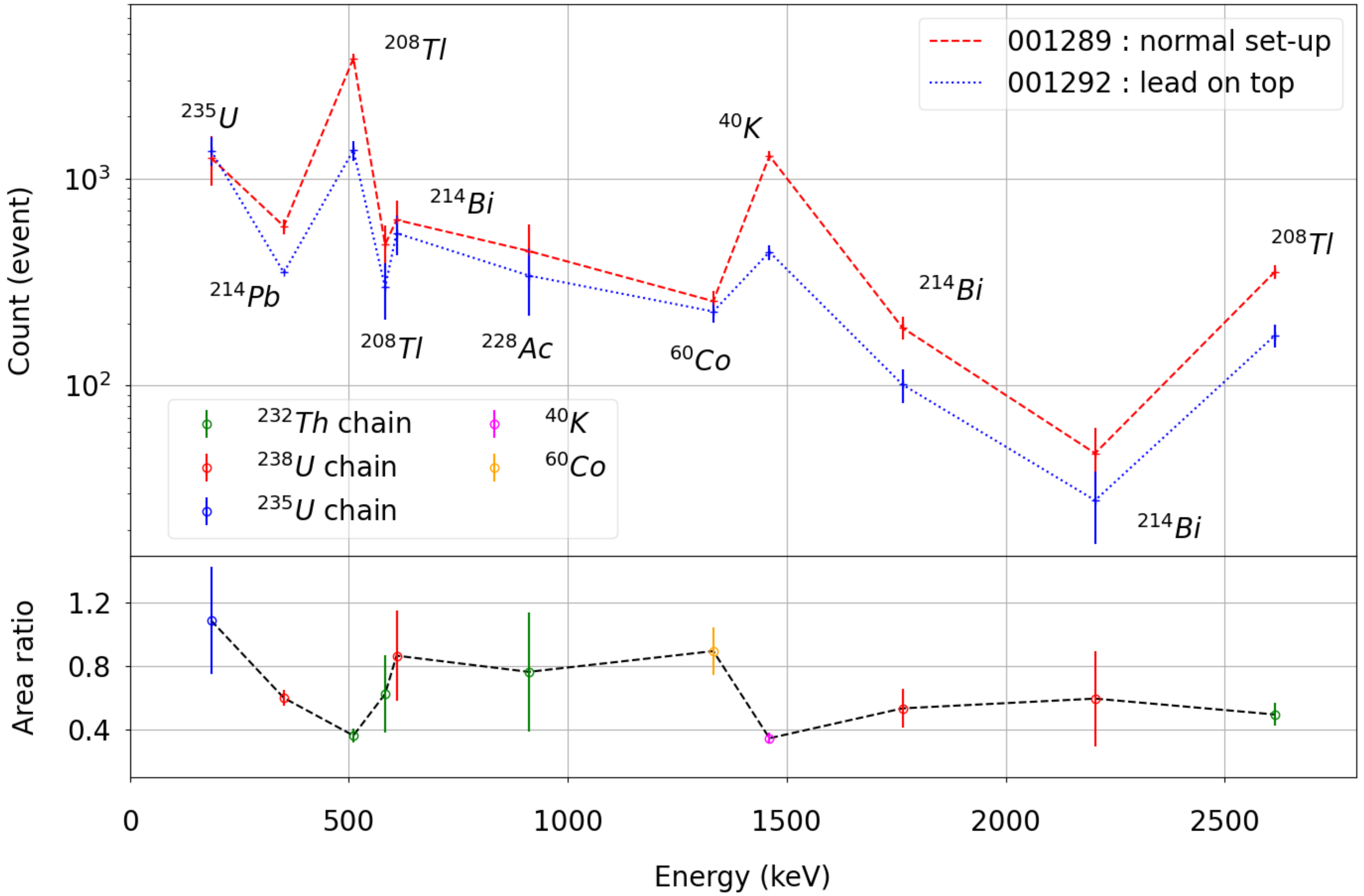

1. Contamination of aluminum parts (supports, cover, etc.)
   - ➢ no significant improvement
2. Contamination by ^{40}K of the detector surface by perspiration
   - ➢ upcoming study

Sources of external contamination

Comparison of photoelectric peak areas as a function of energy

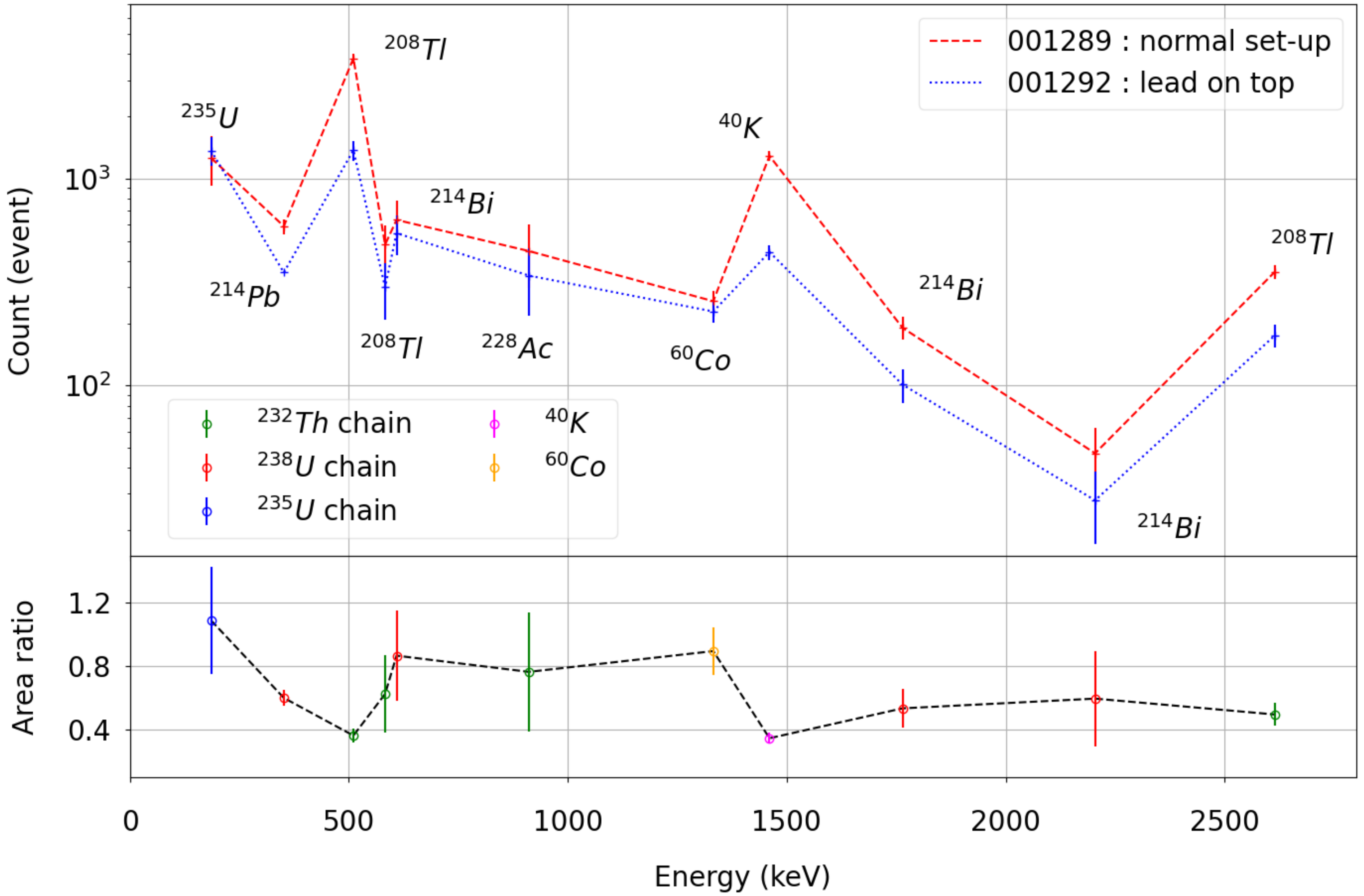

1. Contamination of aluminum parts (supports, cover, etc.)
   - ➢ no significant improvement
2. Contamination by ^{40}K of the detector surface by perspiration
   - ➢ upcoming study
3. Contribution from the ILL transfer canal
   - ➢ HPGe acquisition comparison
   - ➢ significant part comes from channel : from **11%** to **65%**
   - ➢ need to improve simulation

Sources of external contamination

Comparison of photoelectric peak areas as a function of energy

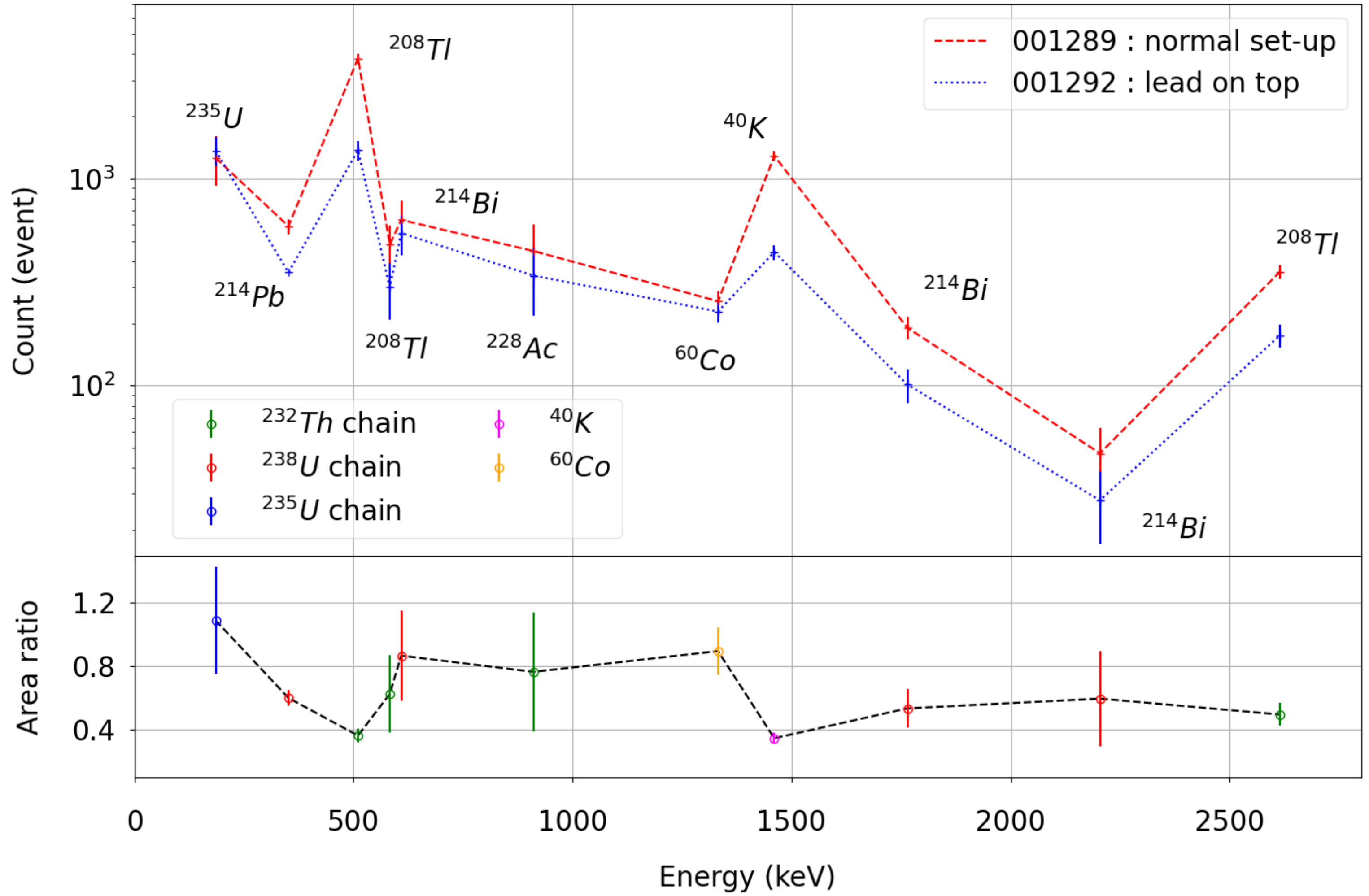

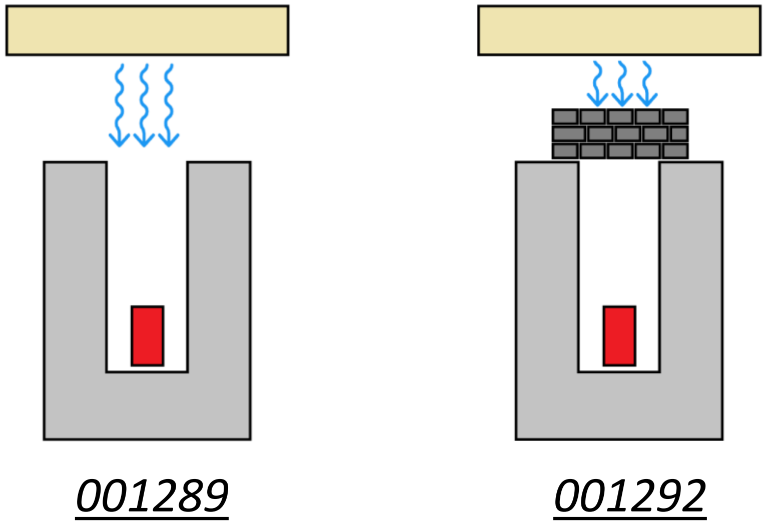

3. Contribution from the ILL transfer canal
   - HPGe acquisition comparison
   - significant part comes from channel : from **11%** to **65%**
   - need to improve simulation

I. Context and state of the art

II. Detection method and calibration

III. Study of γ-background

IV. Measurement of specific activity

IV. Conclusion and prospects

Conclusion of the study

Objective : to combine simulated spectra to reproduce the experimental background spectrum and the LSM measure of activity

Conclusion : radiogenic background from shielding is not dominant, it comes from external sources (Al, slab, etc.)

Preliminary result : adjustment needs improvement to reproduce experimental data. Too many free parameters ?

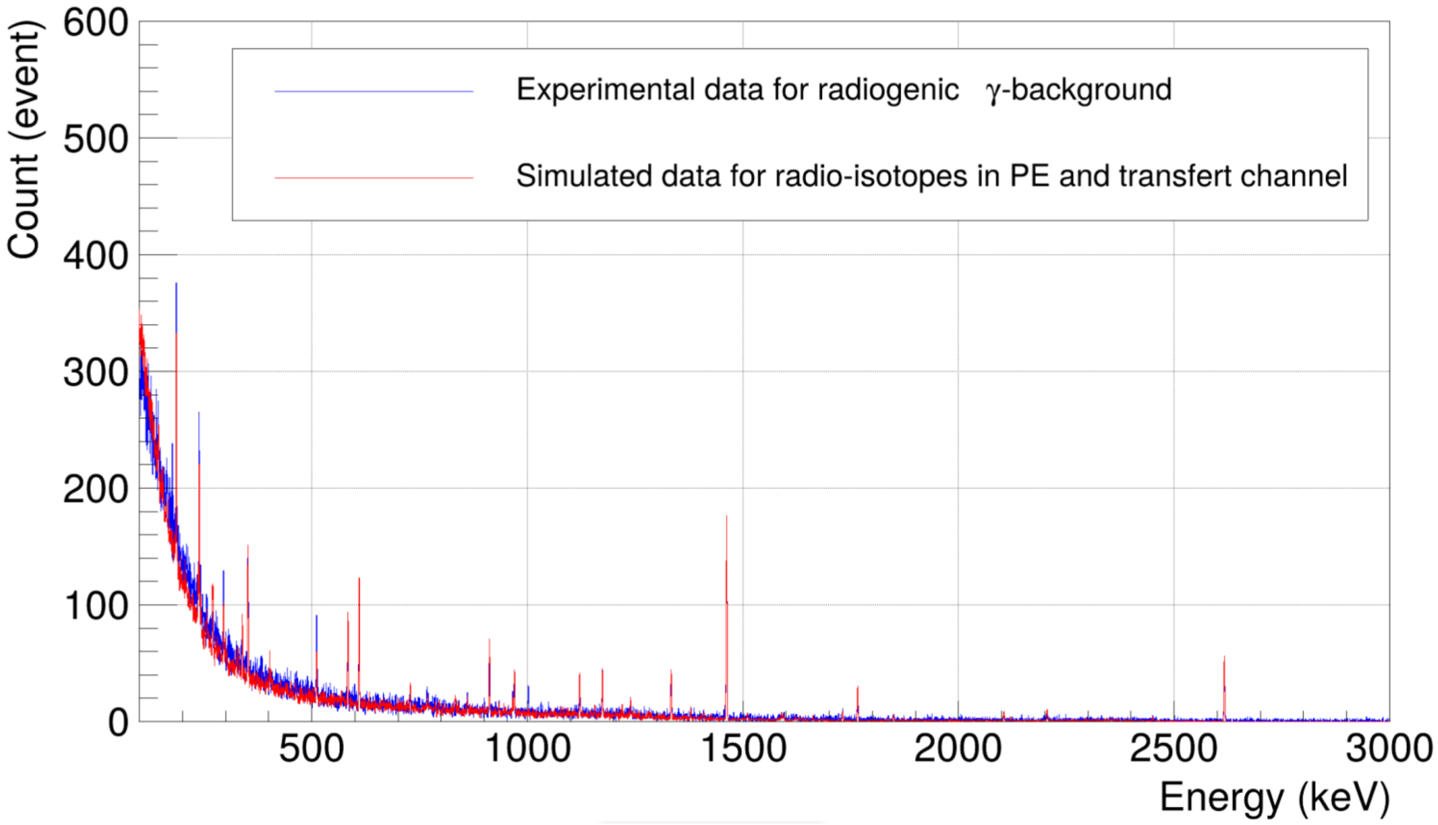

Reconstruction of the radiogenic background spectrum adding the contribution of the ILL transfer channel

Outlook : reactogenic & neutron

Works also completed :

- study of reactogenic background (^{41}Ar)
- GEANT4 environment modifications
- Study of Ricochet bolometer data (RUN013 & RUN014)
- Shift for data acquisition

Outlook :

- Study of reactogenic background outside the shielding with data taking to come
- Analysis of FID nuclear recoil to study neutron background

Comparison of experimental spectra for the OFF and ON reactor

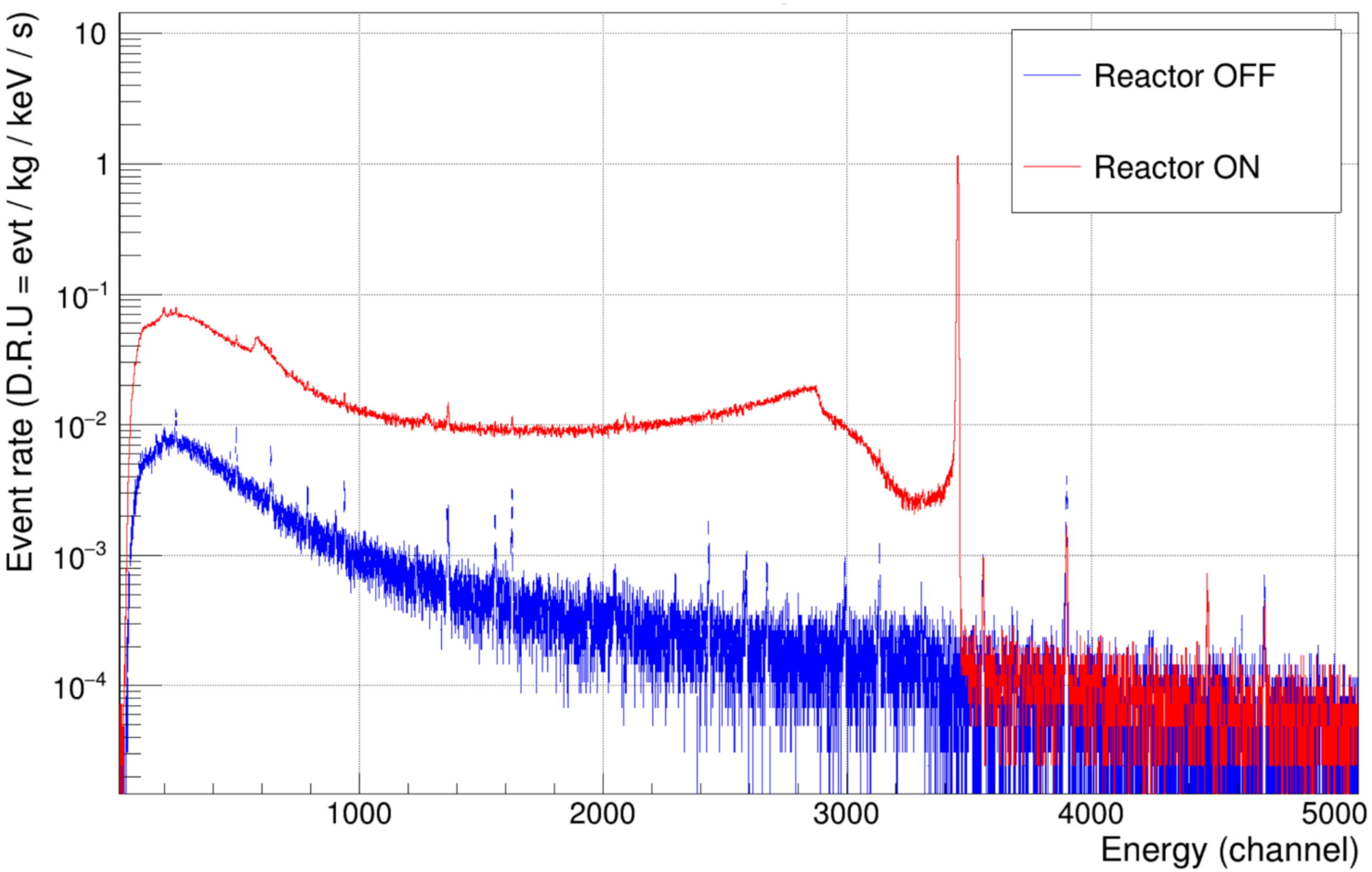

Outlook : reactogenic & neutron

Works also completed :

- study of reactogenic background (^{41}Ar)
- GEANT4 environment modifications
- Study of Ricochet bolometer data (RUN013 & RUN014)
- Shift for data acquisition

Outlook :

- Study of reactogenic background outside the shielding with data taking to come
- Analysis of FID nuclear recoil to study neutron background

RUN014 experimental spectrum for ON reactor and one bolometer

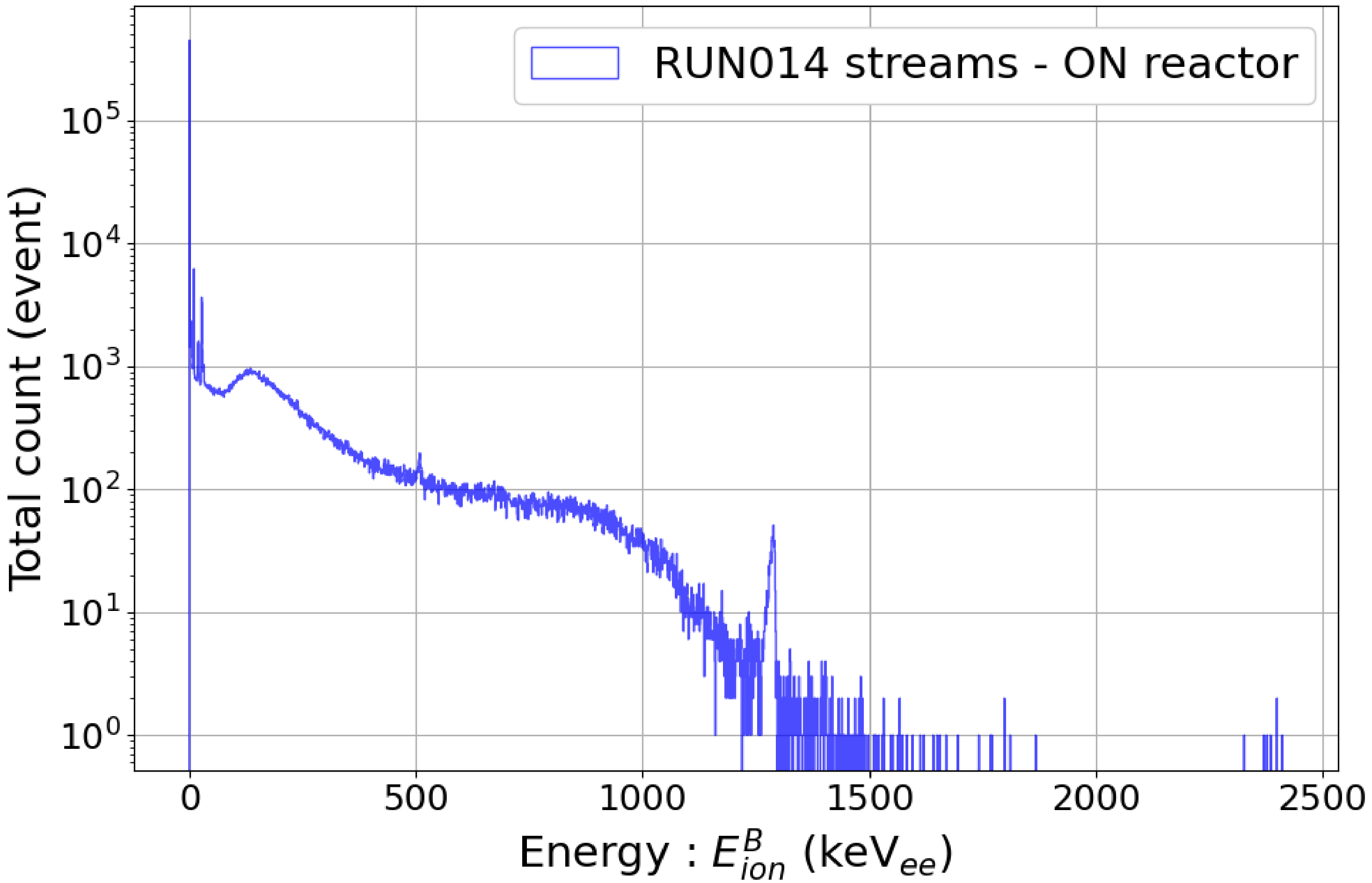

Thank you for your attention!

Back-up

Physical process : CEνNS

[EPL, 143 (2023) 34001, M. Cadeddu & al.]

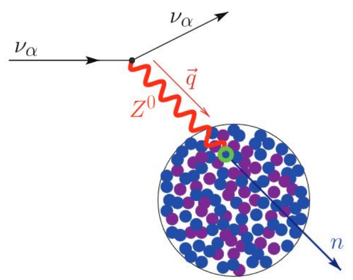

Inelastic and incoherent :

$\lambda_{Z_0} \ll 2R$

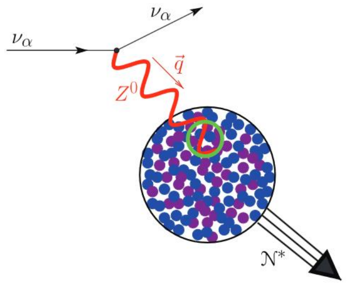

Elastic and incoherent:

$\lambda_{Z_0} \leq 2R$

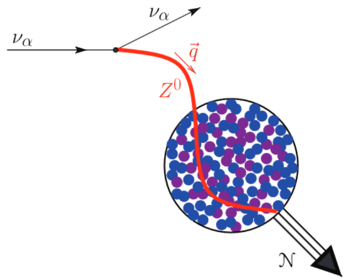

Elastic and coherent :

$\lambda_{Z_0} \geq 2R$

- Technical challenges : very low nuclear recoil
- Ultra-sensitive detectors $\sim 10\ eV$ for Ricochet

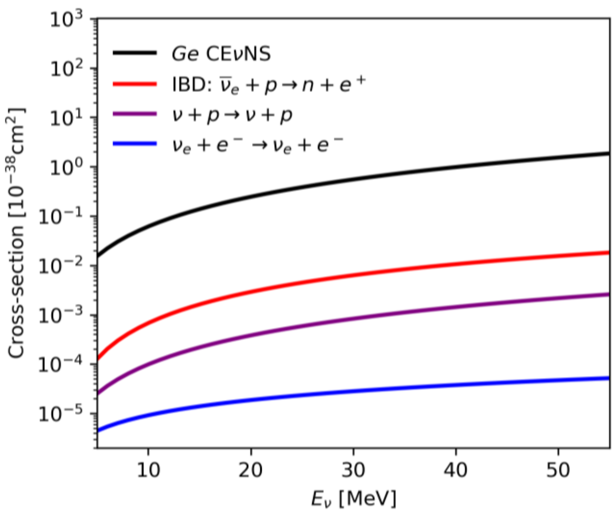

Interactions cross-sections for various processes

Expected interaction rates for the Ricochet experiment

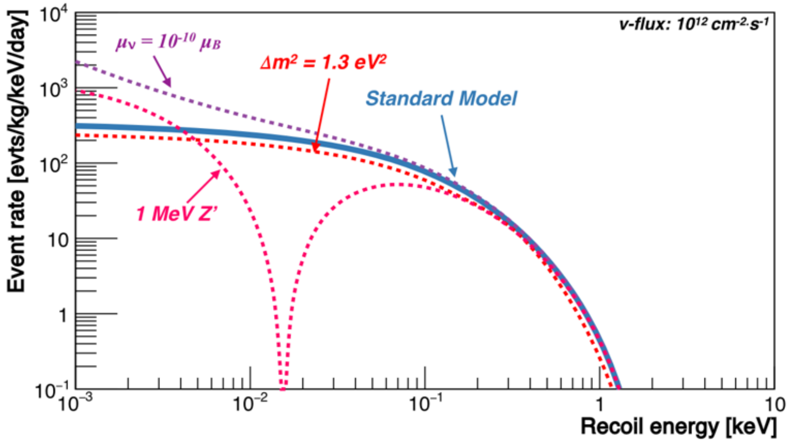

- Non-standard ν-quark interaction
- Neutrino magnetic moment μ_ν
- New mediator boson Z'
- Background for dark matter

[JCAP (2018), J. Billard & al.]

Physical parameter : θ_W

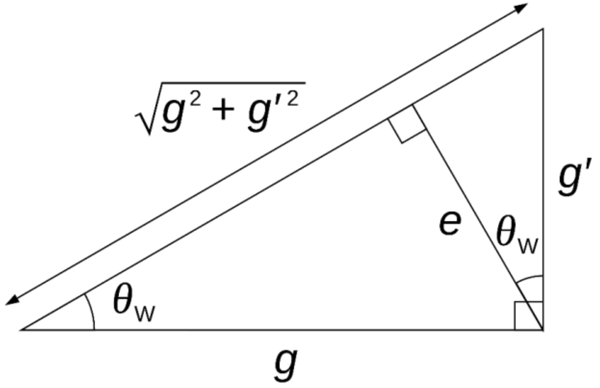

Relationship with coupling constants

$B^\mu, W_3^\mu \rightarrow A^\mu, Z^\mu$

Structure constant :

$$sin^2(\boldsymbol{\theta_W}) = 1 - \left(\frac{M_W}{M_Z}\right)^2$$

Cross section predicted by the Standard Model :

$$\frac{d\sigma_{\nu/N}}{dE_R} = \frac{G_F^2}{4\pi} Q_w^2 \, m_N \left(1 - \frac{m_N \, E_R}{2 \, E_\nu^2}\right) F^2(E_R)$$

With : $Q_w = N - (1 - 4\,\mathbf{sin^2}\,\boldsymbol{\theta_W})\,Z$

Unification of the electromagnetic force and the weak interaction :

- Represents the rotation caused by spontaneous symmetry breaking
- Proportion of weak and electromagnetic interactions in particle interactions

E_R : recoil energy

E_ν : neutrino energy

G_F : Fermi's constant

m_N : nucleus mass

$F(E_R)$: form facteur

Q_w : nucleus weak charge

N : number of neutrons

Z : number of protons

$\boldsymbol{\theta_W}$: weak mixing angle

Beyond the Standard Model

Standard Model prediction :

$$\frac{d\sigma_{SM}}{dE_R} = \frac{G_F^2}{4\pi} Q_w^2\, m_N \left(1 - \frac{m_N\, E_R}{2\, E_\nu^2}\right) F^2(E_R)$$

Non-zero magnetic moment :

$$\frac{d\sigma_\mu}{dE_R} = \frac{\pi\, \alpha^2\, \mu_\nu^2\, Z^2}{m_e} \left(\frac{1}{E_R} - \frac{1}{E_\nu} + \frac{E_R}{4E_\nu^2}\right) F^2(E_R)$$

Scalar boson :

$$\frac{d\sigma_S}{dE_R} = \frac{Q_S^2}{4\pi} \frac{m_N^2\, E_R}{E_\nu^2\, (q^2 + m_S^2)^2} F^2(E_R) \qquad Q_S = g_{\nu,S}\, g_{q,S}\, (15.1\, Z + 14\, N)$$

Tensor boson :

$$\frac{d\sigma_T}{dE_R} = \frac{Q_T^2}{2\pi} \frac{m_N\, (4\, E_\nu^2 - m_N\, E_R)}{E_\nu^2\, (q^2 + m_T^2)^2} F^2(E_R) \qquad Q_T = g_{\nu,T}\, g_{q,T}\, (0.85\, Z + 0{,}08\, N)$$

Vector boson :

$$\frac{d\sigma_V}{dE_R} \propto \frac{d\sigma_{SM}}{dE_R} \qquad Q_W \rightarrow Q_{tot} = Q_W - \frac{\sqrt{2}}{G_F\, q^2} \frac{g_{\nu,V} \left[Z\, (2\, g_{u,V} + g_{d,V}) + N\, (g_{u,V} + 2\, g_{d,V}) \right]}{q^2 + m_V^2}$$

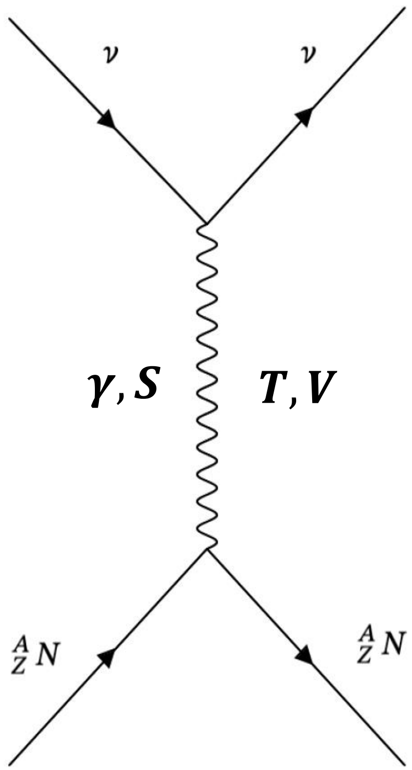

ILL neutrino spectrum

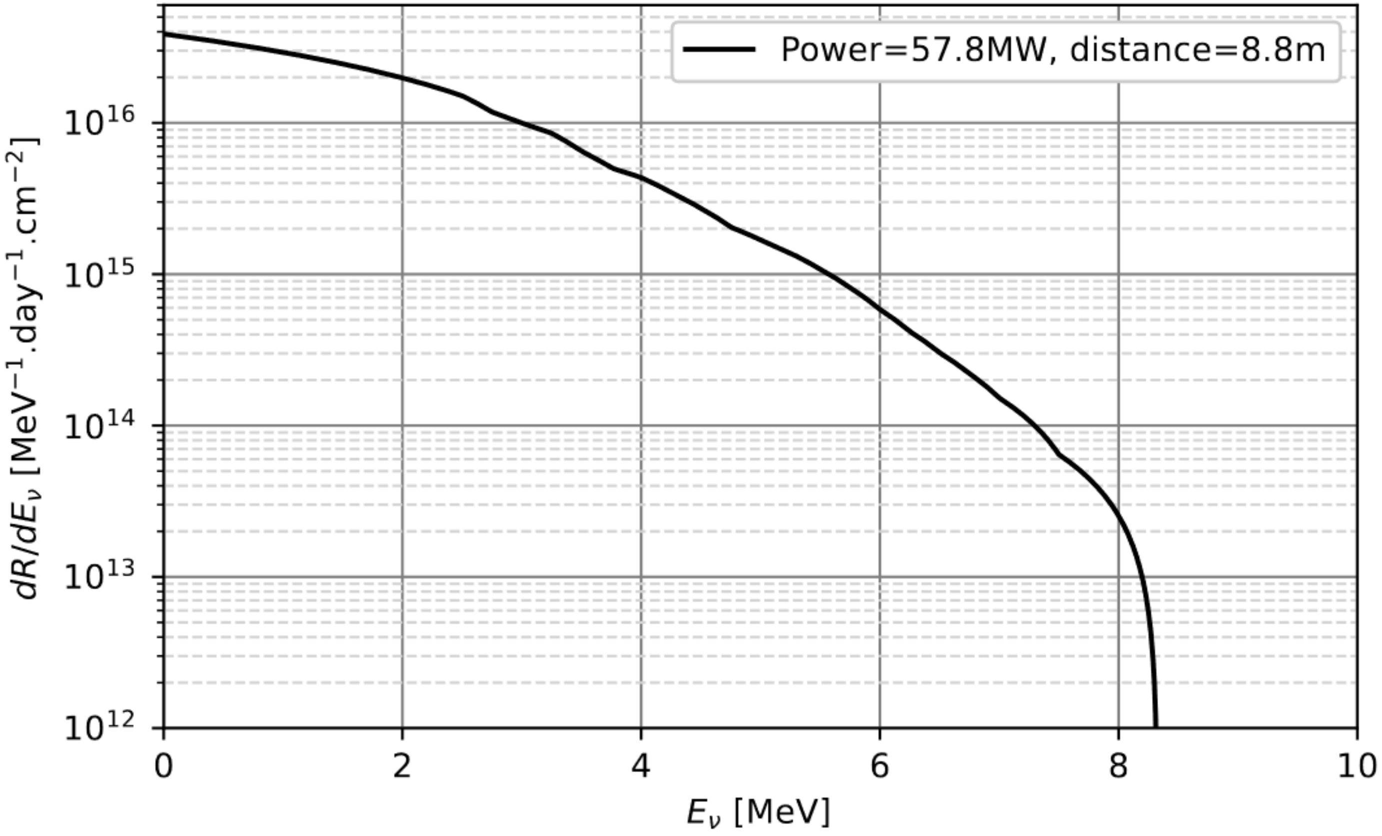

Spectrum of electric anti-neutrinos from the ILL reactor measured by the STEREO experiment

- Reactor with **58 MWth**
- ➢ $E_\nu < 10\ MeV$
- only **8.8 m** to the reactor
- ➢ $\sigma_\nu \sim 10^{12}\ cm^{-2}.s^{-1}$

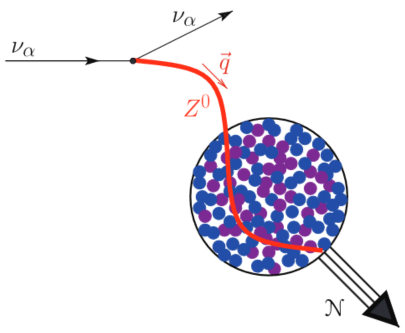

Elastic and coherent :

$\lambda_{Z_0} \geq 2R$

The Ricochet experience at ILL

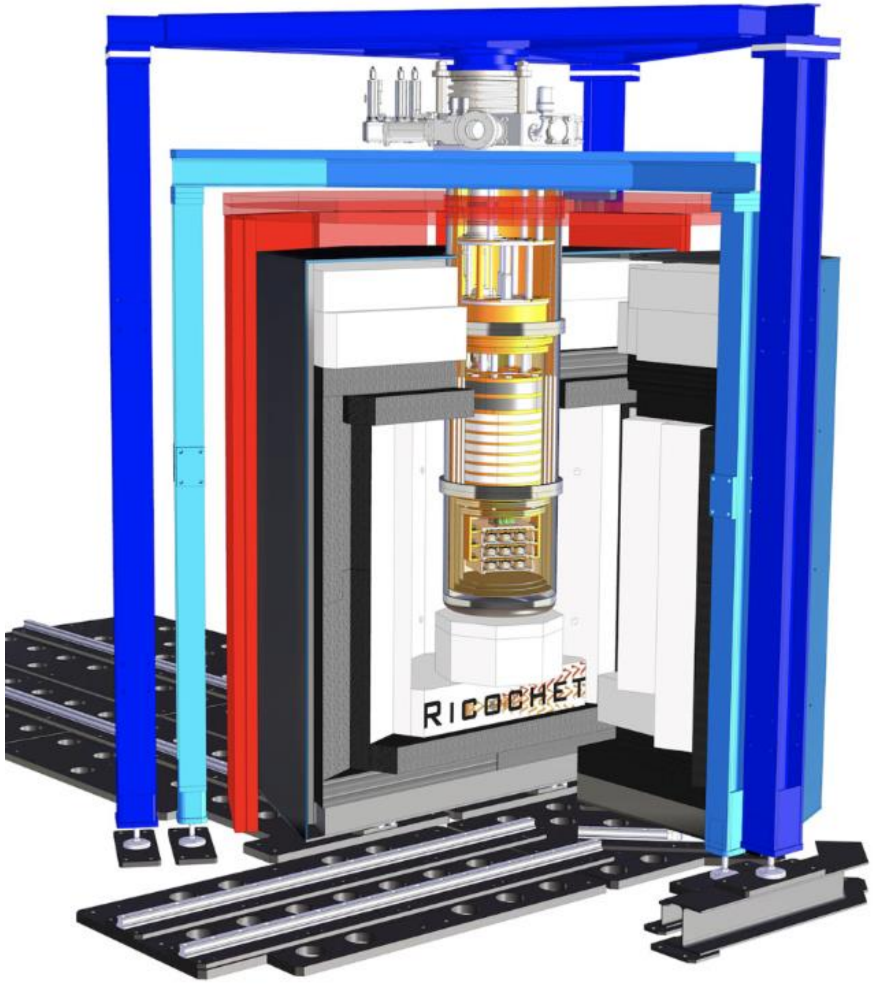

Diagram of Ricochet's shielding and cryostat

[EPJC 83:20 (2023) , Ricochet collaboration]

- International collaboration begins in 2019
- Rare events experiment : ~ **10 DRU**
- Installed at ILL with data acquisition in progress

- Aims to detect $\mathbf{CE\nu NS}$ at low-energy
- 18 germanium **cryogenic calorimeters** : ~ 1 kg at 10 mK
- **Ionization** and **heat** signals : **NR/ER** discrimination

List of detectors

- Neutron detection $\begin{cases} {}^{3}_{2}He \\ H_2 \end{cases}$

- Gamma detection $\begin{cases} \boldsymbol{HPGe} \\ NaI \end{cases}$

- Detectors **inside** & outside shielding

- On and **OFF** reactor periods

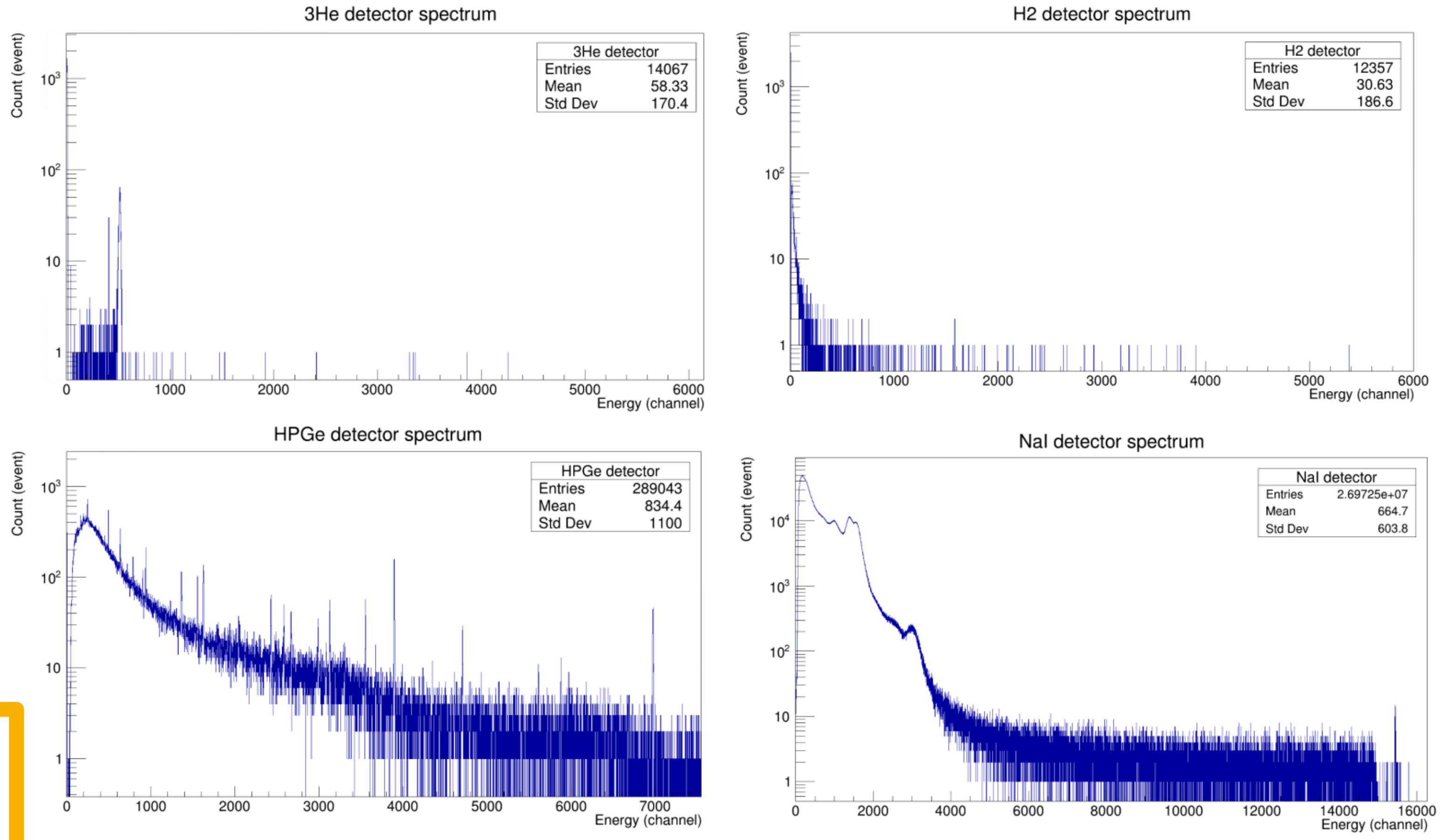

Spectra of the different detectors in the case of OFF reactor (001193)

HPGe detector acquisition

- ILL reactor **OFF** period
- Known $^{152}\boldsymbol{Eu}$ source
- Activity : $\boldsymbol{A} = \mathbf{5,3} \times \mathbf{10^4}\ \boldsymbol{Bq}$
- 4 acquisitions / dispositions

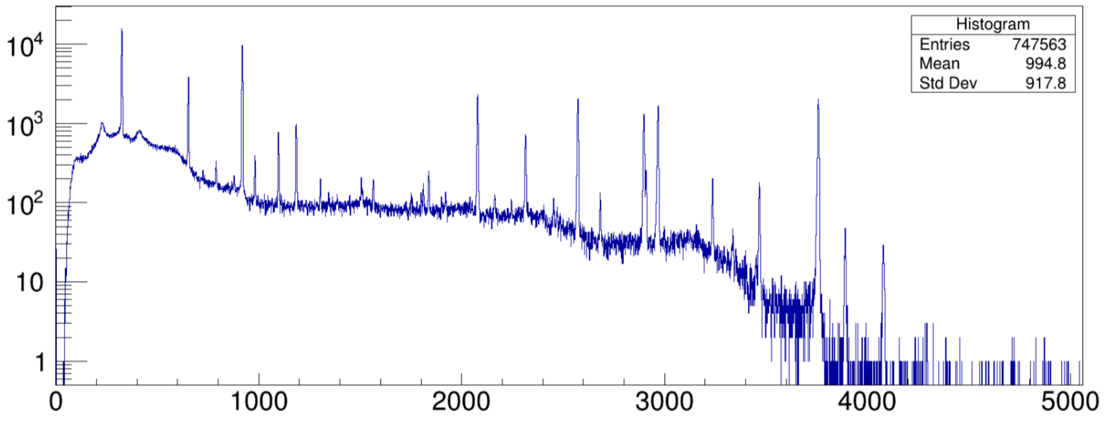

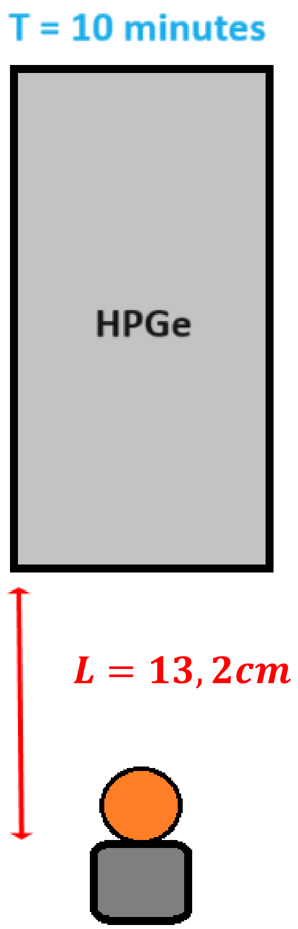

- **Cubix** → ROOT based graphical interface providing a large number of tools for gamma-ray spectroscopy analysis
- Developed by Jérémie Dudouet (IP2I Lyon, CNRS/IN2P3)

Configurations and spectrum

Spectrum analysis with Cubix

- **Cubix** → ROOT based graphical interface providing a large number of tools for gamma-ray spectroscopy analysis
- Developed by Jérémie Dudouet (IP2I Lyon, CNRS/IN2P3)

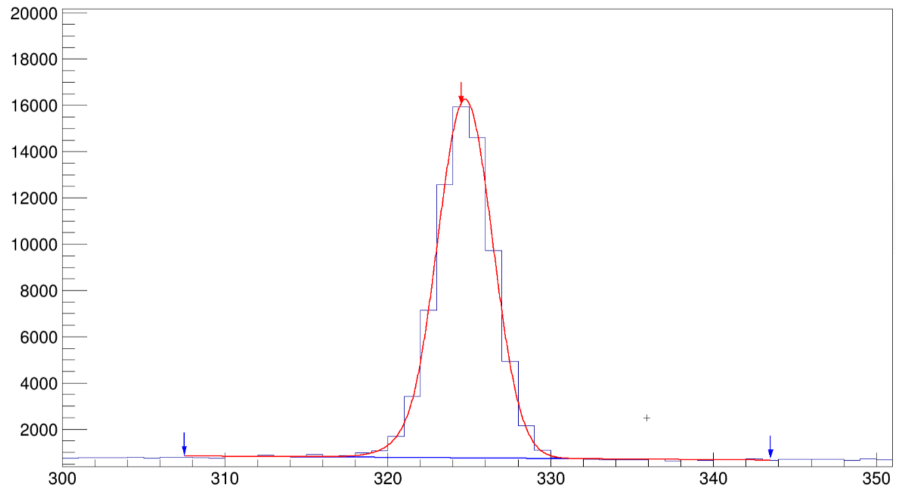

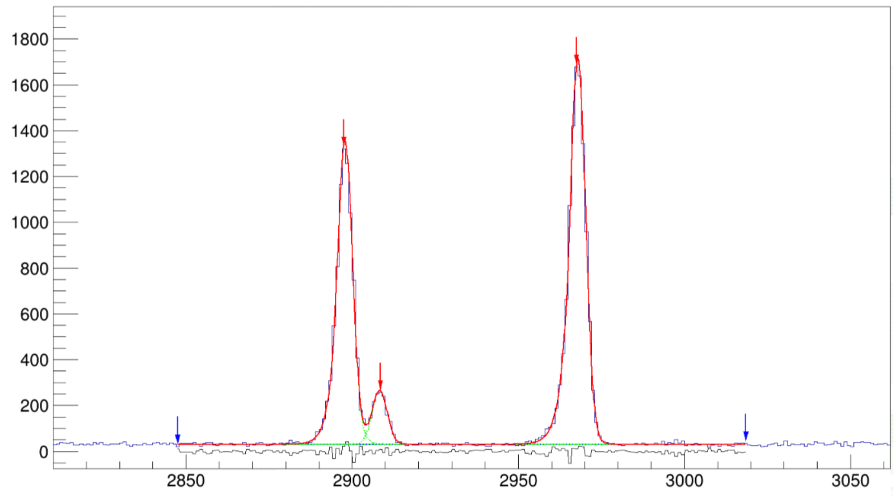

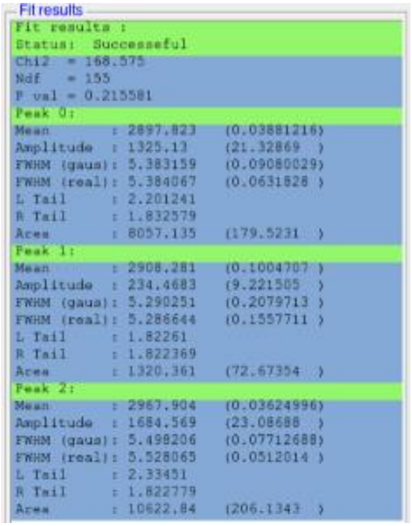

Cubix usage examples for single and double photoelectric peaks

Source decay channels

β^- decay :

$$^{152}_{63}Eu \rightarrow \, ^{152}_{64}Gd + \, ^{0}_{1}e^- + \, ^{0}_{0}\overline{\nu_e}$$

- β^- channel in $27{,}92\%$ of cases
- 6 single peaks, 3 double peaks and 2 triple peaks ⇒ 11 identified peaks

ϵ decay :

$$^{152}_{63}Eu + \, ^{0}_{1}e^- \rightarrow \, ^{152}_{62}Sm + \, ^{0}_{0}\nu_e$$

- ϵ channel in $72{,}08\%$ of cases
- 19 single peaks, 3 double peaks and 4 triples peaks ⇒ 26 identified peaks

γ-background subtraction

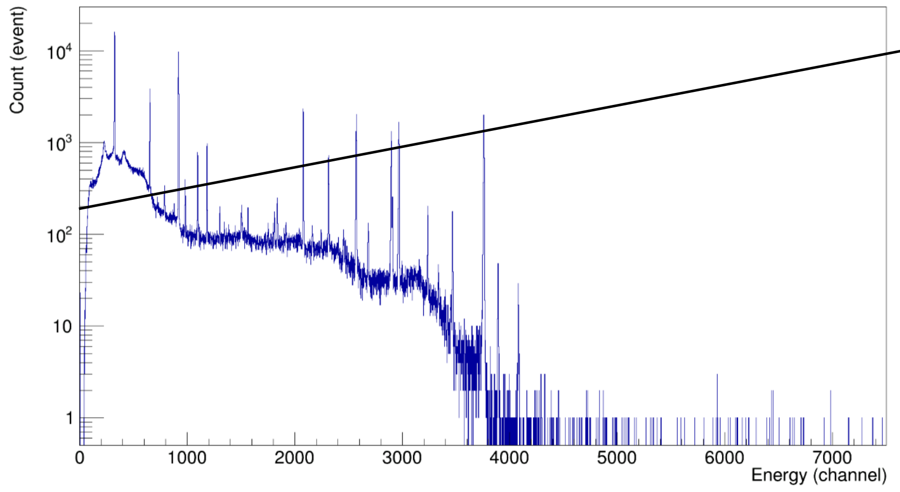

-

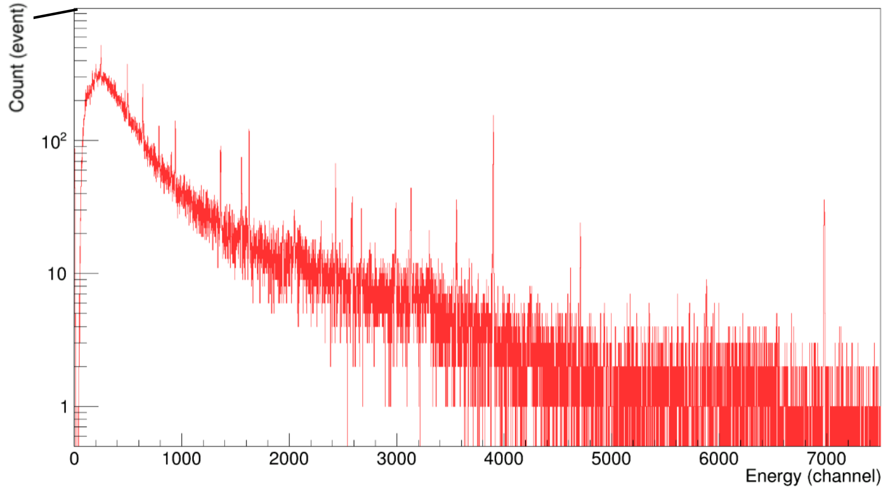

=

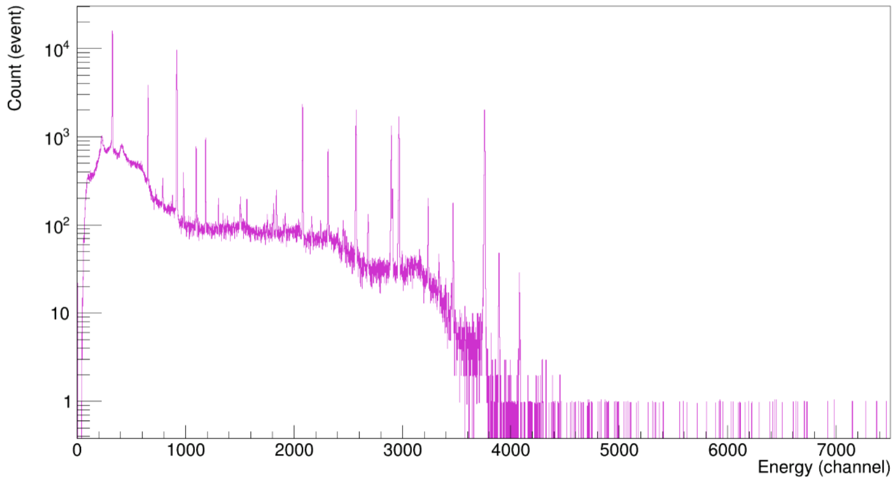

Example of background subtraction for acquisition 1232

- 1232 (blue) → ^{152}Eu source
- 1231 (red) → natural γ-background

➢ Experimental data without background (purple)

Energetic resolution

[G. F. Knoll, Radiation Detection and Measurement : Chapter 12, III.B]

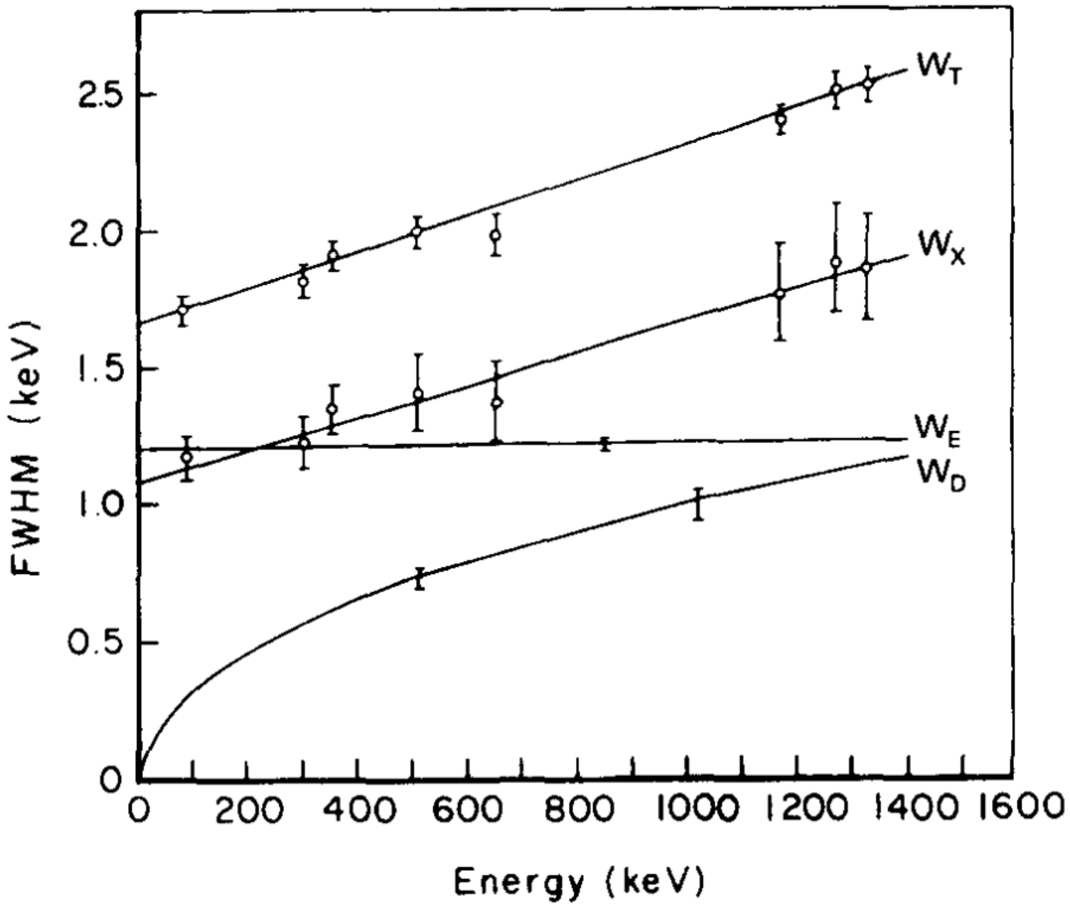

Energetic resolution of a HPGe detector

Energetic resolution = Σ 3 contributions :

- $W_X = aE + b$: incomplete collection of charges
- $W_E = c = cste$: electronic noise
- $W_D = d\sqrt{E}$: statistical fluctuation linked to the number of charge carriers created

Width at half maximum due to detection of a monoenergetic gamma :

$$W_T = \sqrt{W_X^2 + W_D^2 + W_D^2} = \sqrt{\alpha E^2 + \beta E + \gamma}$$

Energy efficiency of detector

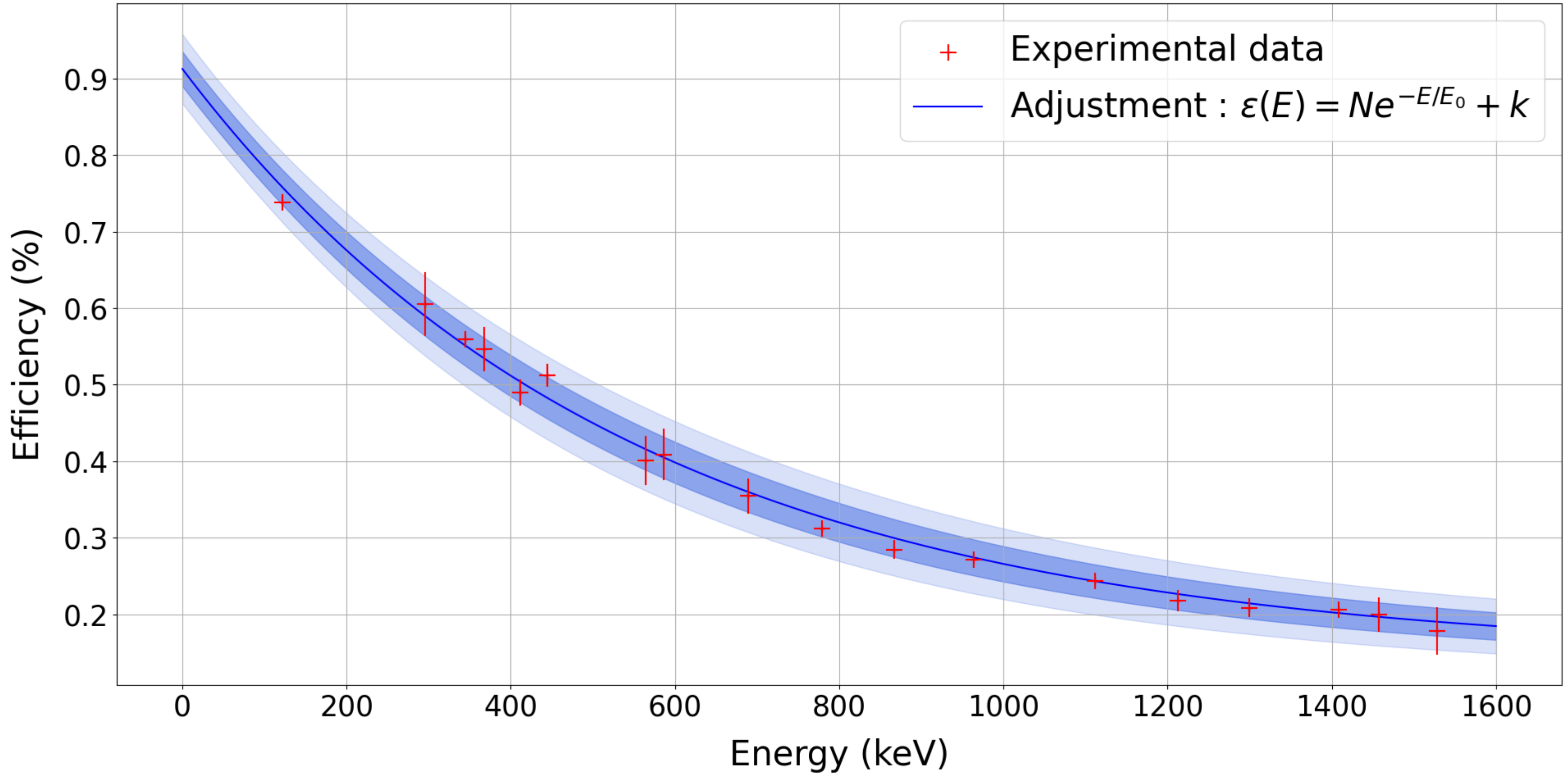

HPGe detector efficiency as a function of energy for the europium source

➢ Corresponds to the expected curve for this type of detector

Experimental efficiency of HPGe detector with the $^{152}_{63}\mathrm{Eu}$ source :

$$\epsilon(E_i) = \frac{N_{pic}(E_i)}{A\left(^{152}_{63}Eu\right) \times T_{exp} \times I_\gamma(E_i)}$$

- E_i : photoelectric peak energy
- $N_{pic}(E_i)$: area of the peak
- $A\left(^{152}_{63}Eu\right)$: source activity
- T_{exp} : acquisition period
- $I_\gamma(E_i)$: intensity of peak

Efficiency for acquisition 1232

- Adjustment $\epsilon = N \times e^{-E/E_0}$
- $\begin{cases} N = (1{,}12 \pm 0{,}03) \times 10^2 \\ E_0 = (9{,}18 \pm 0{,}30) \times 10^2 \ keV \end{cases}$

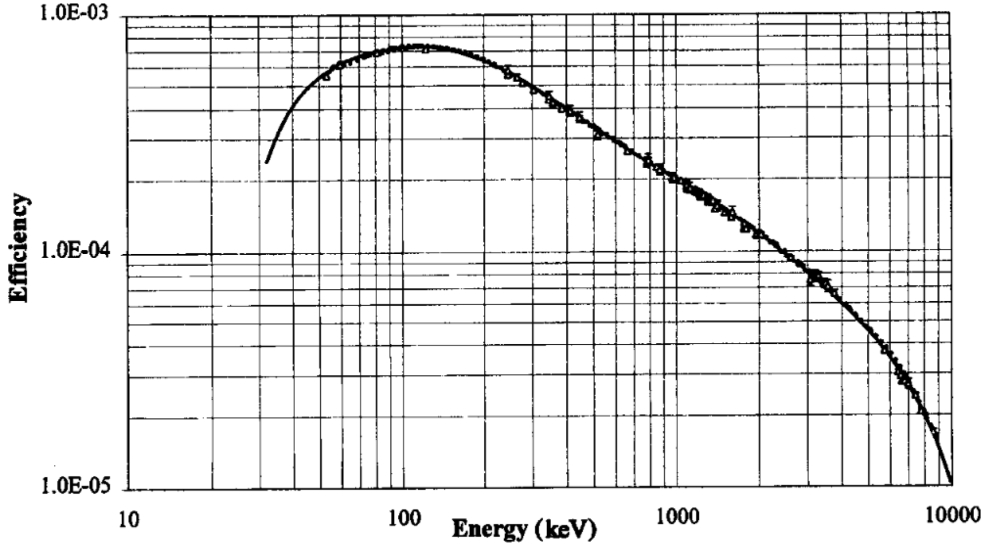

Example of an efficiency curve for an HPGe detector

Relative energy efficiency for acquisition 1232

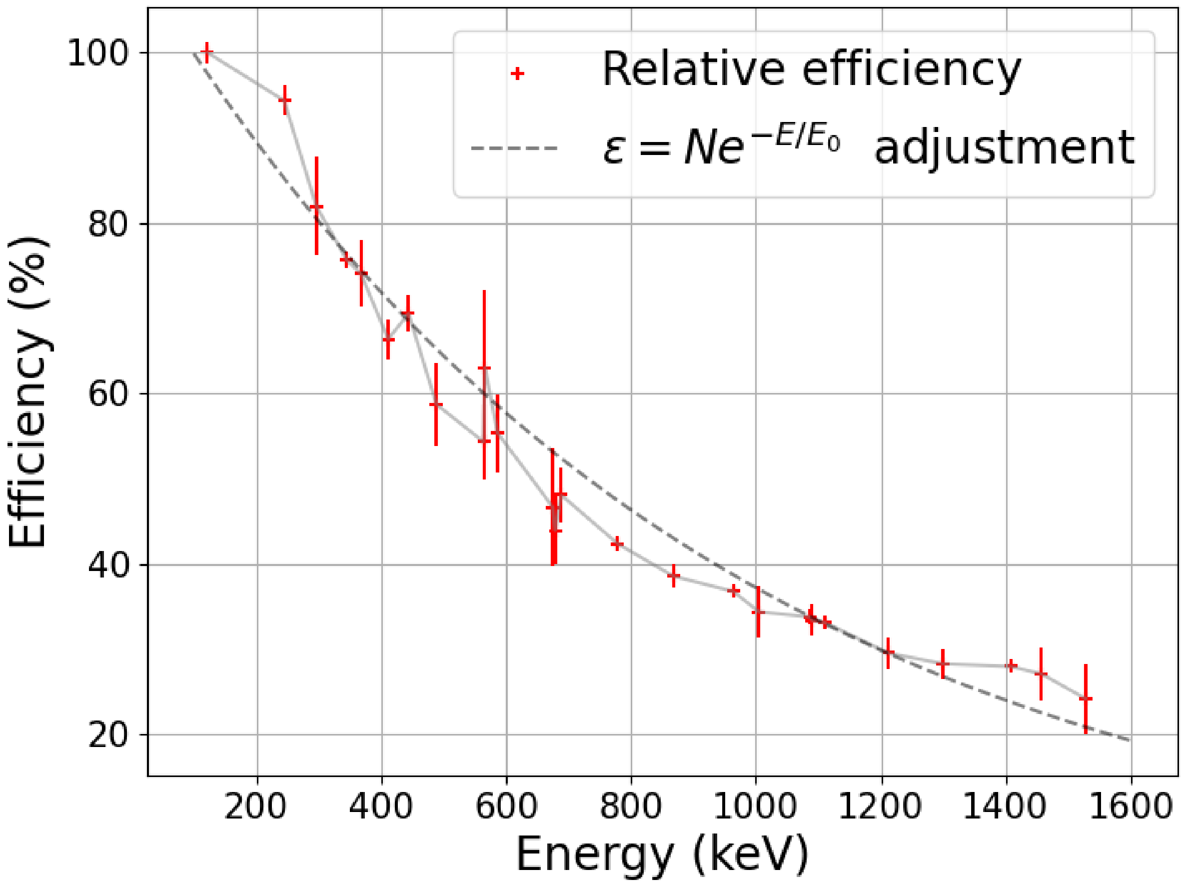

[G. F. Knoll, Radiation Detection and Measurement : Chapter 12, III.B]

Geometry of the detector

- Gamma detection : $\boldsymbol{HPGe}$
- Detector **inside** shielding
- **OFF** period reactor

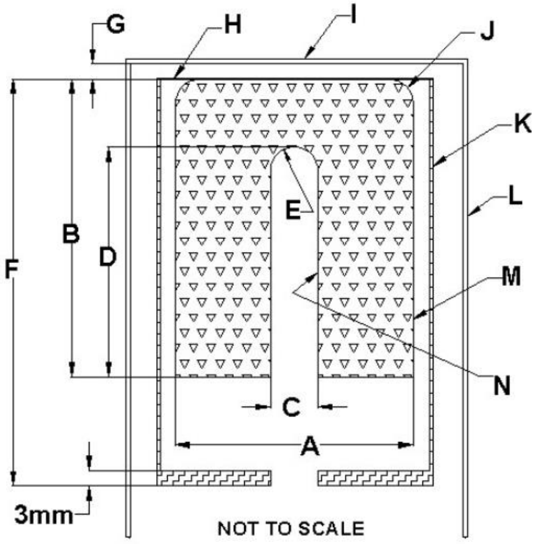

BASIC DETECTOR DIMENSIONS	
DETECTOR DIAMETER (A)	74.8 mm
DETECTOR LENGTH (B)	58.7 mm
DETECTOR END RADIUS (J)	8 mm, NOMINAL
HOLE DIAMETER (C)	9.8 mm
HOLE DEPTH (D)	45.9 mm
HOLE BOTTOM RADIUS (E)	HOLE DIAMETER / 2 mm, NOMINAL

MISCELLANEOUS DETECTOR ASSEMBLY DIMENSIONS AND MATERIALS			
IDENTIFIER	DIMENSION	DESCRIPTION	MATERIAL(S)
F	130 mm	MOUNT CUP, LENGTH	ALUMINUM
G	4 mm	END CAP TO CRYSTAL GAP	N.A.
H	0.03/0.03 mm/mm	INSULATOR/SHIELD	MYLAR/ALUMINUM
I	1 mm	END CAP WINDOW	ALUMINUM
K	0.76 mm	MOUNT CUP WALL	ALUMINUM
L	1.3 mm	END CAP WALL	ALUMINUM
M	700 microns	OUTSIDE CONTACT LAYER	Ge/Li DEAD LAYER
N	0.3 microns	HOLE CONTACT LAYER	Ge/B DEAD LAYER
P	3.2 mm	MOUNT CUP BASE	ALUMINUM

- Dimensions obtained from the manufacturer (ORTEC - GEM60)
- X-ray controlled dimensions at ILL

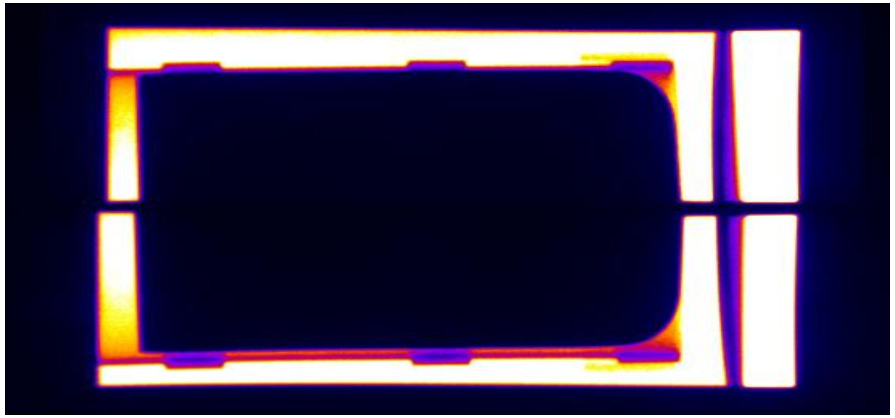

Dimensions and X-ray scan of the detector

Dimensions of HPGe

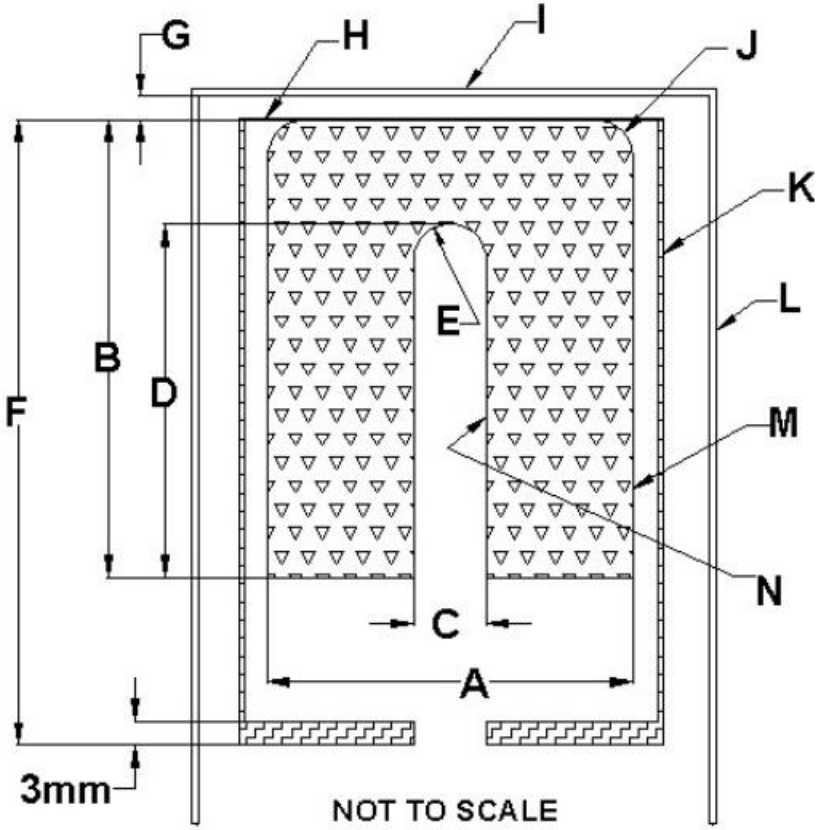

BASIC DETECTOR DIMENSIONS	
DETECTOR DIAMETER (A)	74.8 mm
DETECTOR LENGTH (B)	58.7 mm
DETECTOR END RADIUS (J)	8 mm, NOMINAL
HOLE DIAMETER (C)	9.8 mm
HOLE DEPTH (D)	45.9 mm
HOLE BOTTOM RADIUS (E)	HOLE DIAMETER / 2 mm, NOMINAL

MISCELLANEOUS DETECTOR ASSEMBLY DIMENSIONS AND MATERIALS

IDENTIFIER	DIMENSION	DESCRIPTION	MATERIAL(S)
F	130 mm	MOUNT CUP, LENGTH	ALUMINUM
G	4 mm	END CAP TO CRYSTAL GAP	N.A.
H	0.03/0.03 mm/mm	INSULATOR/SHIELD	MYLAR/ALUMINUM
I	1 mm	END CAP WINDOW	ALUMINUM
K	0.76 mm	MOUNT CUP WALL	ALUMINUM
L	1.3 mm	END CAP WALL	ALUMINUM
M	700 microns	OUTSIDE CONTACT LAYER	Ge/Li DEAD LAYER
N	0.3 microns	HOLE CONTACT LAYER	Ge/B DEAD LAYER
P	3.2 mm	MOUNT CUP BASE	ALUMINUM

Geometry improvement in GEANT4

Comparison of experimental data with spectra simulated by varying the hole diameter of the germanium crystal

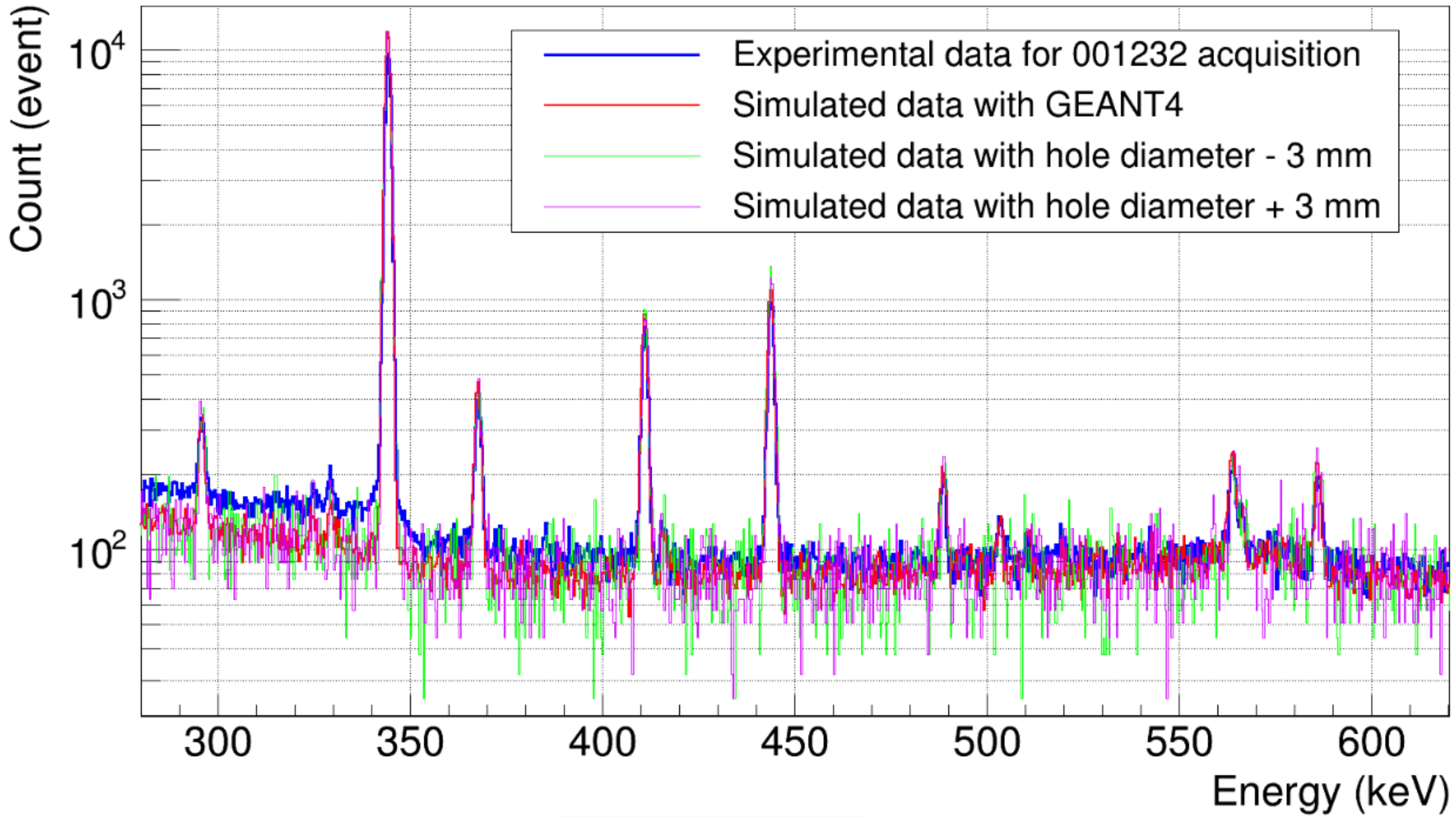

- Compton front deficit in simulation
  - ➢ Internal crystal geometry not observable with X-ray
  - ➢ Variation of crystal hole diameter

BASIC DETECTOR DIMENSIONS	
DETECTOR DIAMETER (A)	74.8 mm
DETECTOR LENGTH (B)	58.7 mm
DETECTOR END RADIUS (J)	8 mm, NOMINAL
HOLE DIAMETER (C)	9.8 mm
HOLE DEPTH (D)	45.9 mm
HOLE BOTTOM RADIUS (E)	HOLE DIAMETER / 2 mm, NOMINAL

MISCELLANEOUS DETECTOR ASSEMBLY DIMENSIONS AND MATERIALS			
IDENTIFIER	DIMENSION	DESCRIPTION	MATERIAL(S)
F	130 mm	MOUNT CUP, LENGTH	ALUMINUM
G	4 mm	END CAP TO CRYSTAL GAP	N.A.
H	0.03/0.03 mm/mm	INSULATOR/SHIELD	MYLAR/ALUMINUM
I	1 mm	END CAP WINDOW	ALUMINUM
K	0.76 mm	MOUNT CUP WALL	ALUMINUM
L	1.3 mm	END CAP WALL	ALUMINUM
M	700 microns	OUTSIDE CONTACT LAYER	Ge/Li DEAD LAYER
N	0.3 microns	HOLE CONTACT LAYER	Ge/B DEAD LAYER
P	3.2 mm	MOUNT CUP BASE	ALUMINUM

Geometry improvement in GEANT4

Relative difference between simulated and experimental spectra for different germanium crystal hole diameters

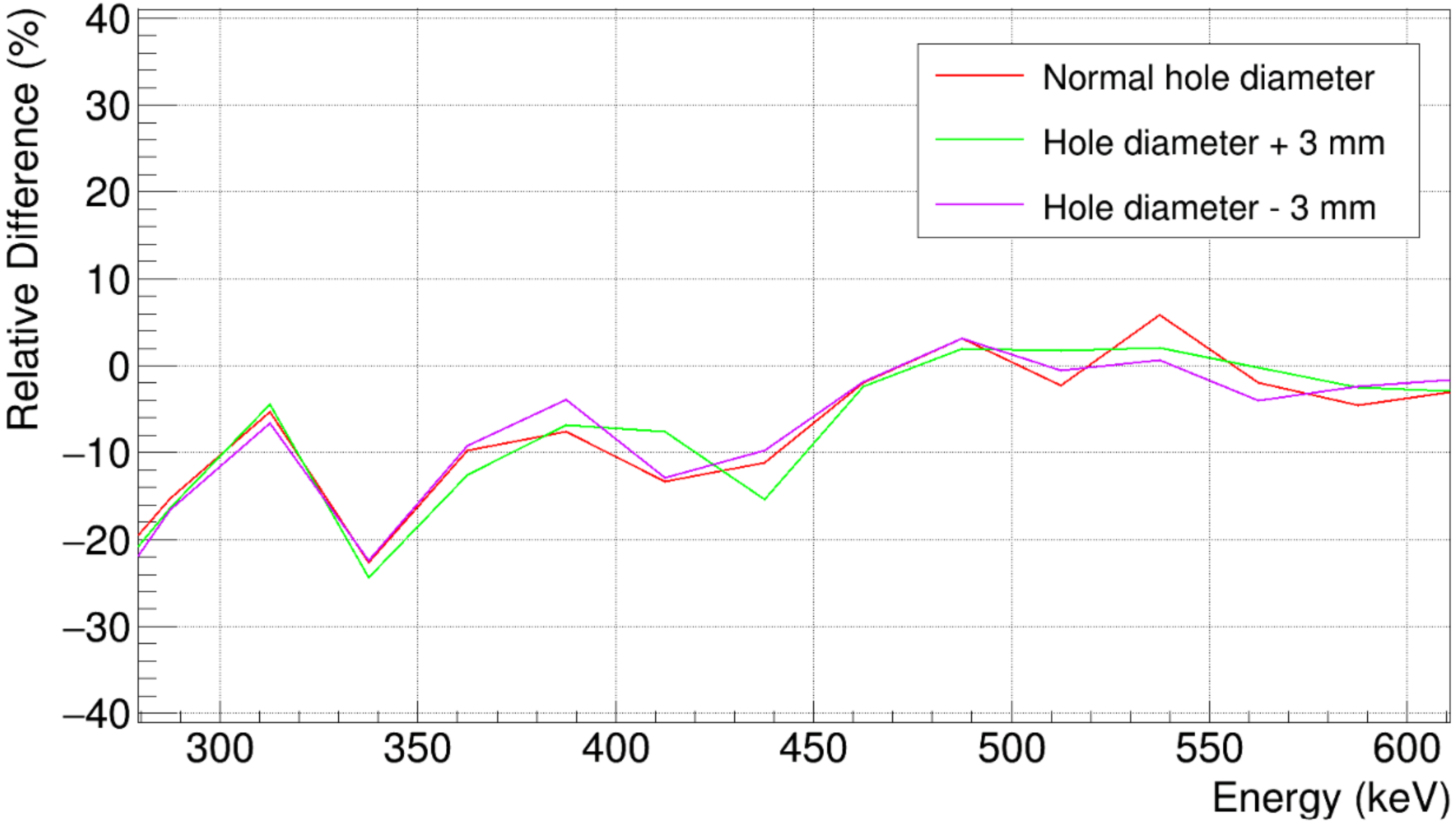

- Compton front deficit in simulation
  - ➢ Internal crystal geometry not observable with X-ray
  - ➢ Variation of crystal hole diameter
- Few differences between simulations ($\pm 3\ mm$)
  - ➢ No trend observed
  - ➢ keep the initial geometry

Modification of crystal height

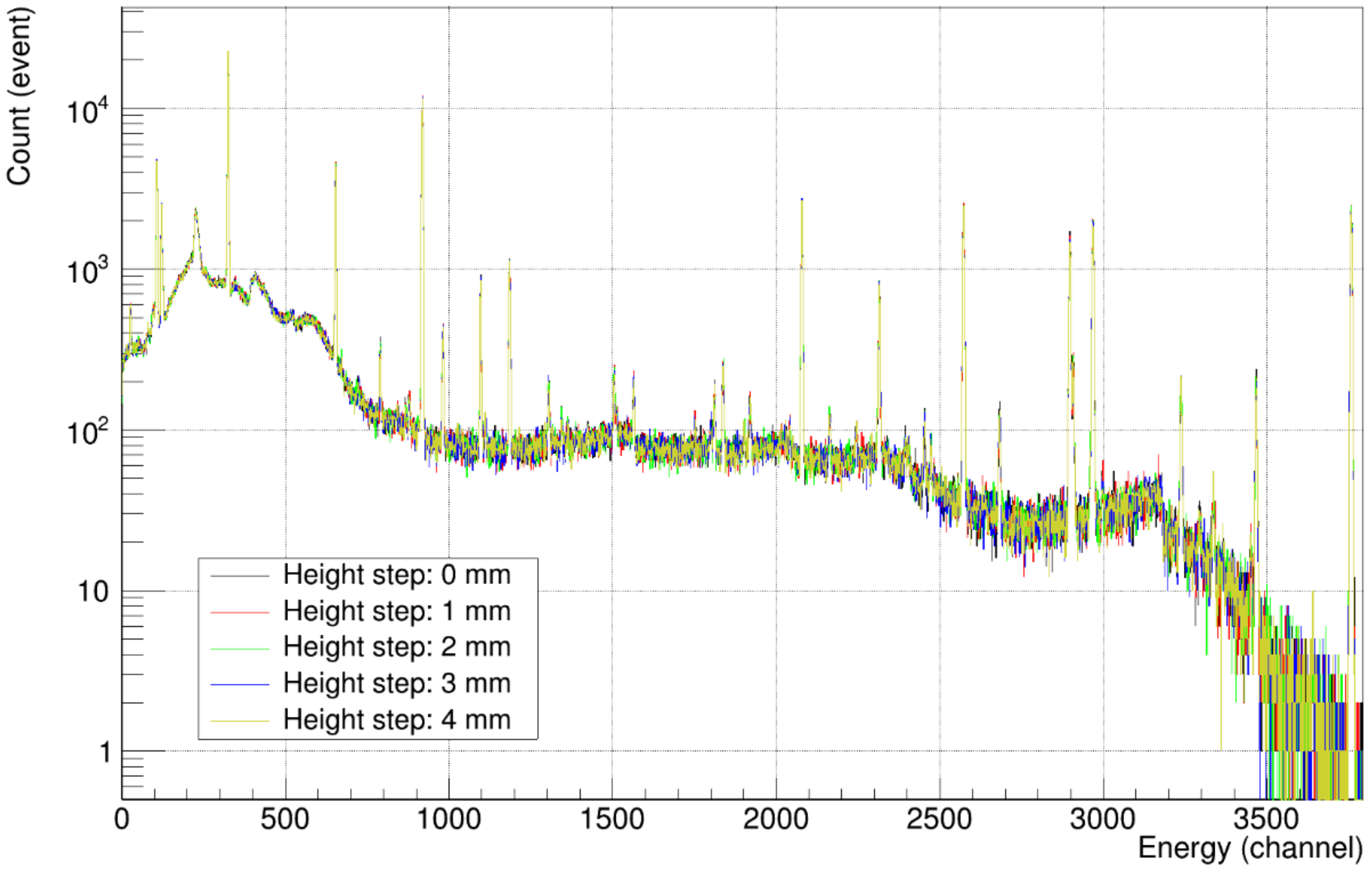

Comparison of spectra for a 152-Eu source

Step i ⇔ -i mm step over height

- Compton front: constant rate
- Photoelectric peaks: amplitude decreases with increasing step

➢ what we expected (Maryvonne)

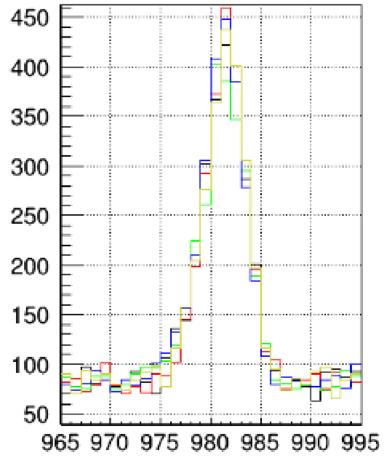

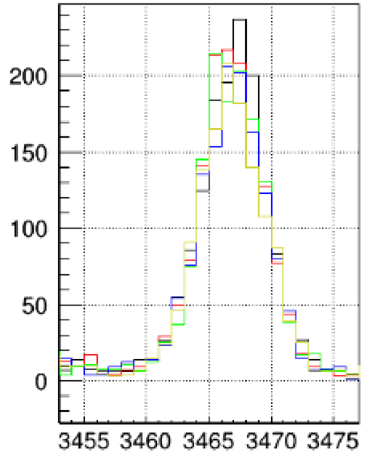

Modification of crystal height

Comparing areas under histogram

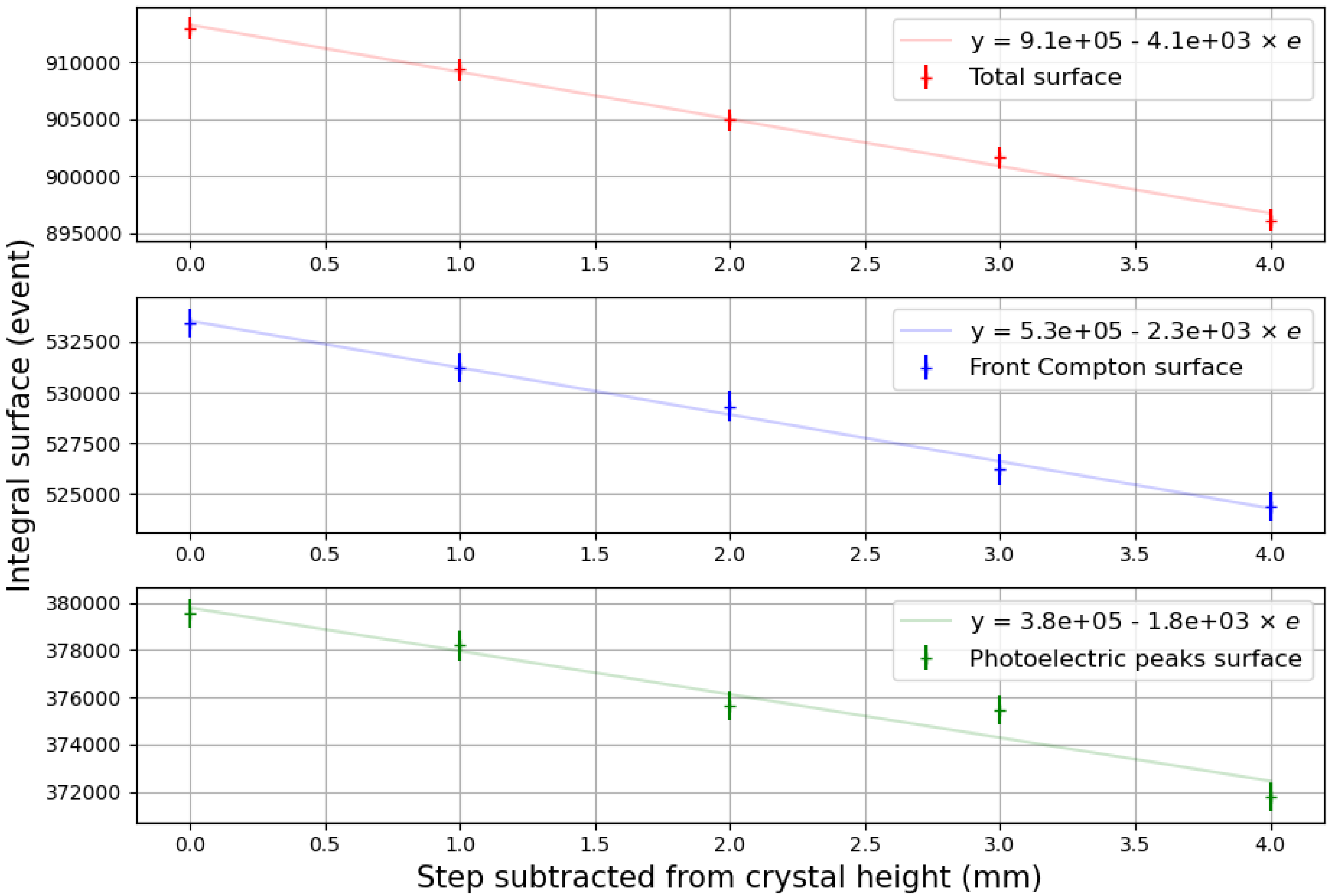

Step i ⇔ -i mm step over height

- Total area ↓ if height ↓
- Compton front area ↓ if height ↓
- Peaks area ↓ if height ↓

Desired speed: Front Compton ↓ slower than photopeaks

➢ Does not compensate for peak amplitude compared to Compton Front

Majoritary radio-isotopes

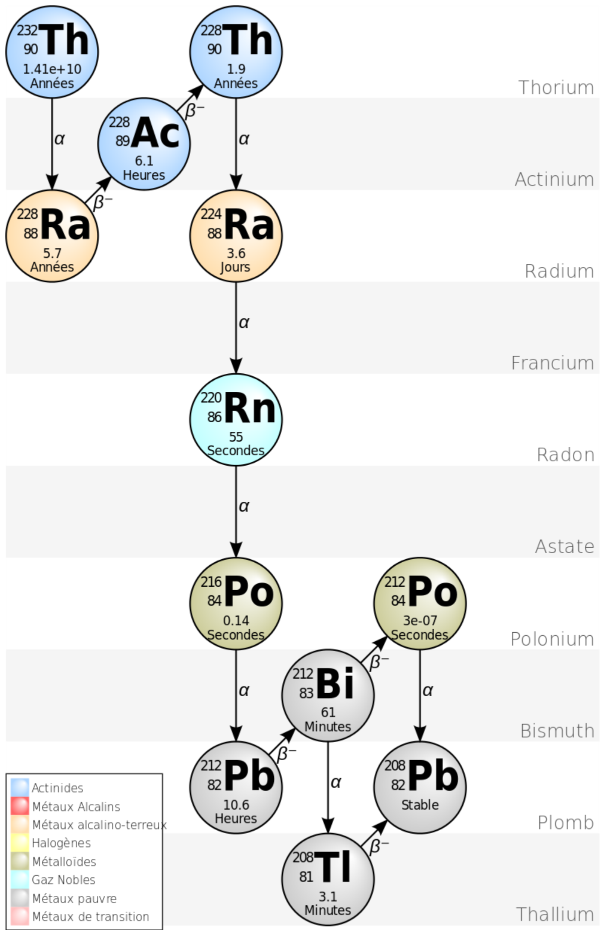

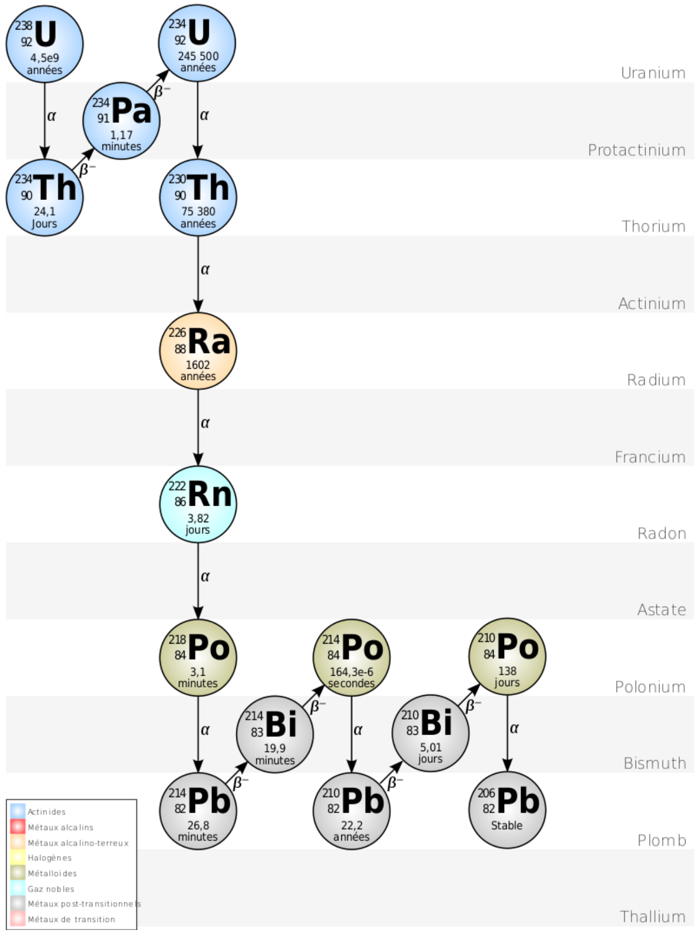

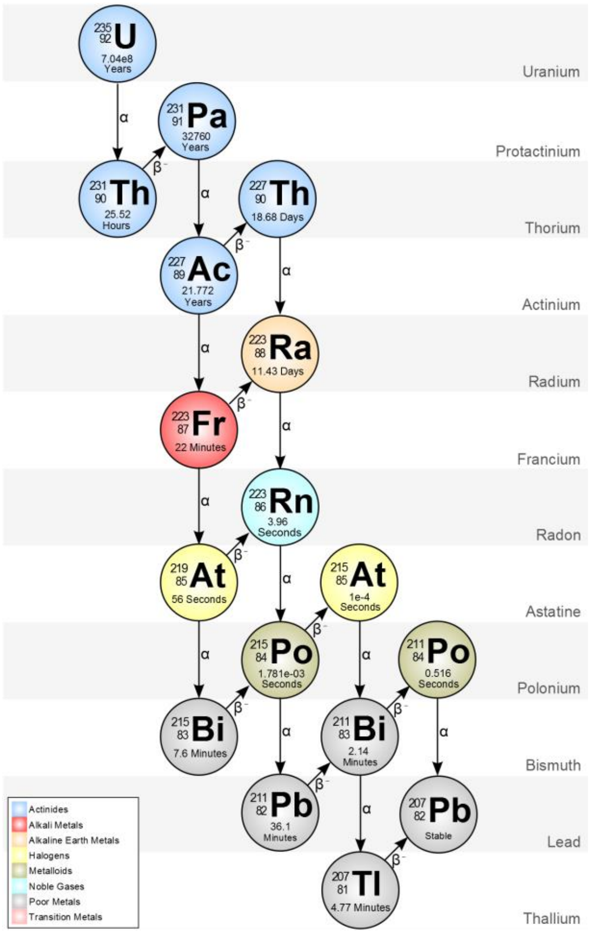

From left to right : 232-Th, 238-U and 235-U chains

From top to bottom : 40-K and 60-Co

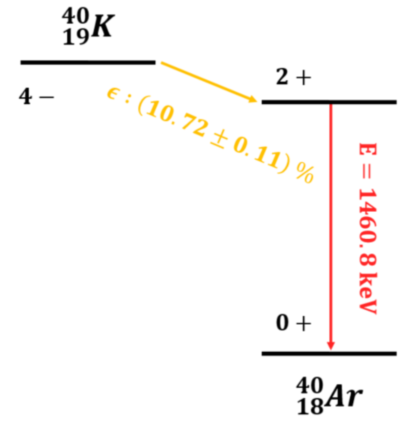

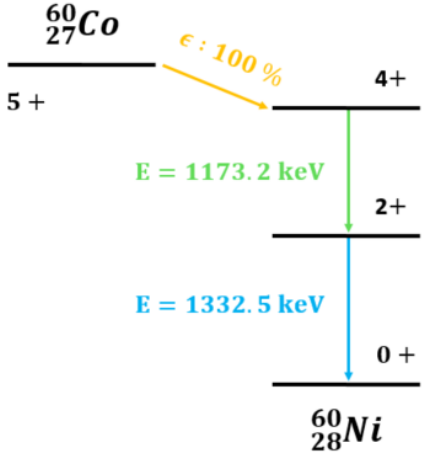

Linear combination of simulations

Linear combination of simulations :

$$Y = \sum_{i=1}^{N} a_i^{PE} y_i^{PE} + \sum_{j=1}^{M} a_j^{Pb} y_j^{Pb}$$

- Y : linear combination
- $y_k^{PE/Pb}$: simulated spectra
- a_k : linear coefficients

Objective : reproduce experimental radiogenic background spectrum and activity

- Number of generations required in **polyethylene** shielding :

$^{232}Th \rightarrow (1.96 \pm 0.07) \times 10^7$

$^{238}U \rightarrow (1.67 \pm 0.07) \times 10^7$

$^{40}K \rightarrow (6.56 \pm 0.88) \times 10^7$

$^{235}U \rightarrow (1.56 \pm 0.07) \times 10^7$

Polyethylene

- Number of generations required in **lead** shielding :

$^{232}Th \rightarrow (4.06 \pm 0.54) \times 10^7$

$^{238}U \rightarrow (6.08 \pm 0.64) \times 10^7$

$^{40}K \rightarrow (8.82 \pm 0.54) \times 10^8$

$^{235}U \rightarrow (4.97 \pm 2.84) \times 10^7$

$^{60}Co \rightarrow (3.70 \pm 0.02) \times 10^7$

Lead

Linear combination of simulations

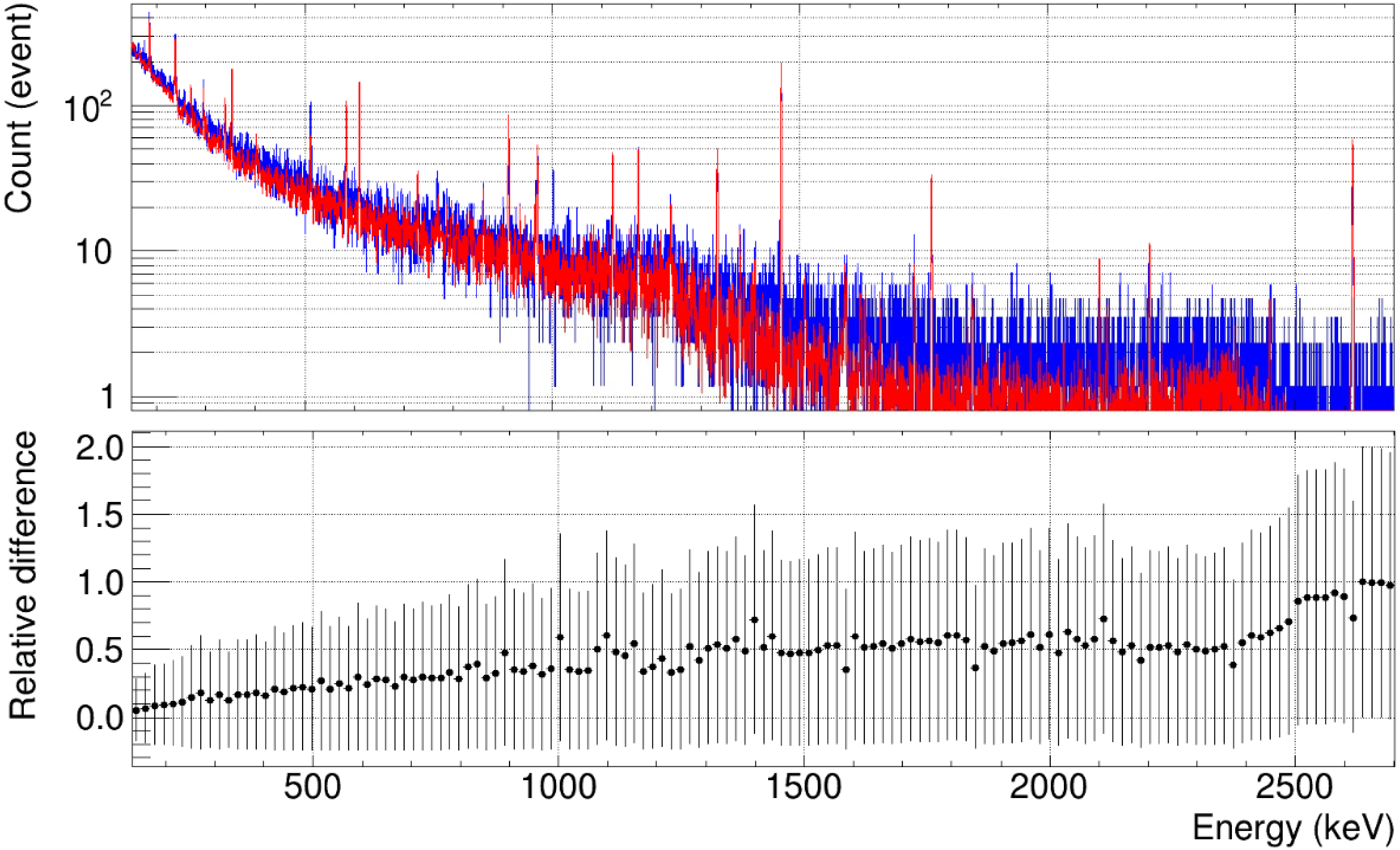

Best adjustment : $\chi^2 = 1.9$

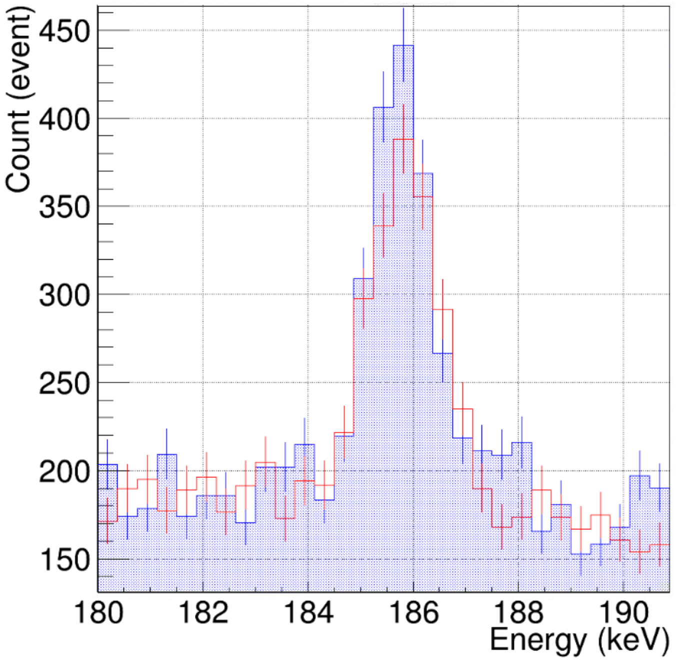

235-U peak at 186 keV

Linear combination of simulations

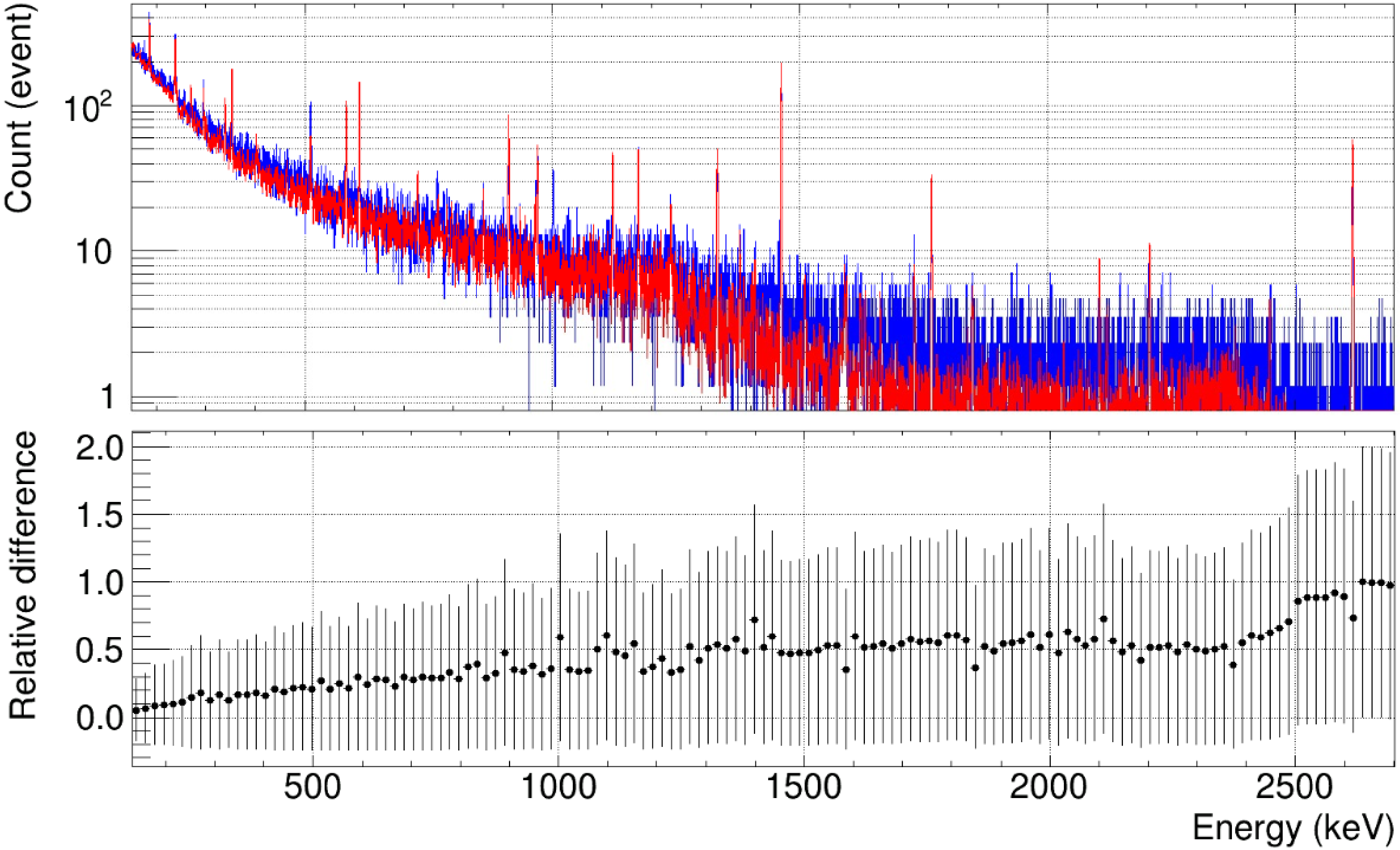

Best adjustment : $\chi^2 = 1.9$

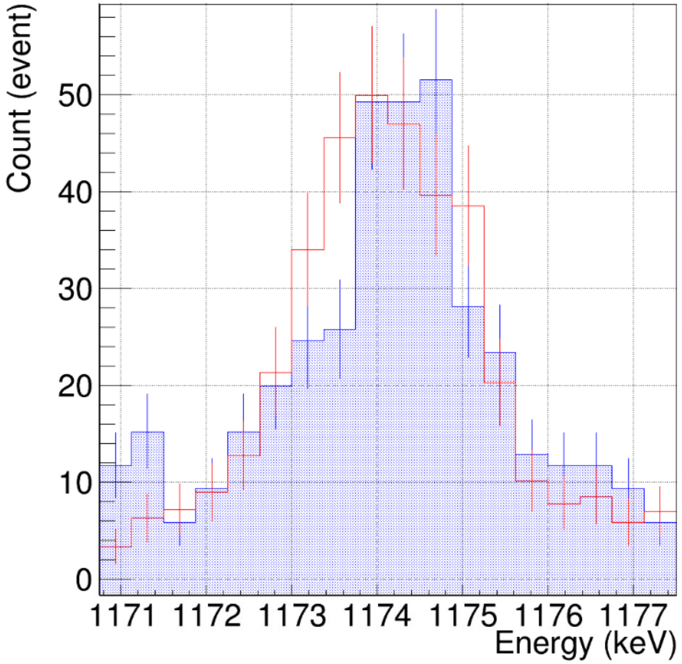

60-Co peak at 1173 keV

Linear combination of simulations

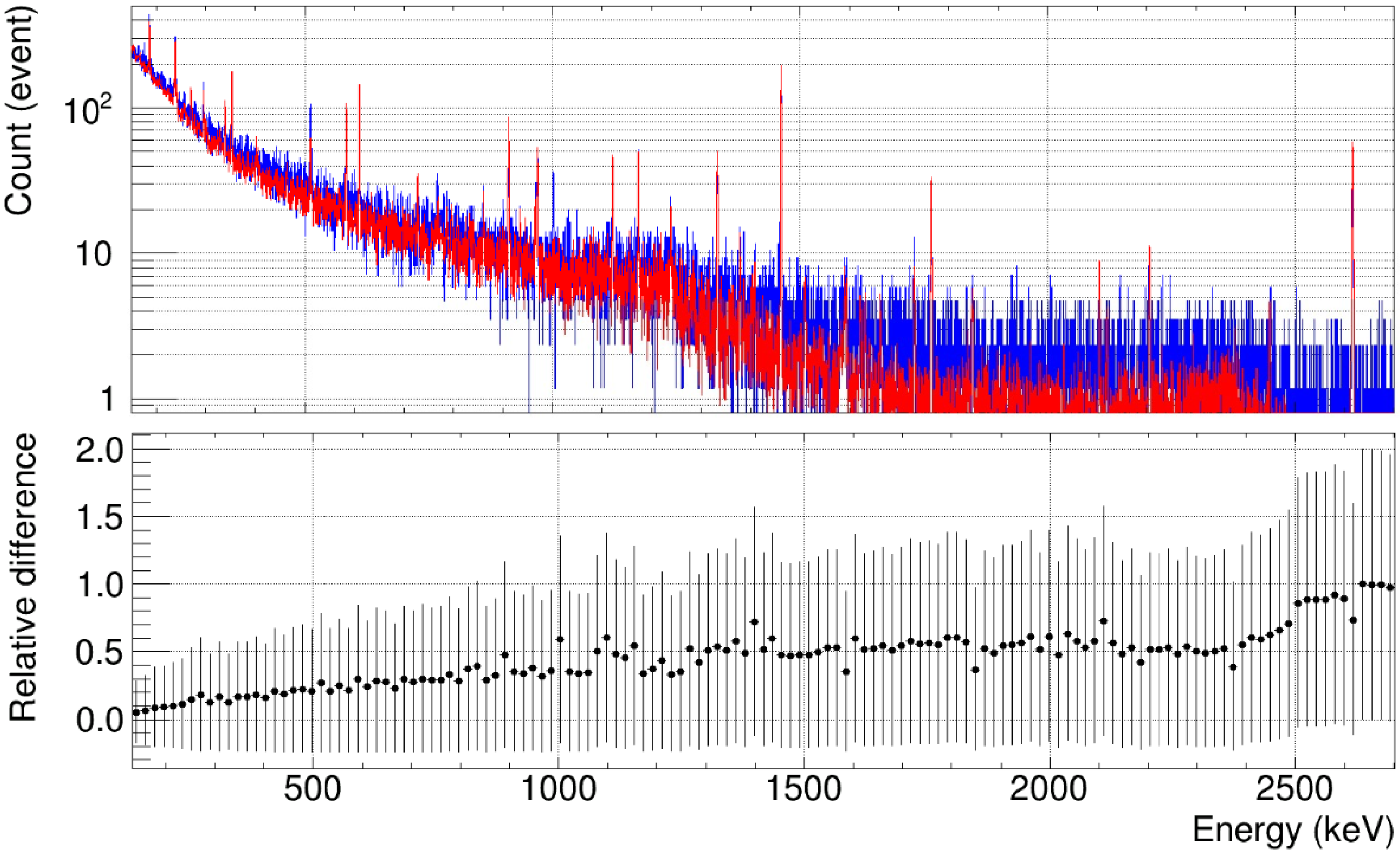

Best adjustment : $\chi^2 = 1.9$

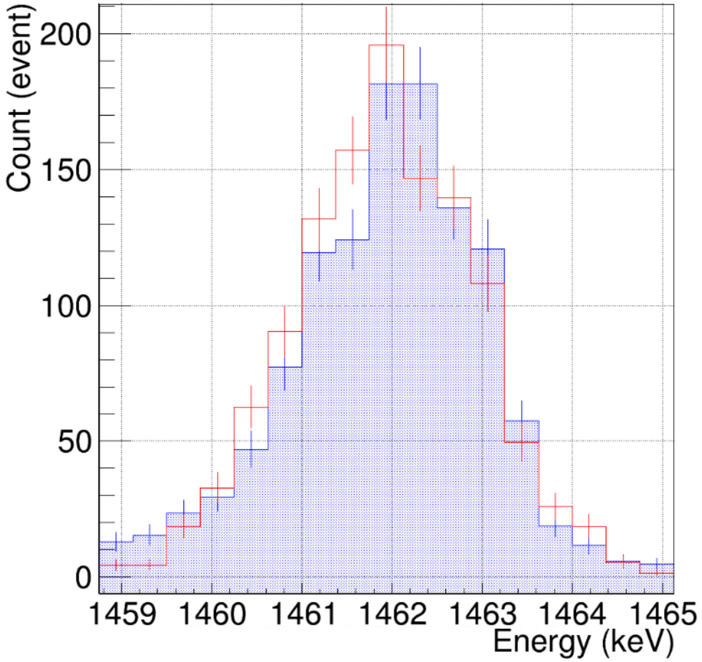

40-K peak at 1461 keV

Linear combination of simulations

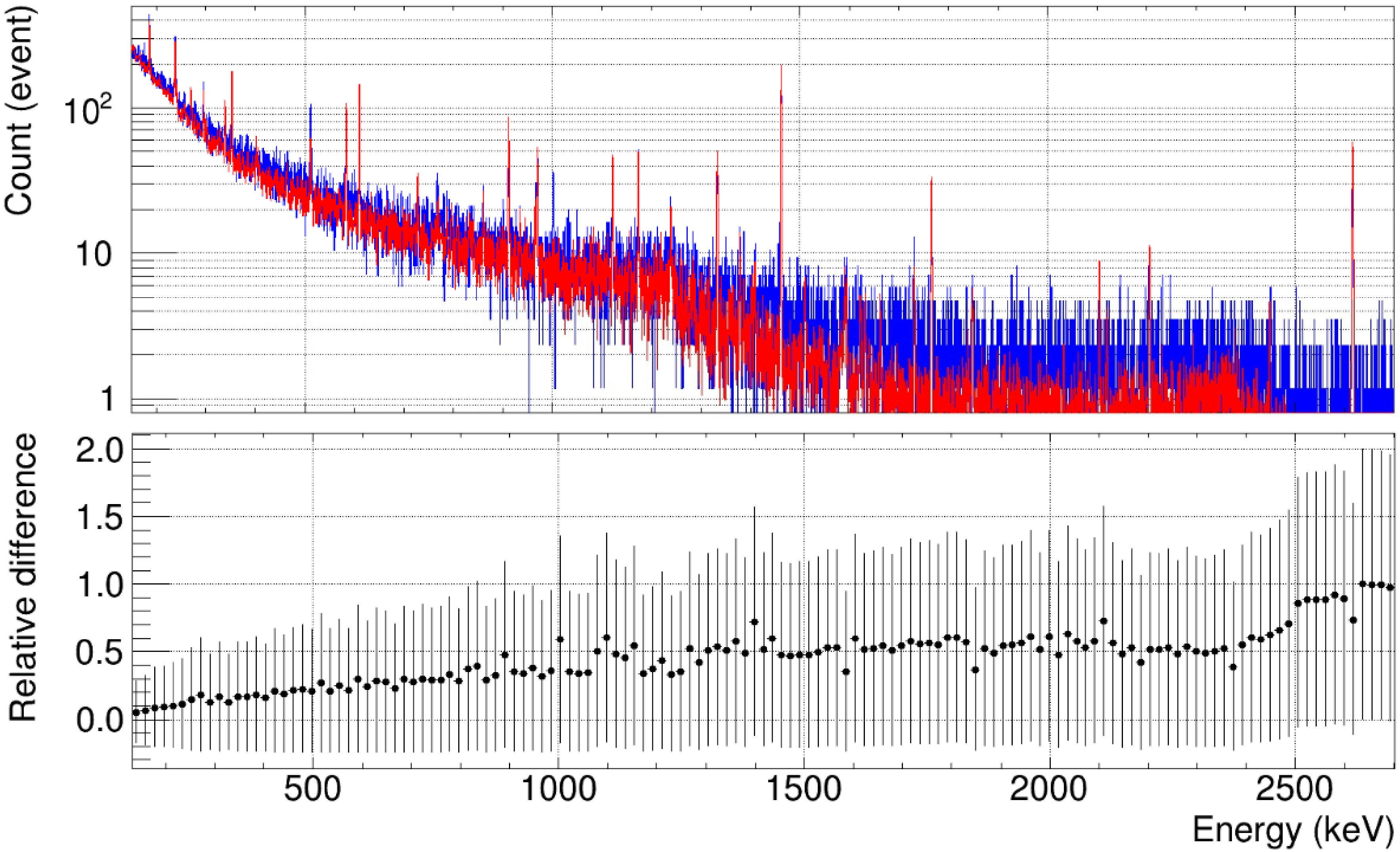

Best adjustment : $\chi^2 = 1.9$

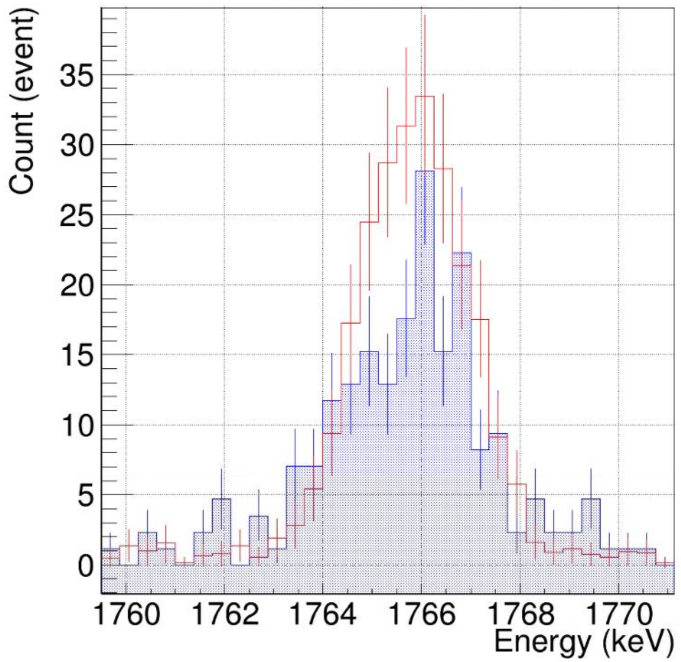

214-Bi peak at 1764 keV

Linear combination of simulations

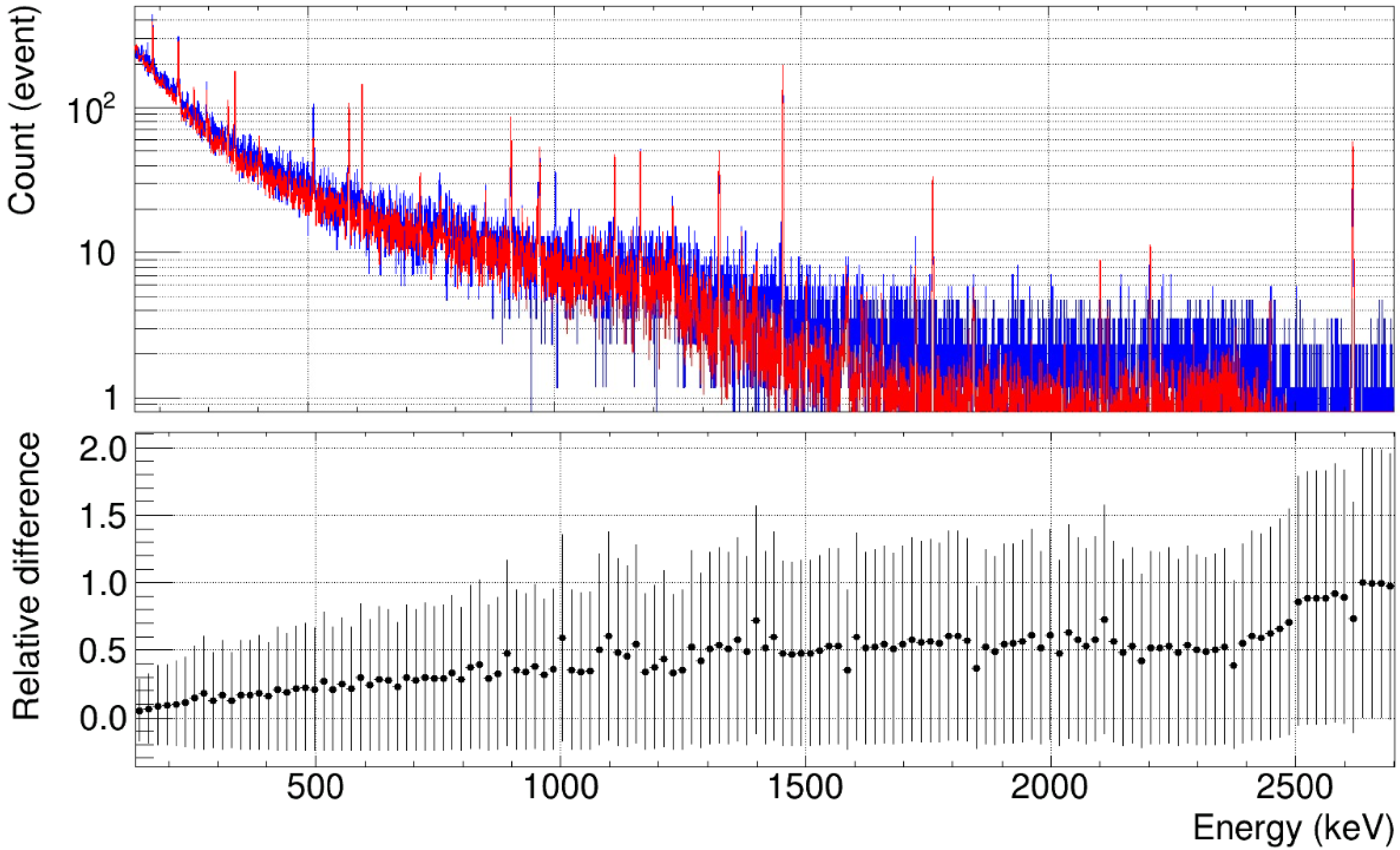

Best adjustment : $\chi^2 = 1.9$

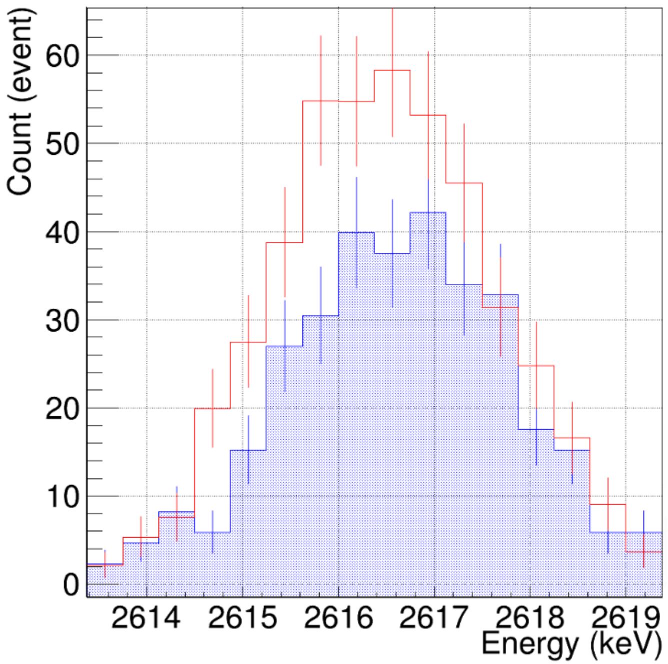

208-Tl peak at 2614 keV

Activity measurement : LSM

1) **^{232}Th chain** :

- ^{212}Pb : $E = 239$ keV $\Rightarrow$ $A = (2.1 \pm 0.9)$mBq/kg
- ^{208}Tl : $E = 583$ keV $\Rightarrow$ $A = (2.4 \pm 0.7)$ mBq/kg
- ^{208}Tl: $E = 2614$ keV $\Rightarrow$ $A < 6.9$ mBq/kg
- ^{228}Ac : $E = 911$ keV $\Rightarrow$ $A < 9.7$ mBq/kg

3) **^{40}K radio-isotope** :

- ^{40}K : $E = 1461$ keV $\Rightarrow$ $A = (22.7 \pm 13.0)$mBq/kg

2) **^{238}U chain** :

Visible experimental data :

- ^{214}Pb : $E = 295$ keV $\Rightarrow$ $A = (3.2 \pm 2.2)$ mBq/kg
- ^{214}Pb : $E = 352$ keV $\Rightarrow$ $A = (2.6 \pm 1.6)$ mBq/kg
- ^{214}Bi: $E = 609$ keV $\Rightarrow$ $A = (1.9 \pm 1.6)$ mBq/kg
- ^{214}Bi : $E = 1765$ keV $\Rightarrow$ $A < 28.6$ mBq/kg

Experimental data not visible :

- ^{226}Ra : $E = 499$ keV $\Rightarrow$ $A < 17.0$ mBq/kg
- ^{210}Pb : $E = 46$ keV $\Rightarrow$ $A < 52.8$ mBq/kg

Polyethylene

Activity measurement : LSM

1) **^{232}Th chain** :

- ^{232}Th : $A \in [0.1\ ;0.2]$ Bq/kg
- ^{228}Ra : $A \in [0.1\ ;0.3]$ Bq/kg
- ^{228}Ac : $A \in [0.1\ ;0.3]$ Bq/kg
- ^{212}Pb : $A \in [0.1\ ;0.2]$ Bq/kg
- ^{208}Tl : $A \in [0.1\ ;0.2]$ Bq/kg

3) **^{40}K radio-isotope** :

- ^{40}K : $A \in [0.4\ ;0.8]$ Bq/kg

2) **^{238}U chain** :

- ^{238}U : $A \in [0.5\ ;1.0]$ Bq/kg
- ^{234}Th : $A \in [0.5\ ;1.0]$ Bq/kg
- ^{234}U : $A \in [0.5\ ;1.0]$ Bq/kg
- ^{230}Th : $A \in [0.5\ ;1.0]$ Bq/kg
- ^{226}Ra : $A \in [2.0\ ;4.0]$ Bq/kg
- ^{214}Pb : $A \in [0.1\ ;0.2]$ Bq/kg
- ^{214}Bi : $A \in [0.09\ ;0.17]$ Bq/kg
- ^{210}Pb : $A = (570 \pm 290)$ Bq/kg

Lead

Example of mono-energetic peaks

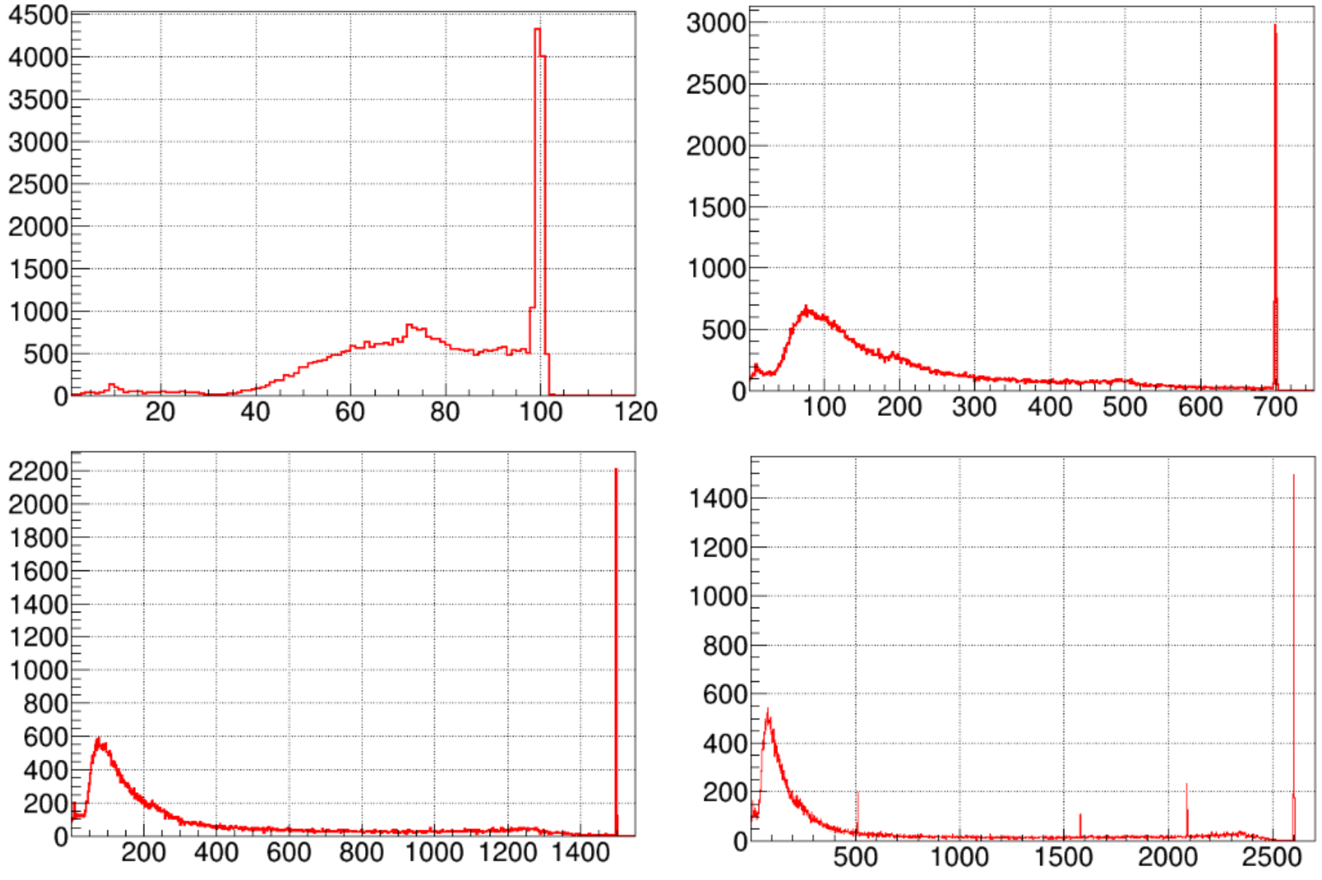

Example of spectra for single-energy peaks : 100, 700, 1500 and 2600 keV

Efficiency obtained only with GEANT4 : generations of **27 mono-energetic** peaks

Total efficiency calculated from :

$$\epsilon_{G4}(E) = \frac{N_{peak}(E)}{N_{gen}}$$

- $N_{peak}(E)$: peak area at energy E
- N_{gen} : number of single-energy photons generated

Specific activity : 232-Th example

Mass of polyethylene : $M_{PE} = 2\ T$

Acquisition time : $T_{RUN} = 60314\ s$

Chains generated : $N_{gen} = 1.3 \times 10^8$

Linear coefficient : $\mathrm{a} = 0.1506 \pm 0.0047$

$$\mathrm{A^{eq}} = \frac{a \times \mathrm{N_{gen}}}{\mathrm{T_{RUN}}}$$

Chains in secular equilibrium with GEANT4 :

$$\mathrm{A^{eq}}(^{232}Th) = (1.62 \pm 0.06) \times 10^2\ mBq/kg$$

Number of events : $N_{peak}^{G4} = (2.37 \pm 0.10) \times 10^3$

Intensity of the peak : $I_\gamma = (25.8 \pm 0.4)\ \%$

Total efficiency : ϵ^{G4} ⇒ interpolation

Specific activity for the 228-Ac peak at 911 keV of the 232-Th chain :

$$\mathrm{A_{peak}^{G4}}(^{228}Ac) = (1.61 \pm 0.09) \times 10^2\ mBq/kg$$

$$\mathrm{A_{peak}^{G4}}(^{228}Ac) = \frac{\mathrm{a} \times \mathrm{N_{peak}^{G4}}}{\mathrm{T_{RUN}} \times I_\gamma \times \epsilon}$$

Impact of secular chain equilibrium

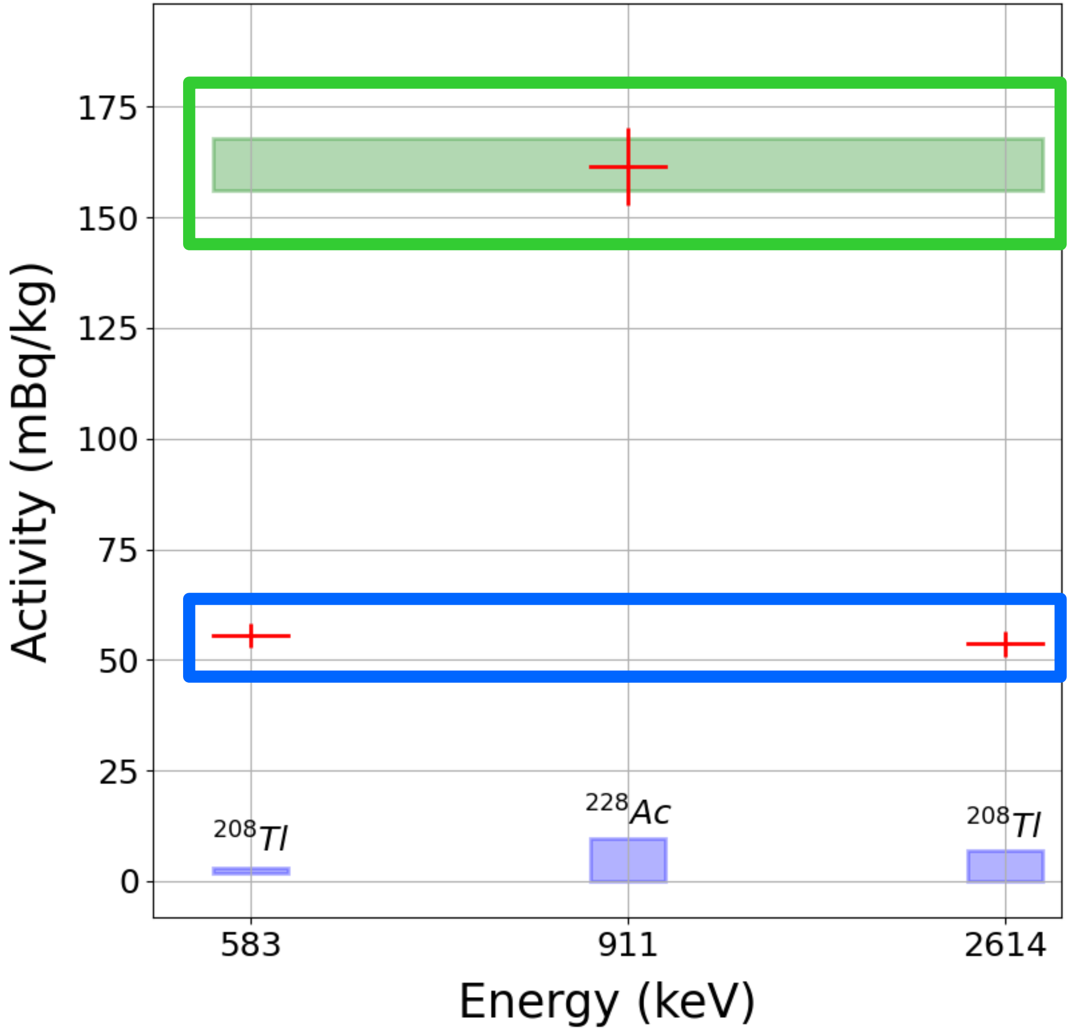

Example for the 232-Th chain in PE

Impact of secular chain equilibrium

First equilibrium down to Ra-isotope

Break in equilibrium

Second equilibrium from Rn-isotope

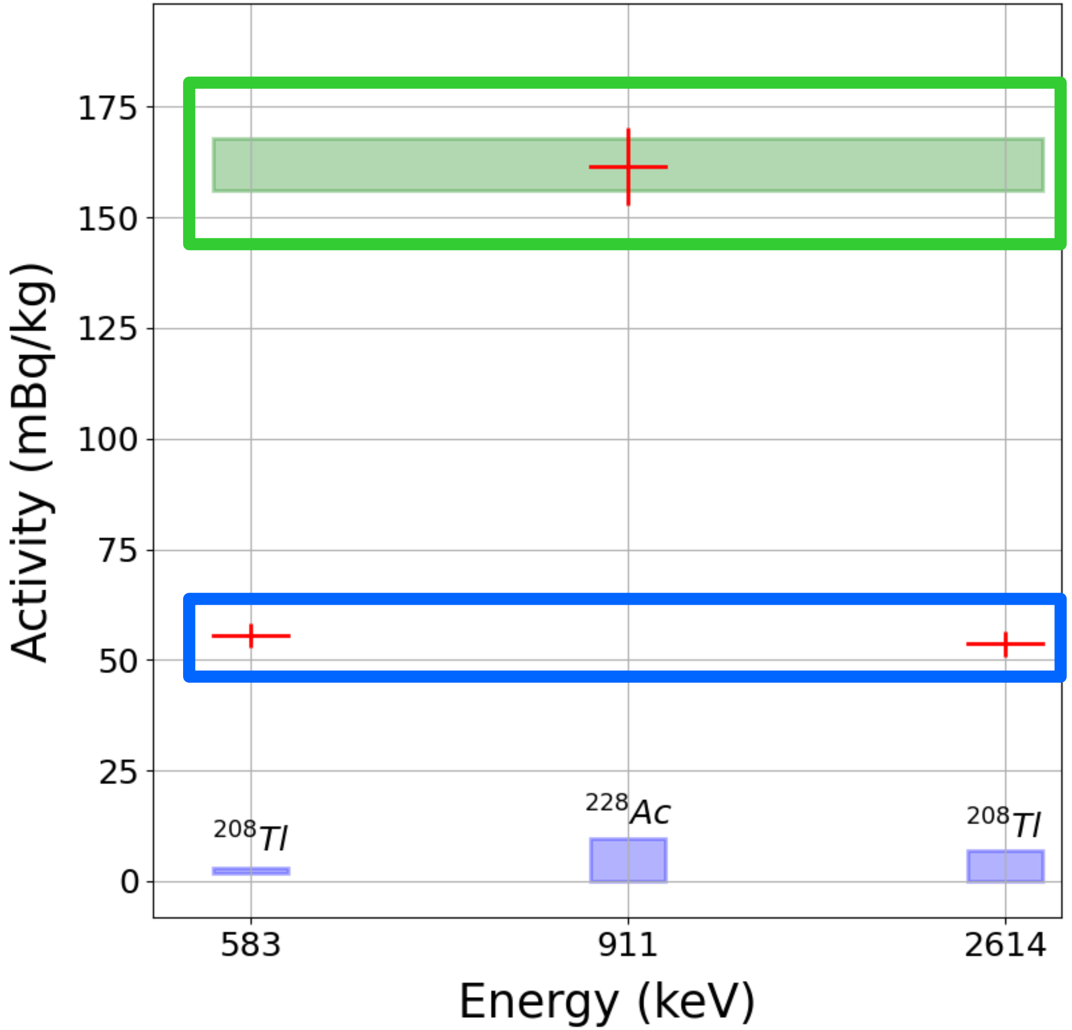

Example for the 232-Th chain in PE

Impact of secular chain equilibrium

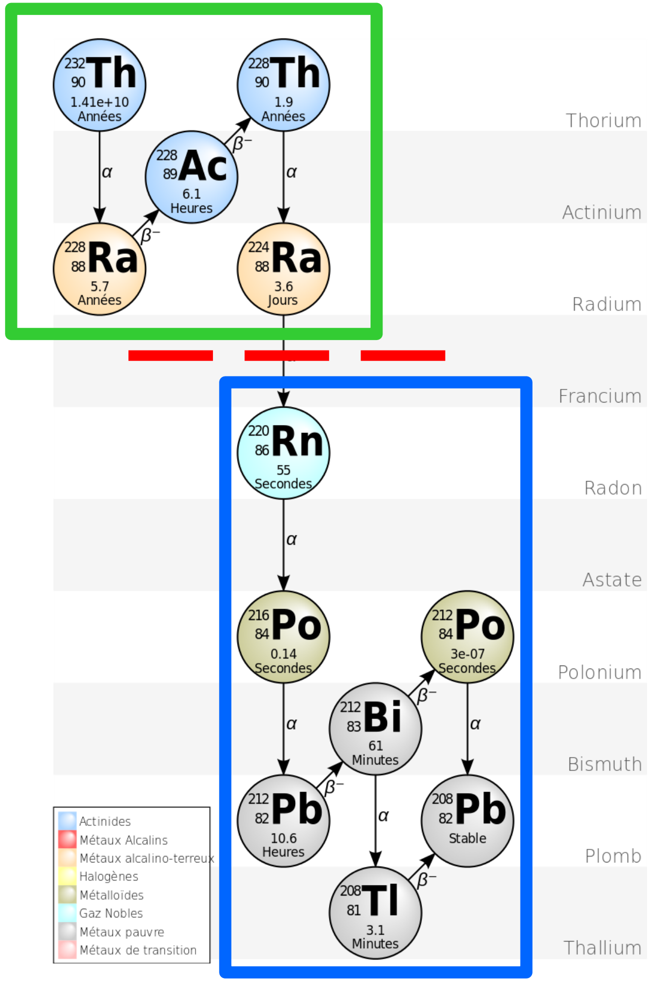

232-Th decay chain

- First equilibrium down to Ra-isotope
- Break in equilibrium
- Second equilibrium from Rn-isotope

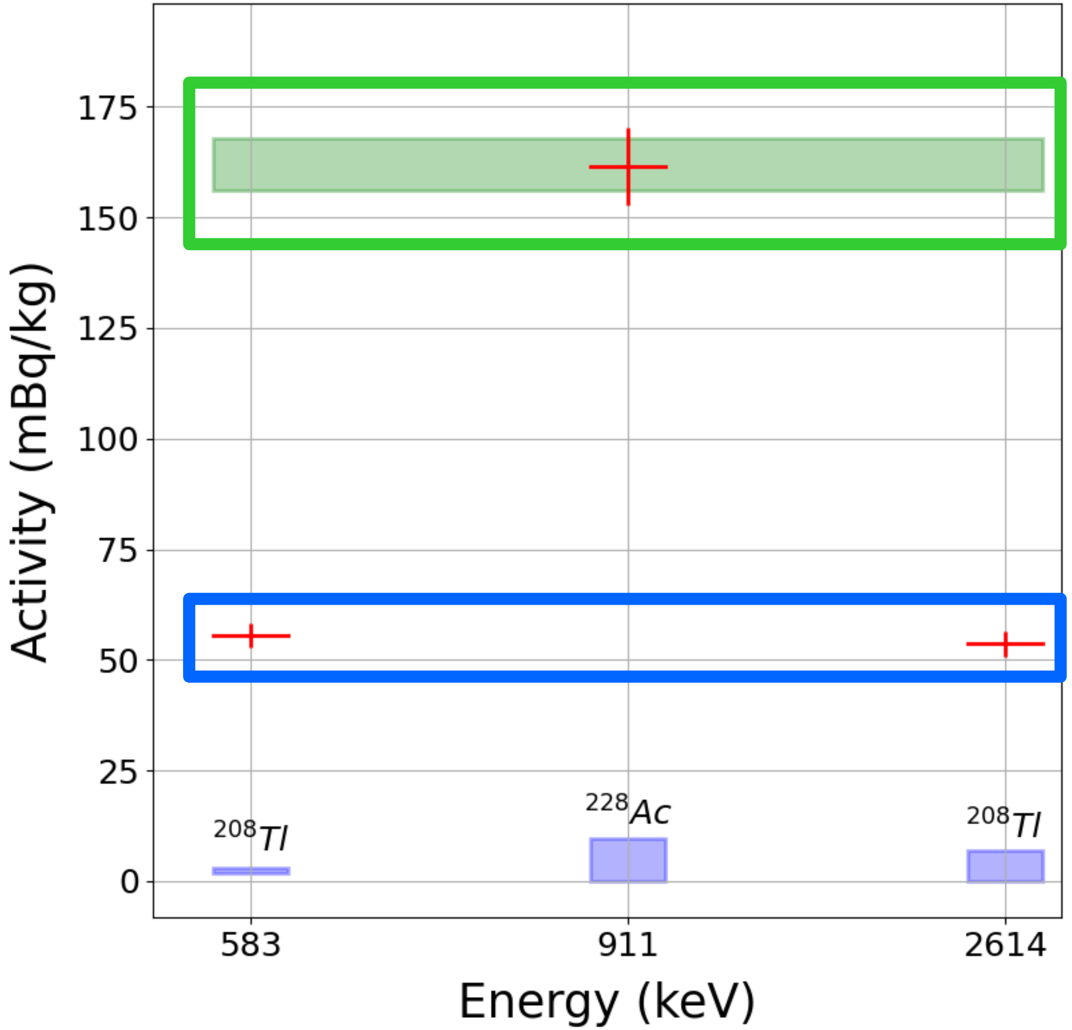

Example for the 232-Th chain in PE

Impact of secular chain equilibrium

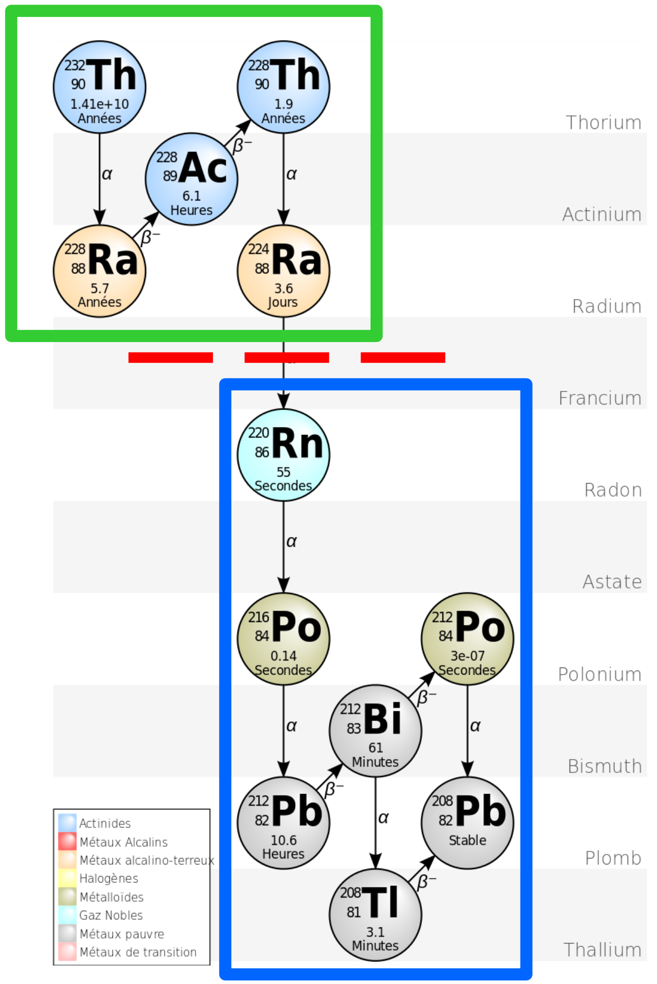

232-Th decay chain

First equilibrium down to Ra-isotope

Break in equilibrium

Second equilibrium from Rn-isotope

Two different equilibrium levels visible in GEANT4 data :

- First coherent with secular equilibrium of the chain
- Second not coherent
- Neither is consistent with LSM data !

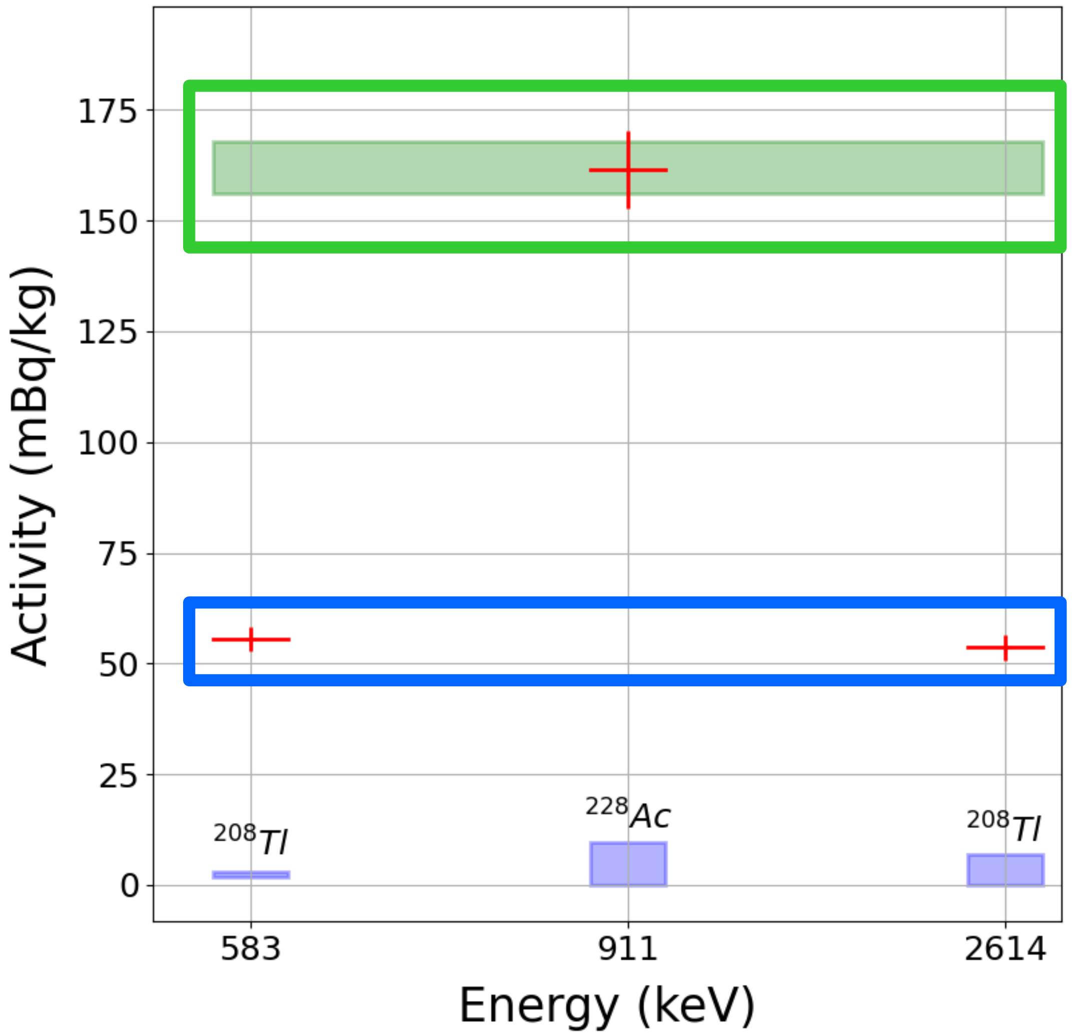

Example for the 232-Th chain in PE

Activity measurement : peak by peak

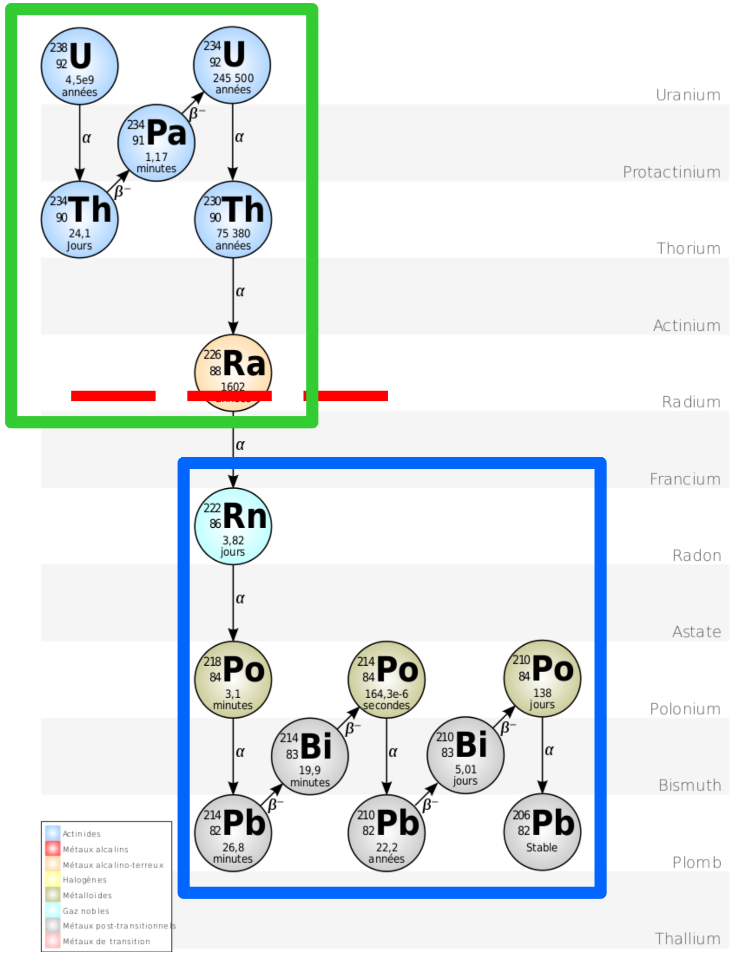

238-U decay chain

First equilibrium down to Ra-isotope

Second equilibrium from Rn-isotope

Only one equilibrium level visible in GEANT4 data :

- Coherent with secular equilibrium
- Not coherent with LSM experimental data !

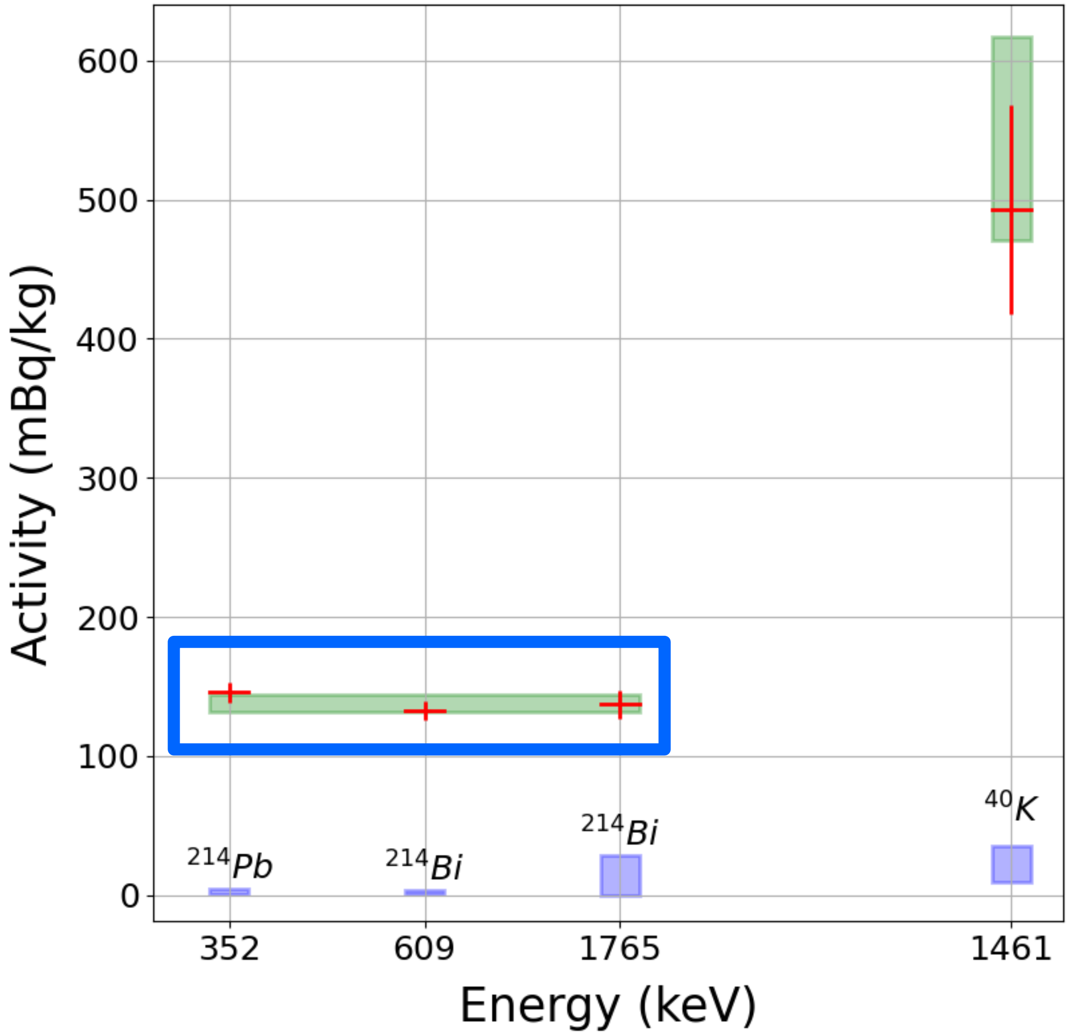

Example for the 238-U chain and 40-K

GEANT4 simulations in shielding

Simulations of the 5 chains in both shielding : $\boldsymbol{PE}$ & $\boldsymbol{Pb}$

- Place these radioactive isotopes in the shielding to obtain a gamma background model
- As homogeneous in lead or polyethylene shielding with **GPSInMaterial** method
- Modification of the lead shielding macro ***OutershieldingBuilder.cc*** :
  - separation into two lead layers to save calculation time during simulations
  - Radio-isotope generation in the **first cm** only

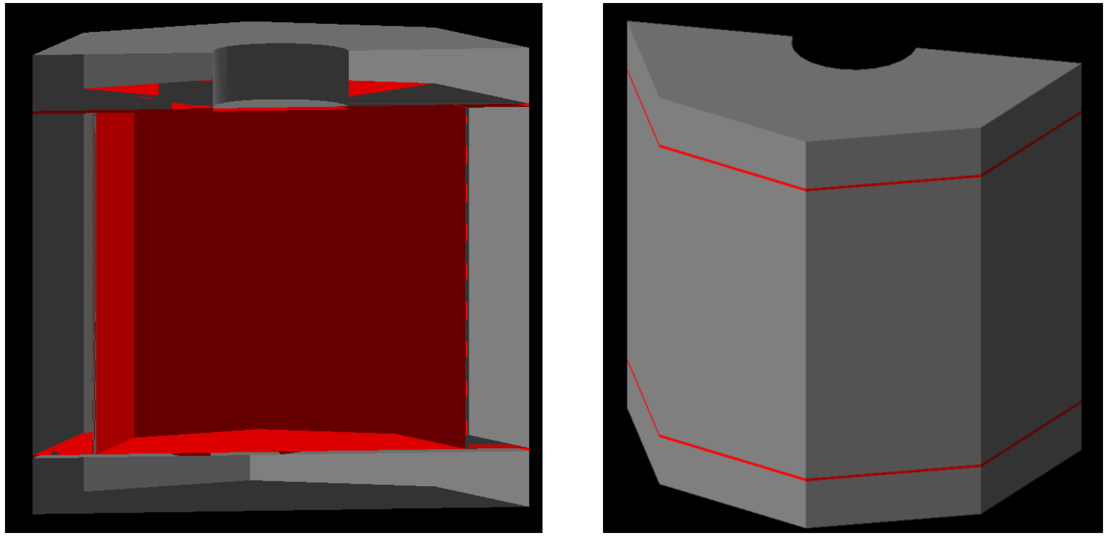

OuterShielding_Lead_Bot_1_physical [0]
OuterShielding_Lead_Bot_2_physical [0]
OuterShielding_Lead_Mid_1_physical [0]
OuterShielding_Lead_Mid_2_physical [0]
OuterShielding_Lead_Top_1_physical [0]
OuterShielding_Lead_Top_2_physical [0]

Example with the first centimeter of lead in red

GEANT4 simulations in lead

Area of a regular octagon :

$$A = 2\left(1+\sqrt{2}\right)a^2$$
$$= 2\sqrt{2}\,R^2$$
$$= 8\left(\sqrt{2}-1\right)r^2$$

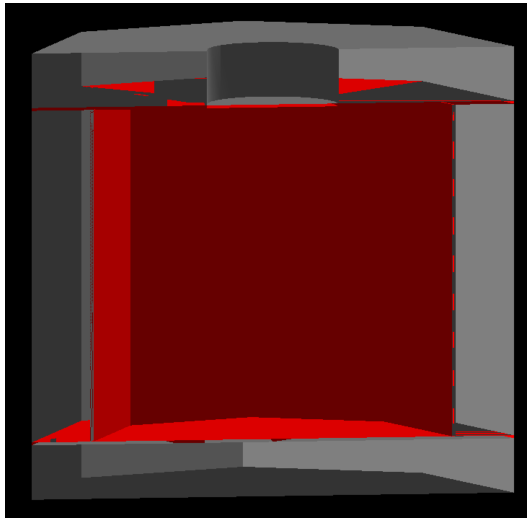

- ☑ OuterShielding_Lead_Bot_1_physical [0]
- ☑ OuterShielding_Lead_Bot_2_physical [0]
- ☑ OuterShielding_Lead_Mid_1_physical [0]
- ☑ OuterShielding_Lead_Mid_2_physical [0]
- ☑ OuterShielding_Lead_Top_1_physical [0]
- ☑ OuterShielding_Lead_Top_2_physical [0]

- $R = \frac{a}{2\sin\left(\frac{\pi}{8}\right)} = \frac{a}{\sqrt{2-\sqrt{2}}}$: circumscribed radius
- $r = \frac{a}{2}\cot\left(\frac{\pi}{8}\right) = \frac{a}{2}\left(1+\sqrt{2}\right)$: inscribed radius

Volume of lead shielding : $V = A \times H$

Mass of lead : $M = V \times \rho = 20.35\ T$

Mass in first centimeter : $M_{1cm} = 936\ kg$

Modification of the lead layer

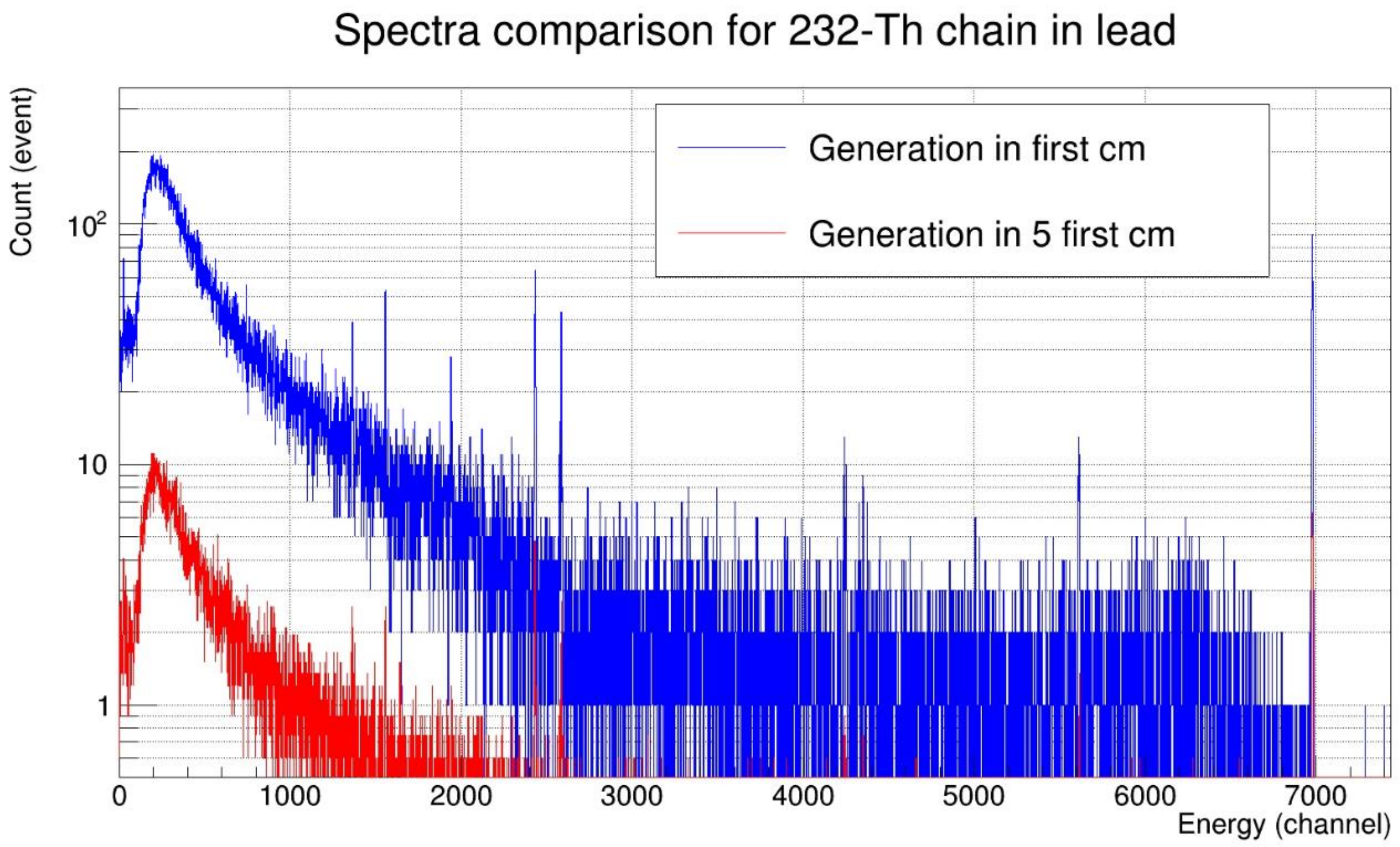

Comparison of 232-Th chain spectra in lead

New volumes for lead shielding :

- Using **G4Polyhedra**
- Creation of a new **Lead2** material
- Testing with the radioactive chains

➢ Expected pattern: number of events ↓ if thickness ↑ (attenuation)

Modeling the transfer channel slab

ILL transfer channel slab = concrete + steel + stainless steel

Dimensions and properties obtained from plans supplied by ILL (Stéphane FUARD)

$\rho = 84\ kg/m^2$ for steel

$\rho = 47\ kg/m^2$ for stainless steel

$d = 2{,}3\ g/cm^3$ for concrete

} simplification by creating a composite, homogeneous material $\Rightarrow\ d_m^T = 2{,}393\ g/cm^3$

Modify **"MaterialsBuilder.cc"** and **"OuterShieldingBuilder.cc"** to add this slab to the simulation

Modeling the transfer channel slab

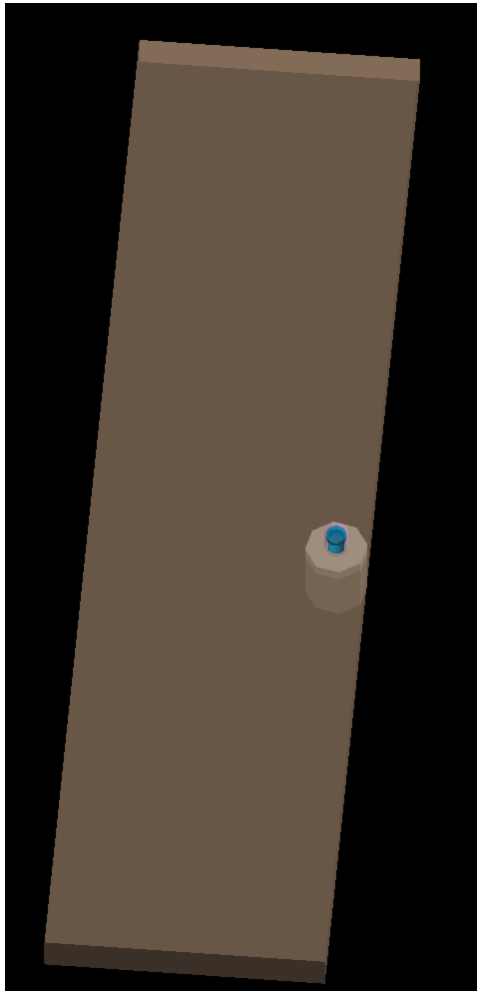

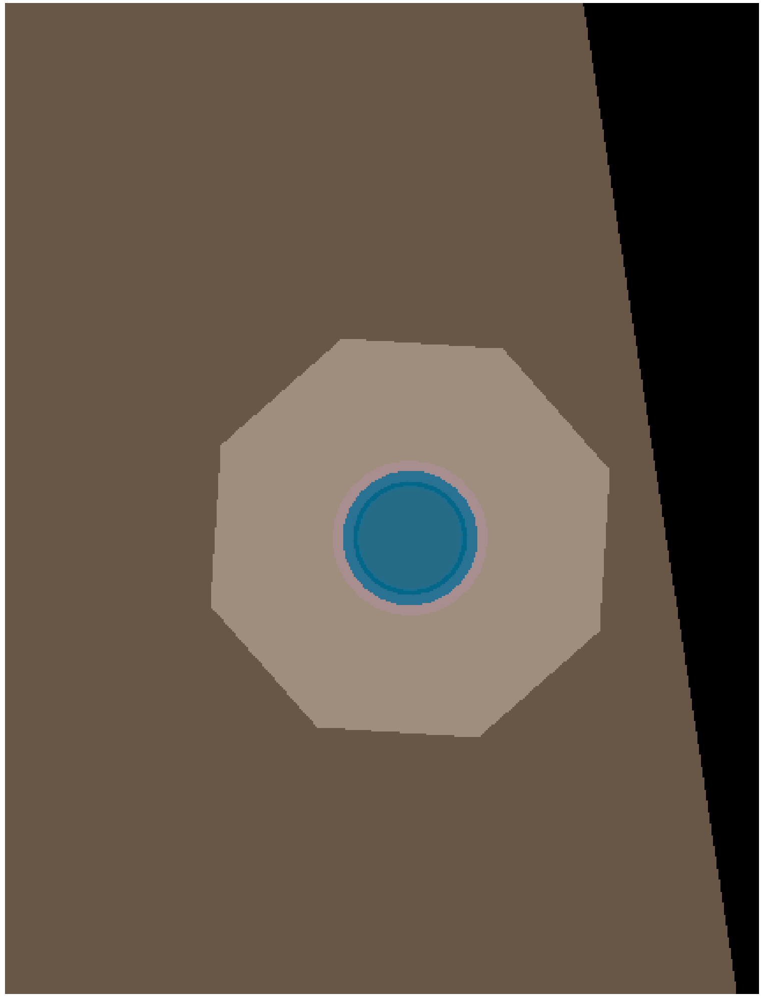

True transfer channel dimensions :

- Width : $x = 755\ cm = 7.55\ m$
- Length : y= $3000\ cm = 30\ m$
- Height : z= $100\ cm = 1\ m$
- Volume : $V = 226.5\ m^3$
- Rotation/shielding : $\alpha = 9.6°$
- x translation : $\mathrm{T_x} = -280.5\ cm$
- → volume too large: simulation not optimized

Modeling the transfer channel slab

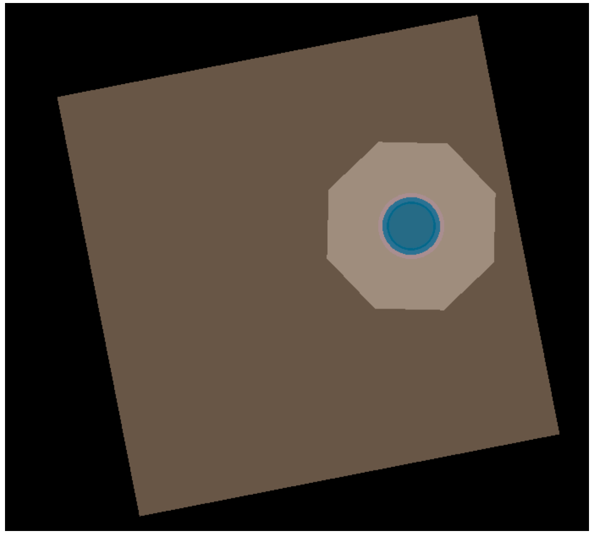

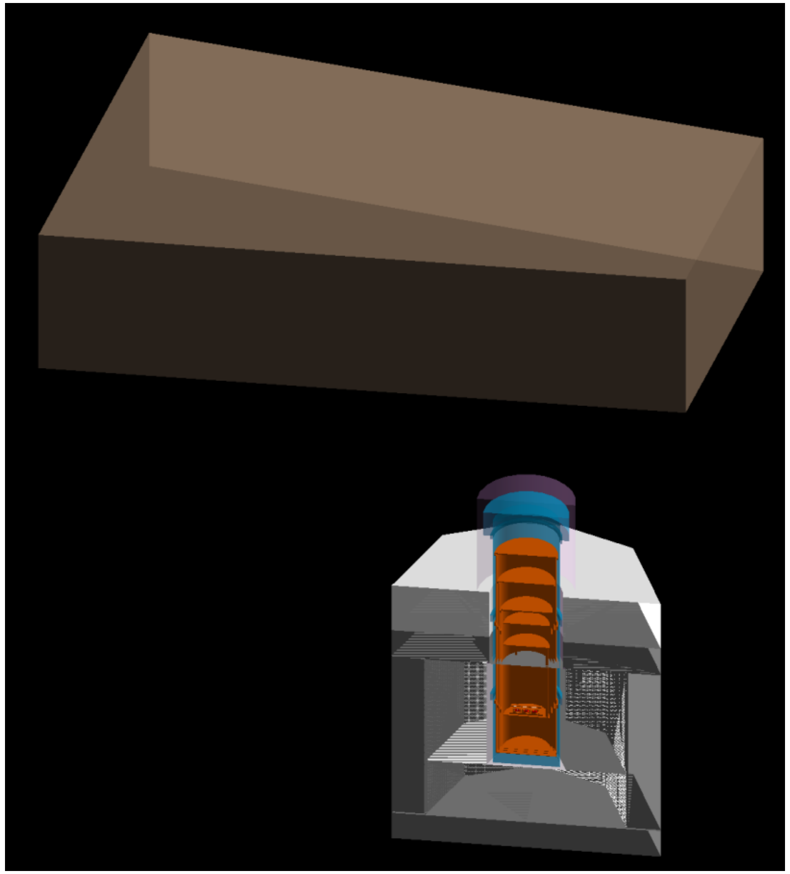

GEANT4 transfer channel dimensions :

- Width : $x = 400\ cm = 4\ m$
- Length : y$= 400\ cm = 4\ m$
- Height : z$= 100\ cm = 1\ m$
- Volume : $V = 4\ m^3$
- Rotation/shielding : $\alpha = 9.6°$
- x translation : $T_x = -103\ cm$
- → volume reduced by 98% : less computing time

Ricochet RUN013

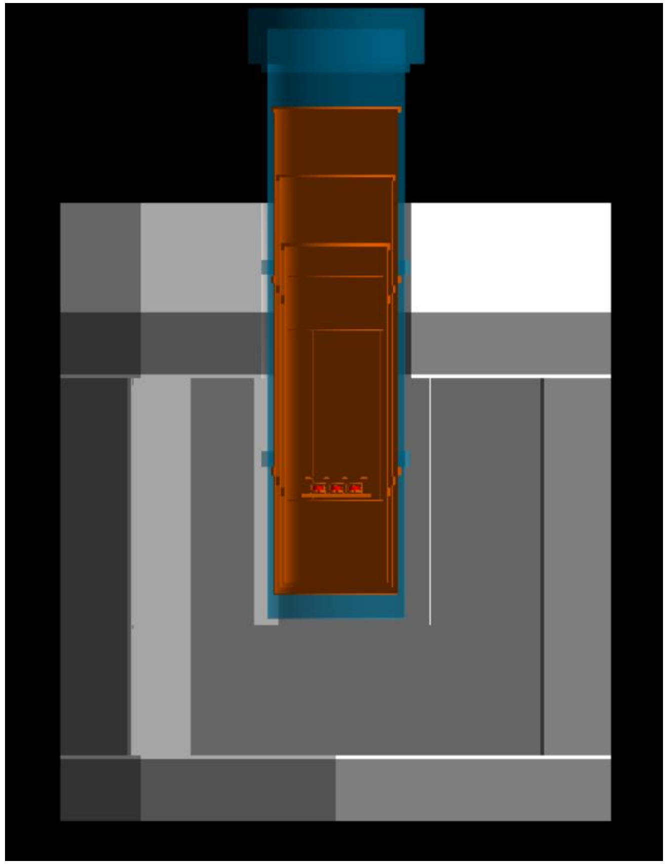

GEANT4 simulation for Ricochet RUN013 (G. Chemin)

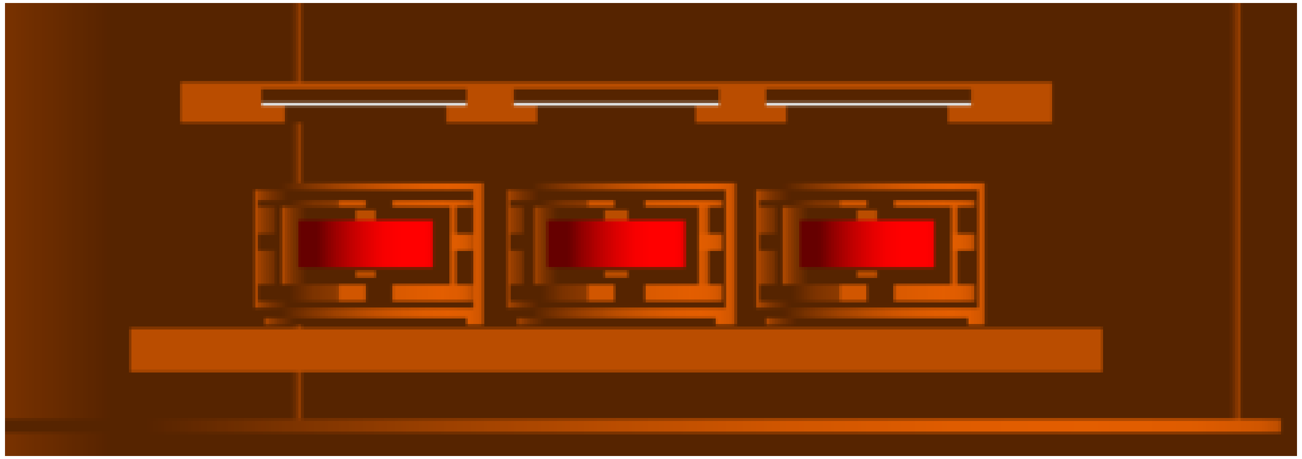

- 1 MiniCryoCube
- 2-part lead shielding
- Generation in the first centimeter of lead and throughout the polyethylene
- 3 detectors but only one sensitive volume
- No internal shielding

Activity measurement : peak by peak

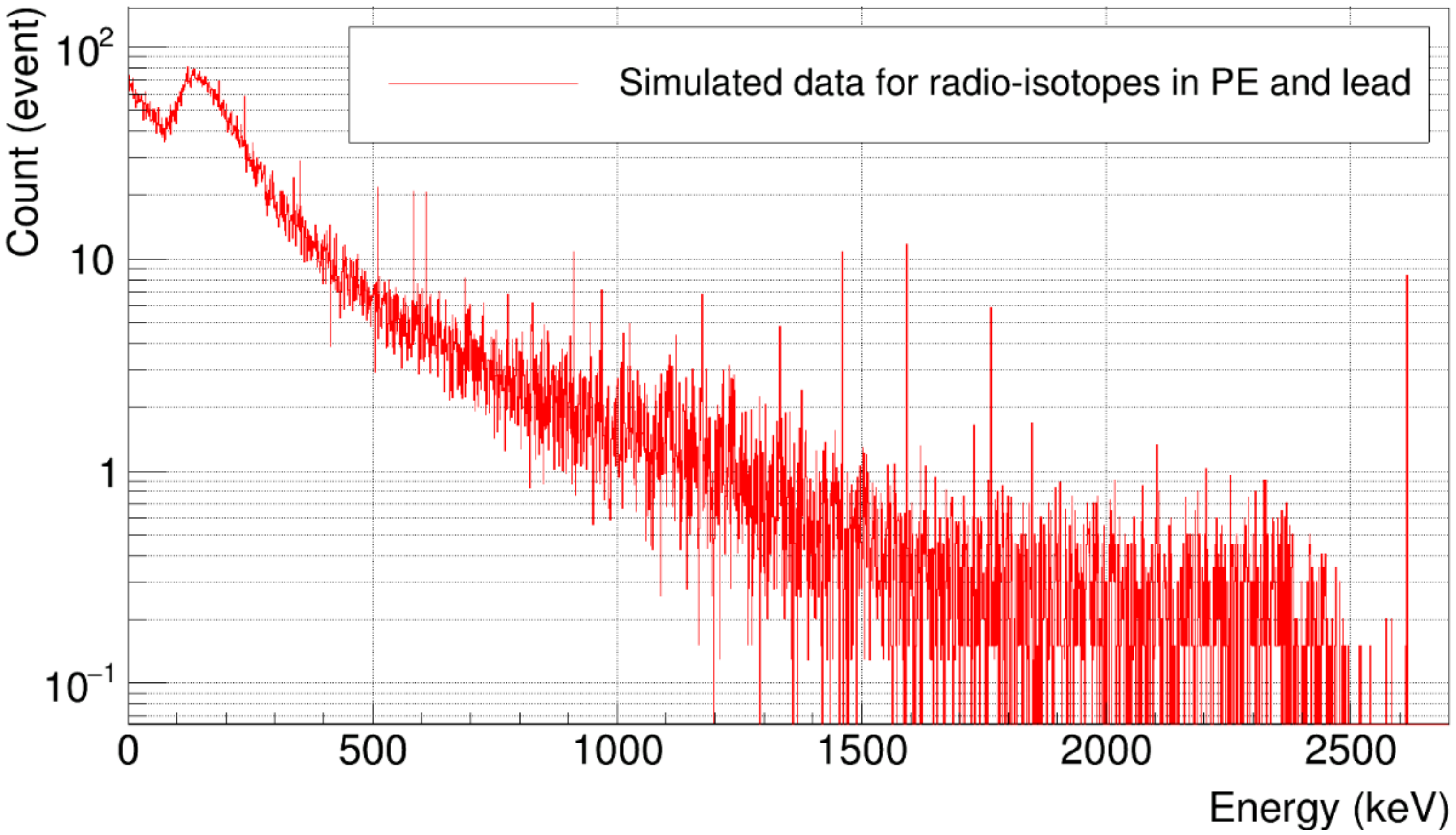

Linear combinaison of the radiogenic simulations for RUN013

- Obtained with the same linear coefficients as the HPGe study
- Requires convolution with energy resolution
- Requires convolution with energy efficiency

- Maximum energy experimentally detected by RUN013 : 700 keV
- Peaks not visible the radiogenic background for RUN013

Activity measurement : peak by peak

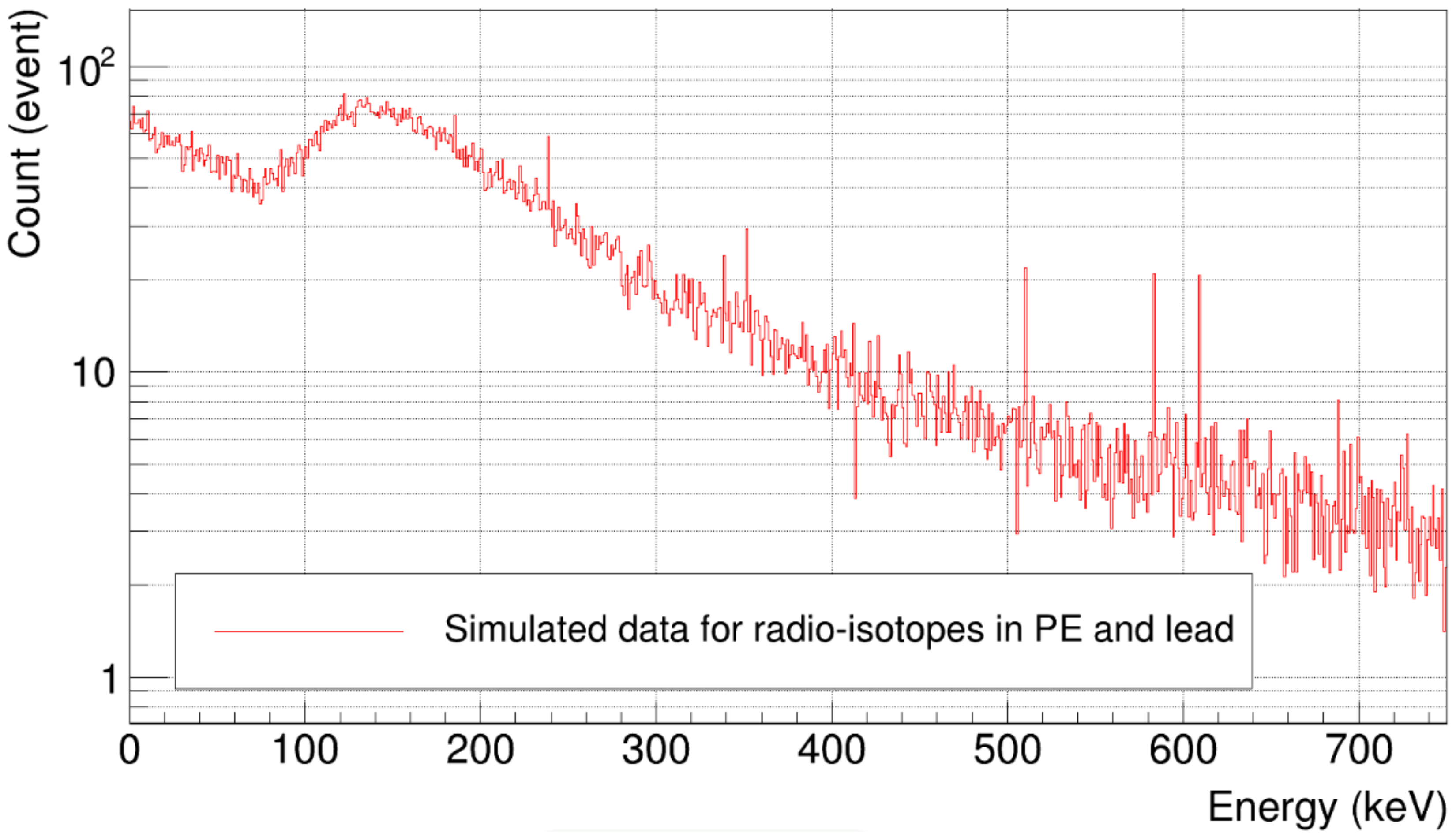

Linear combinaison of the radiogenic simulations for RUN013

- Obtained with the same linear coefficients as the HPGe study
- Requires convolution with energy resolution
- Requires convolution with energy efficiency

- Maximum energy experimentally detected by RUN013 : 700 keV
- Peaks not visible the radiogenic background for RUN013

Reactogenic background : 41-Ar

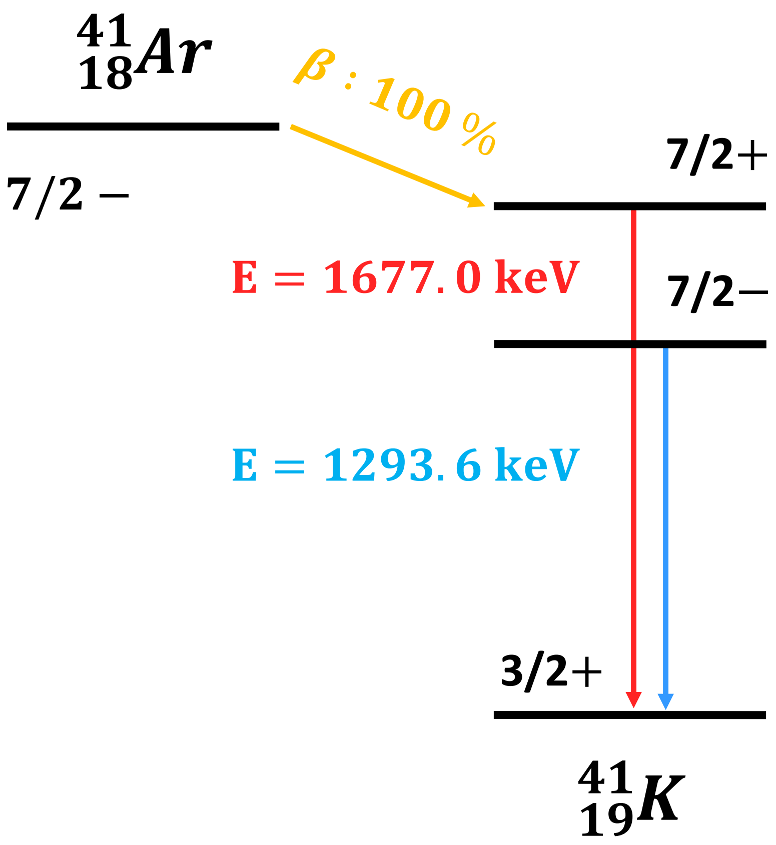

Argon-41 decay diagram

Reactor **ON** → $^{41}_{18}\mathbf{Ar}$ activation with $\tau_{1/2} = 109.61\ m$

$$^{40}_{18}Ar + {}^{1}_{0}n \rightarrow {}^{41}_{18}Ar \rightarrow {}^{41}_{19}K + {}^{0}_{1}e^{-} + {}^{0}_{0}\overline{\nu}_e$$

Method 1 : generate argon in the entire GEANT4 *World*

- $N_{gen} = 10^9\ evts \rightarrow N_{det} \sim 10^3\ evts$
- Output file too large and few statistics !

Method 2 : generate argon in central part of the cryostat

- Add argon-filled tube and subtract other volumes
- $N_{gen} = 10^8\ evts \rightarrow N_{det} = 5 \times 10^5\ evts$

Ricochet RUN013 : ^{41}Ar contamination

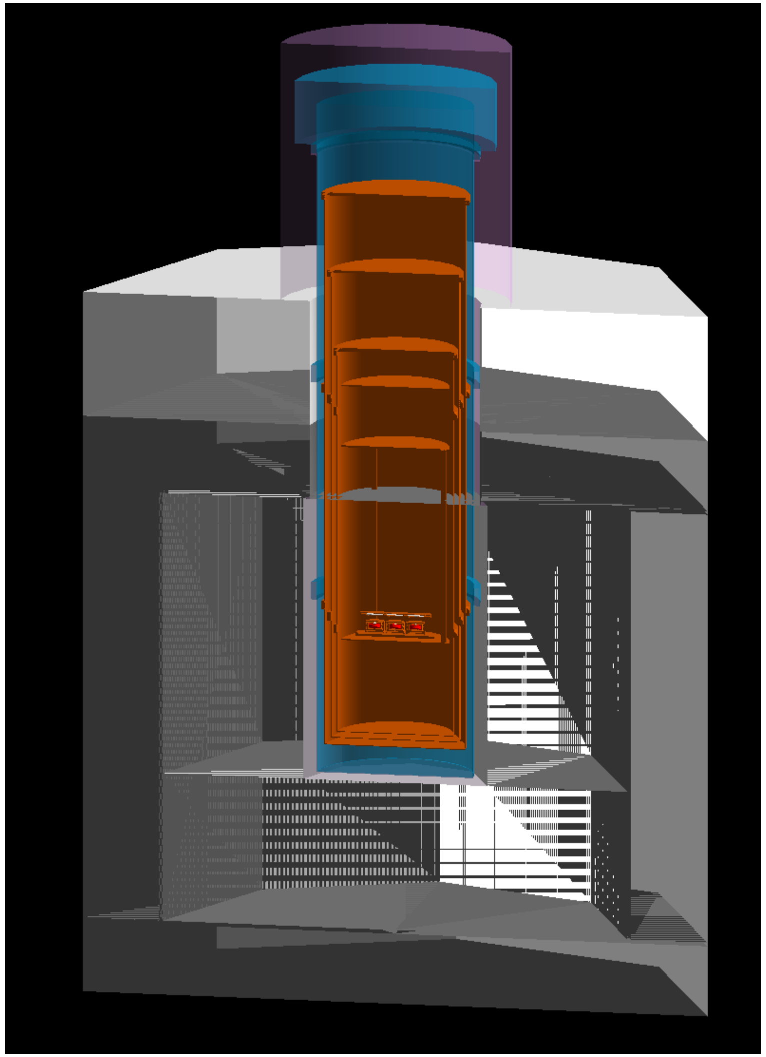

- Addition of an argon-filled layer between the Ricochet shield and the cryostat
- Addition of an argon-filled zone on top of the cryostat
- ➢ Shown here in yellow

- 1 MiniCryoCube
- 2-part lead shielding
- No Veto and CryoVeto
- 3 detectors but only one sensitive volume
- No inner shielding

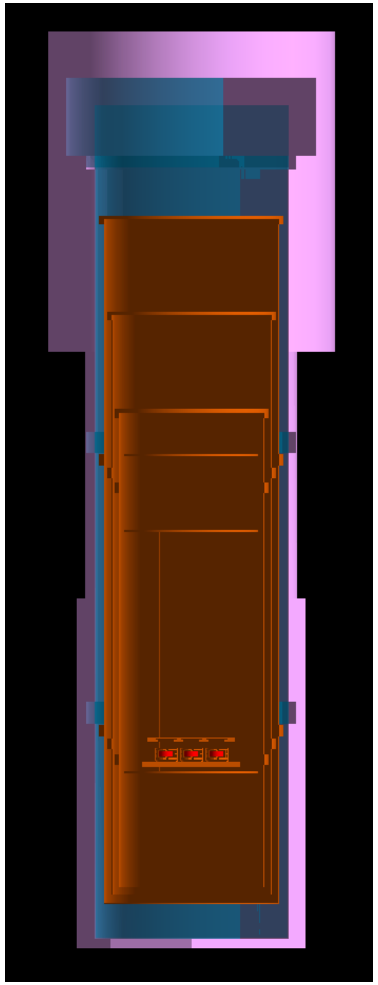

Simulated spectrum for 41-Ar

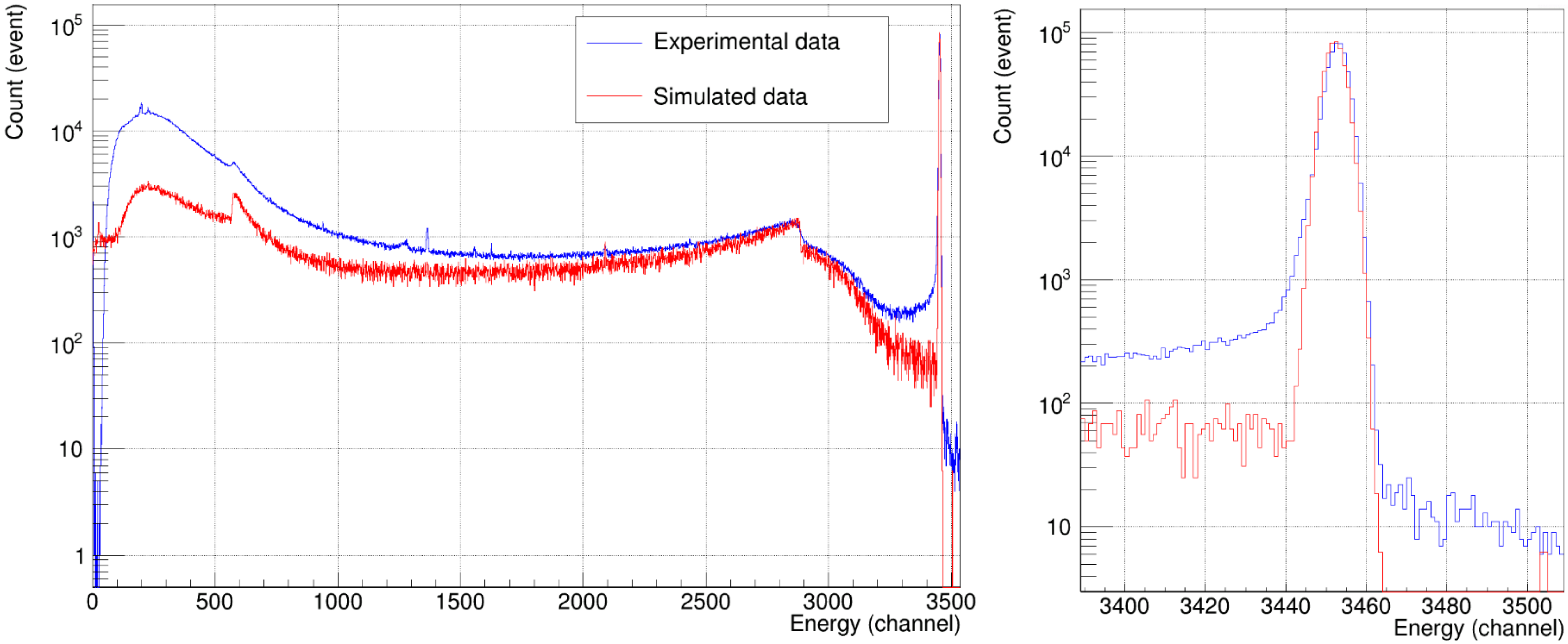

Comparison of experimental (blue) and simulated (red) spectra during an ON cycle of the reactor

Simulated spectrum for 41-Ar

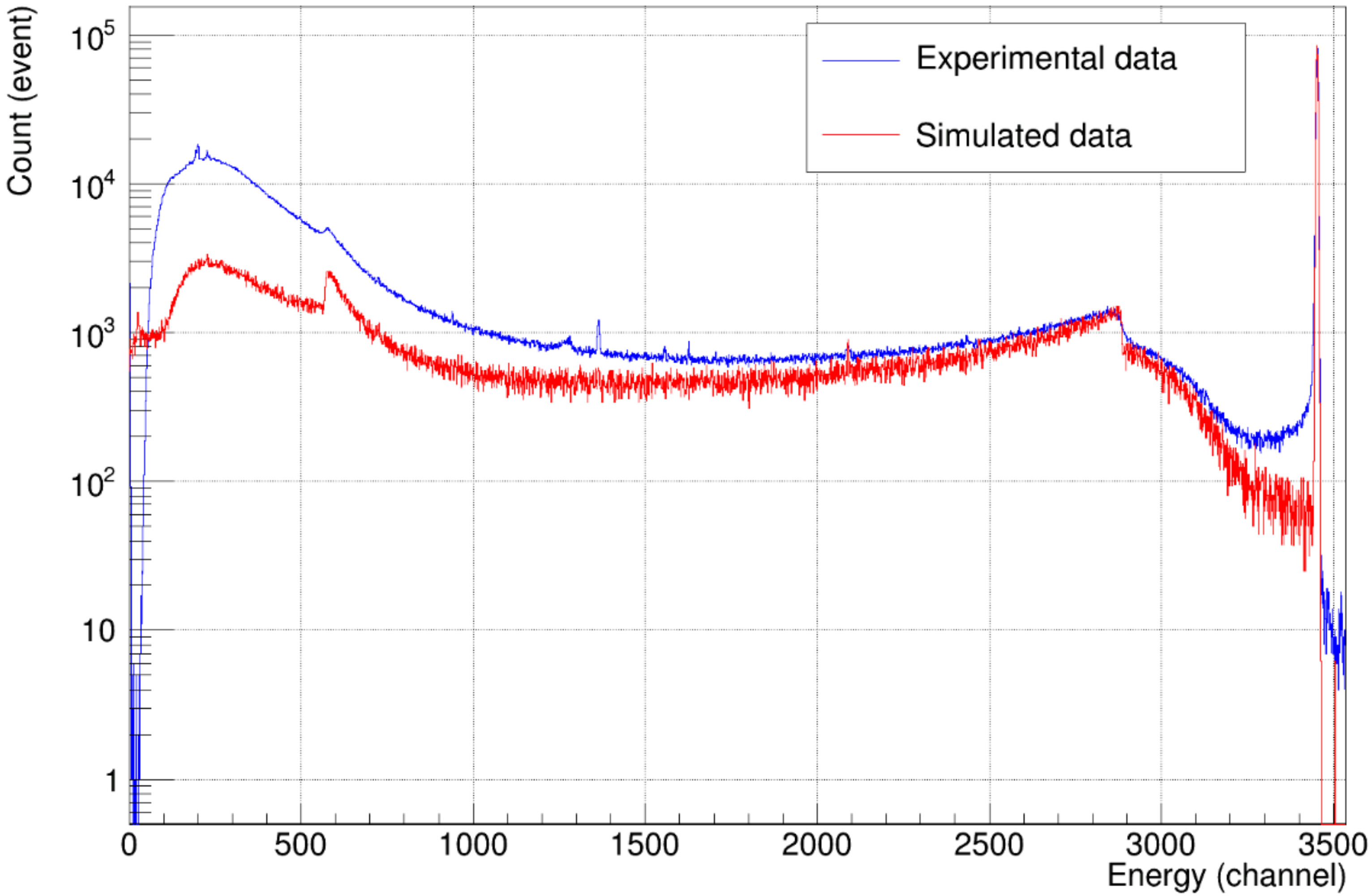

Comparison of experimental (blue) and simulated (red) spectra during an ON cycle of the reactor

GEANT4 simulation :

- Very good reconstruction of the peak at $E_0 = 1293.6\ keV$
- Poor reproduction of the Compton front under E_0

Hypothesis :

- Activation of high-energy γ- isotopes
- Interstices in Ricochet's shielding increase the quantity of argon-41